A SWITCHED SYSTEMS FRAMEWORK FOR NONLINEAR DYNAMIC SYSTEMS
WITH INTERMITTENT STATE FEEDBACK

By

HSI-YUAN CHEN

A DISSERTATION PRESENTED TO THE GRADUATE SCHOOL
OF THE UNIVERSITY OF FLORIDA IN PARTIAL FULFILLMENT
OF THE REQUIREMENTS FOR THE DEGREE OF
DOCTOR OF PHILOSOPHY

UNIVERSITY OF FLORIDA

2018

To my father, Chih-Man Chen, and my mother, Shu-Fen Yeh, for their invaluable support and encouragement.

TABLE OF CONTENTS

LIST OF FIGURES

7

8

Abstract of Dissertation Presented to the Graduate School
of the University of Florida in Partial Fulfillment of the
Requirements for the Degree of Doctor of Philosophy

A SWITCHED SYSTEMS FRAMEWORK FOR NONLINEAR DYNAMIC SYSTEMS
WITH INTERMITTENT STATE FEEDBACK

By

Hsi-Yuan Chen

December 2018

Chair: Warren E. Dixon
Major: Mechanical Engineering

Inspired by applications in which autonomous systems are tasked to operate in a feedback-denied region, this dissertation focuses on the development of a novel switched systems-based control framework to allow intermittent state feedback for systems under such unfavorable scenarios. Specifically, the developed approach utilizes a model of the controlled systems to predict the state of the systems when feedback is unavailable. Inherently, the systems can be further divided into subsystems based on feedback availability, where the behavior of each subsystem is unique. Based on the design of nonlinear controllers, observers and reset maps, Lyapunov-based, switched systems stability analysis methods are developed to determine the stabilizing dwell-time conditions for the subsystems. The stability analysis provides a framework for achieving operations in the presence of intermittent feedback.

CHAPTER 1
INTRODUCTION

1.1 Motivation

Acquiring state feedback is at the core of ensuring stability in control designs. However, factors such as the task definition, operating environment, or sensor modality can result in temporary loss of feedback for autonomous systems. For example, feedback may be provided by sensors such as cameras which are limited by sensing distance and field-of-view (FOV) constraints and are vulnerable to occlusions. Inspired by such factors, previous literature have introduced various path-planning and control methods seeking uninterrupted feedback (cf., [1–13]). However, the trajectory or behavior of the system from such results are inherently constrained. For instance, results such as [14–16] yield sharp-angled and non-smooth trajectories for nonholonomic systems, such as wheeled mobile robots (WMR), to maintain a landmark in the camera's FOV in visual servoing applications. In addition, such designs for control or trajectory may not be feasible for operations that are confined by the environment. Other applications beyond vision-based guidance control are also limited by this restriction. For example, the operational range of an autonomous vehicle may be hindered in areas with limited feedback such as GPS denied regions, poor signal coverage, and communication-restricted zones. Therefore, despite the best efforts of various solutions, loss of feedback can still occur for some sensor modalities and environmental factors.

In this dissertation, rather than trying to constrain the system to ensure continuous feedback is available, a novel framework is developed using a switched systems approach to relax this constraint and allow for autonomous operations under the influence of intermittent feedback availability. Navigational tasks can still be potentially achieved when feedback is not available by utilizing a state estimate to predict the state during feedback-denied periods. Consequently, the effect of intermittent feedback divides the system into stable and unstable subsystems for periods with and without

11

state feedback, respectively. Specifically, even if the system is exponentially stable when state feedback is available, the error dynamics are unstable without feedback, and therefore the overall system may diverge in the limit if the feedback is denied for sufficiently long periods of time. By leveraging switched systems theory, sufficient conditions can be developed to maximize the time that the system can spend outside without state feedback, while guaranteeing the stability of the overall system.

1.2 Literature Review

To compensate for intermittent feedback, a method for state estimation is required for periods of time when feedback is unavailable. Stability considerations are also important to ensure the estimation error is bounded. The networked control systems community has investigated problems such as [17–20] where communication rates are limited, i.e., a reduced frequency in data transmission. Typically in these results, state feedback updates are event-triggered, where an independently designed decision maker is used to broadcast sensor information between systems whenever prescribed conditions are reached. Other works, such as [21–23], model data loss as random missing outputs and noisy measurements, where stability is proven in a stochastic sense. In each case, state estimates are propagated by a model of the controlled system during the periods when the state measurement is missing. In this dissertation, the system must be physically within a feedback-available region to receive state information, introducing a unique challenge where the system's stability ultimately depends on its ability to return to the feedback-available region before the prescribed conditions are reached.

Stability of systems that experience random state feedback has been analyzed in works such as [22, 24–45]. In such results, the intermittent loss of measurement is modeled as a random Bernoulli process with a known probability. Resulting trajectories are then analyzed in a probabilistic sense, where the expected value of the estimation error

12

is shown to converge asymptotically. In addition to the aforementioned physical constraint on feedback availability, the framework developed in this dissertation examines the behavior of the actual tracking and estimation errors where the state measurements are completely denied for a prescribed time-frame.

Another state estimation application domain is visual-odometry. Methods for systems using imaging sensors for state feedback have been developed to relax the requirement of keeping landmarks in the FOV (cf., [46] and [47]). In [46], the topology of multiple landmarks are related via a daisy-chaining approach where new landmarks are mapped onto the initial world frame and are used to provide state feedback after initial landmarks have left the FOV. In [47], a method is presented where feature points in the background are related to a landmark in a similar fashion to provide state estimate for a WMR to navigate around a landmark without constantly keeping it in the FOV. However, the state estimate in both results are treated as state feedback, and the effects from measurement noise and disturbances are not discussed. Therefore, daisy-chaining-based approaches may provide local state feedback estimates and may well in an ideal or simulated scenario; however, the accuracy of the feedback eventually degrades and diverges in many cases, such as those with measurement noise and disturbances in the dynamics. This phenomenon is notable in conventional approaches to the simultaneous localization and mapping (SLAM) problem, such as in [48–50], which use relationships between features or landmarks to simultaneously estimate the pose (i.e., position and orientation) of the sensor and the landmarks with respect to the world frame. For monocular or vision-based sensors, a feature-rich environment with sufficient measurements are typically required for SLAM methods to perform well. Similar to the daisy-chaining approaches, a well-known and common drawback with SLAM algorithms is the drift in estimate due to the accumulation of measurement noise over time (cf., [51, 52]). The common practice to overcome the error accumulation is through a global loop closure process that constantly searches for potential loop

closures to optimize the estimates [53, 54]. However, achieving a global loop closures is computationally heavy and a bound on the estimate drift is not guaranteed. Motivated by these drawbacks, the work in this dissertation presents sufficient conditions that are derived via a Lyapunov-based switched systems analysis to ensure the global loop closure of the state estimates are achieved, guaranteeing the boundedness of the estimate errors by a desired bound. While this framework may be integrated with existing SLAM algorithms, the development in this dissertation utilizes a dead-reckoning approach to demonstrate the worst case scenario, where only system models are used to predict the state estimates when state feedback is not available. Applications that may potentially benefit from this approach include underwater operations where submerged vehicles must resurface to acquire position information via the Global Positioning System (GPS) occasionally and exploration of regions where absolute positioning systems have not been previously established.

As discussed in [55], arbitrary switching between stable subsystems may potentially lead to instability. The strategy for proving stability for slow switching between stable subsystems typically involves developing switching conditions to stabilize the overall system. The results in [55] shows that overall stability can be proven if a common Lyapunov function exists for all subsystems so that the time derivative of the Lyapunov function is upper bounded by a common negative definite function. However, multiple subsystem-specific Lyapunov functions may also be used in cases where a common Lyapunov function cannot be determined. These Lyapunov functions may be discontinuous and discrete jumps may occur over switching interfaces, requiring the enforcement of switching conditions to ensure the respective subsystems are decreasing over a cycle of activation, and switching conditions must be imposed on the subsystems to enforce a decrease in the subsystem-specific Lyapunov functions over a cycle of successive activation of the respective subsystems. As described in [55], the switching conditions typically manifest as (average) dwell-time conditions, which specify the duration for

14

which each subsystem must remain active. In [56], a stability analysis is provided for switched systems with stable and unstable linear time invariant (LTI) subsystems, and an average dwell-time condition is developed. Similarly, the authors in [57] developed dwell-time conditions for switched systems with stable and unstable nonlinear subsystems. In [58], the authors developed an observer to estimate the depths of feature points in a image from a monocular camera and use a predictor to propagate the state estimates when the features are occluded or outside the FOV. Based on the error system formulation, the subsystem for the observer is stable, while the subsystem for the predictor is unstable. An average dwell time condition is developed to ensure the stability of the switched system. However, dwell-time conditions in these results typically require the stable subsystems to be activated longer than the unstable subsystems, as indicated in [56].

Motivated by past literature and the prevalent nature of the problem, this dissertation aims to develop a framework for achieving control objectives despite intermittent loss of feedback. Unlike previous results, the focus in this work is to prolong and maximize the amount of time a system can spend in a feedback-denied region. Based on a Lyapunov-based, switched systems analysis, sets of stabilizing dwell time conditions are developed for stable and unstable subsystems to ensure stability for the overall system.

1.3   Outline of the Dissertation

In Chapter 2 and the development in [59], a novel control method is presented to relax the aforementioned landmark visibility constraint. In contrast to [47], a switched systems analysis is used to develop a set of dwell time conditions based on landmark visibility to ensure stability of the overall observer. Similar to [58], the state estimate update, governed by a nonlinear observer, is shown to be stable when the landmark is in the FOV. When the landmark is not in the FOV, a predictor is utilized to update the state estimates. Specifically, a Lyapunov-based stability analysis is used to determine the minimum and maximum periods of time the landmark can be in and out of the

FOV, respectively. To achieve a trajectory tracking objective, a controller similar to the development in [60] is designed to maintain stability through intermittent periods when the landmark leaves the FOV. The stability analysis indicates the controller ensures the tracking error is GUUB despite intermittent landmark sensing. A simulation and an experiment are provided using a Bézier curve trajectory design, inspired by results such as [61–64], to demonstrate the performance of the approach.

In Chapter 3 and [65], dwell-time conditions and a control method is developed for a generic class of holonomic dynamic systems. The novelty of this chapter is the generalization of the developed approach to allow a system to temporarily leave a feedback-available region and track a trajectory without state feedback. A simulation is provided for a nonlinear dynamical system, and an experiment is performed on a quadcopter to illustrate the robustness and stability of the developed scheme.

In Chapter 4 and [66], a generalized framework for systems operating under intermittent state feedback is investigated. The development in this chapter improves on the result of Chapter 3 to eliminate any alteration to the design and stability analysis when using an existing observer and controller in the presence of intermittent state feedback. In addition, the development in Chapter 4 also allows for the use of reset maps when the system is inside a feedback-available region, yielding a much better performance than the results in Chapter 3. Two experiments are performed. One experiment uses an observer to yield a continuous state estimate and the other utilizes reset maps for comparison.

In Chapter 5, a method for assisted path-following in a feedback-denied region is presented, where a relay agent intermittently updates the state estimation for an exploring agent operating in the feedback-denied region by traveling back and forth from the feedback-available region. Expanding on the framework developed in Chapter 4, unknown drift dynamics are assumed for the relay agent. Specifically, a neural network is utilized to approximate the uncertainty in the dynamics. Similar to previous

chapters, dwell-time conditions are derived for both agents, and through a Lyapunov-based, switched systems analysis, the path-following error is shown to be bounded by a user-defined parameter.

1.4 Notation

In the following, $\mathbb{R}$ denotes the set of real numbers, $\mathbb{R}^n$ and $\mathbb{R}^{n \times m}$ denote the sets of real n-vectors and $n \times m$ matrices, and $\mathbb{R}_{\geq a}$ and $\mathbb{R}_{>a}$ denote the sets of real numbers greater than or equal to a and strictly greater than a, respectively, where $a \in \mathbb{R}$. The $n \times n$ identity matrix is denoted by I_n. The $n \times m$ matrix of zeros and ones is denoted by $0_{n \times m}$ and $1_{n \times m}$, respectively. The notation $(\cdot)^T$ denotes the transpose of a matrix or vector.

CHAPTER 2
A SWITCHED SYSTEMS APPROACH TO VISION-BASED TRACKING CONTROL OF WHEELED MOBILE ROBOTS

Conventional methods for image-based guidance, navigation, and control of a WMR require continuous, uninterrupted state feedback at all times. However, tracked features may be lost due to occlusions or the trajectory of the WMR. In this chapter and [59], a set of dwell-time conditions that can be used for trajectory design are developed to relax the constant visibility constraint, while maintaining the ability to self-localize and track a desired trajectory. The use of a predictor for state estimates when landmark features are not visible helps to extend the time before image feedback of landmark features is required. Using a Lyapunov-based switched systems analysis, maximum and minimum dwell-time conditions are derived for periods when features are visible or not. A simulation and an experiment are performed with a trajectory formed by Bézier splines to demonstrate a globally uniformly ultimately bounded trajectory tracking result despite intermittent measurements.

2.1 System Model

The kinematic model for a unicycle with an exogenous disturbance is

$$\dot{q}(t) = S(q)v(t) + d(t) \tag{2-1}$$

where $q(t)$, $\dot{q}(t) \in \mathbb{R}^3$ are defined as

$$q(t) \triangleq \begin{bmatrix} x(t) & y(t) & \theta(t) \end{bmatrix}^T, \ \dot{q}(t) \triangleq \begin{bmatrix} \dot{x}(t) & \dot{y}(t) & \dot{\theta}(t) \end{bmatrix}^T, \tag{2-2}$$

where $x(t)$, $y(t)$, $\theta(t) \in \mathbb{R}$ denote the linear position and orientation of the WMR, respectively, and $\dot{x}(t)$, $\dot{y}(t)$, $\dot{\theta}(t) \in \mathbb{R}$ denote the Cartesian components of the linear velocity and angular velocity, respectively. The matrix $S(q(t)) \in \mathbb{R}^{3 \times 2}$ is defined as

$$S(q\,(t)) \triangleq \begin{bmatrix} \cos\theta\,(t) & 0 \\ \sin\theta\,(t) & 0 \\ 0 & 1 \end{bmatrix}, \tag{2–3}$$

and the input velocity vector $v(t) \in \mathbb{R}^2$ is defined as

$$v(t) \triangleq \begin{bmatrix} v_1(t) & v_2(t) \end{bmatrix}^T = \begin{bmatrix} v_1(t) & \dot{\theta}(t) \end{bmatrix}^T, \tag{2–4}$$

where $v_1(t),\ v_2(t) \in \mathbb{R}$ denotes the input linear and angular velocity of the WMR, respectively. The disturbance $d(t) \in \mathbb{R}^3$ is defined as

$$d(t) \triangleq \begin{bmatrix} d_1(t) & d_2(t) & d_3(t) \end{bmatrix}^T, \tag{2–5}$$

where $\|d(t)\| \leq \bar{d} \in \mathbb{R}_{\geq 0}$. A reference trajectory for the WMR is generated by

$$\dot{q}_d(t) \triangleq S(q_d\,(t))v_d(t), \tag{2–6}$$

where $q_d(t) \triangleq [x_d(t)\,y_d(t)\,\theta_d(t)]^T \in \mathbb{R}^3$ denotes the desired Cartesian position and orientation with respect to time, and $v_d \triangleq [v_{d1}\,v_{d2}]^T \in \mathbb{R}^2$ denotes the desired linear and angular velocity. The desired Cartesian trajectory and the time-varying velocity signal are constructed to ensure that $v_d(t),\ \dot{v}_d(t),\ q_d(t),\ \dot{q}_d(t) \in \mathcal{L}_\infty \forall t$, and that the starting and ending pose must allow for image feedback of the landmark features. Additionally, the desired trajectory must satisfy the dwell-time conditions developed in subsequent analysis.

Based on the WMR kinematic model and subsequent stability analysis, when image feedback is present an image-based observer is designed as

$$\dot{\hat{q}}(t) \triangleq S(\hat{q}\,(t))v(t) + R(t), \tag{2–7}$$

19

where $\hat{q}(t) \triangleq \begin{bmatrix} \hat{x}(t) \ \hat{y}(t) \ \hat{\theta}(t) \end{bmatrix}^T \in \mathbb{R}^3$ denotes the position and orientation estimates, respectively, $R(t) \triangleq [r_1(t) \ r_2(t) \ r_3(t)]^T \in \mathbb{R}^3$ is a subsequently designed update term. When the landmark features are not available, the state estimates are updated by a predictor designed as

$$\dot{\hat{q}}(t) \triangleq proj(S(\hat{q}(t))v(t)), \tag{2–8}$$

where $proj(\cdot)$ is a smooth projection operator (e.g. [67], [68]).

Assumption 2.1. The states, $q(t)$, can be obtained directly and instantly from image processing. Methods to obtain the states include geometric reconstruction approach with a known distance between two features, as described in [69–71], and fiducial marker systems such as [72, 73].

2.2 State Estimate and Control Objective

The relaxation of the constant landmark visibility constraint implies that landmark features become unavailable when the camera is required to point away from the landmark, and hence, cannot be used to generate state feedback when the landmark is not visible. When the landmark returns to the FOV, state feedback is assumed available under Assumption 2.1. Due to intermittent state feedback, the tracking error is defined based on state estimate as

$$e_1(t) \triangleq \begin{bmatrix} \tilde{x}(t) \\ \tilde{y}(t) \\ \tilde{\theta}(t) \end{bmatrix} = \begin{bmatrix} \hat{x}(t) - x_d(t) \\ \hat{y}(t) - y_d(t) \\ \hat{\theta}(t) - \theta_d(t) \end{bmatrix}. \tag{2–9}$$

To facilitate the subsequent development, a state transformation is defined similar to [60] as

$$
\begin{bmatrix} w(t) \\ z_1(t) \\ z_2(t) \end{bmatrix} \triangleq \begin{bmatrix} -\tilde{\theta}(t)\cos\hat{\theta}(t) + 2\sin\hat{\theta}(t) & -\tilde{\theta}(t)\sin\hat{\theta}(t) - 2\cos\hat{\theta}(t) & 0 \\ 0 & 0 & 1 \\ \cos\hat{\theta}(t) & \sin\hat{\theta}(t) & 0 \end{bmatrix} e_1(t), \quad (2\text{–}10)
$$

where $w(t) \in \mathbb{R}$ and $z(t) \triangleq [z_1(t)\ \ z_2(t)]^T \in \mathbb{R}^2$ are the auxiliary tracking error variables. To quantify the state estimation objective, let the state estimate error, $e_2(t) \in \mathbb{R}^3$ be defined as,

$$
e_2(t) \triangleq \begin{bmatrix} x(t) - \hat{x}(t) \\ y(t) - \hat{y}(t) \\ \theta(t) - \hat{\theta}(t) \end{bmatrix}. \tag{2–11}
$$

2.2.1 Control Development

Taking the time derivative of (2–10) and utilizing (2–1)-(2–6), the open-loop system of the transformed state error can be expressed as [60]

$$
\begin{aligned}
\dot{w}(t) &= u^T(t)J^T z(t) + f(t), & (2\text{–}12) \\
\dot{z}(t) &= u(t),
\end{aligned}
$$

where $J \in \mathbb{R}^{2\times 2}$ is defined as

$$
J \triangleq \begin{bmatrix} 0 & -1 \\ 1 & 0 \end{bmatrix}, \ J^T = -J, \ J^T J = I_{2x2}, \tag{2–13}
$$

and $f(t) \in \mathbb{R}$ is defined as

$$
f(t) \triangleq 2\left(v_{d2}(t)z_2(t) - v_{d1}(t)\sin z_1(t)\right) + 2\left(\sin\left(\hat{\theta}(t)\right)r_1(t) - \cos\left(\hat{\theta}(t)\right)r_2(t)\right). \tag{2–14}
$$

The auxiliary controller $u(t) = [u_1(t) \ u_2(t)]^T \in \mathbb{R}^2$ is defined as

$$u(t) \triangleq T^{-1}(t) \begin{bmatrix} v_1(t) \\ v_2(t) + r_3(t) \end{bmatrix} - \begin{bmatrix} v_{d2}(t) \\ v_{d1}(t) \cos \tilde{\theta}(t) - \left(\cos \left(\hat{\theta}(t) \right) r_1 + \left(\sin \hat{\theta}(t) \right) r_2 \right) \end{bmatrix},$$

(2–15)

where $T(t) \in \mathbb{R}^{2 \times 2}$ is defined as

$$T(t) \triangleq \begin{bmatrix} \left(\tilde{x}(t) \sin \hat{\theta}(t) - \tilde{y}(t) \cos \hat{\theta}(t) \right) & 1 \\ 1 & 0 \end{bmatrix},$$

(2–16)

and hence, (2–4) can be expressed as

$$v(t) = T(t)u(t) + \begin{bmatrix} v_{d1}(t) \cos \tilde{\theta}(t) + v_{d2}(t) \left(\tilde{x}(t) \sin \hat{\theta}(t) - \tilde{y}(t) \cos \hat{\theta}(t) \right) - L(t) \\ v_{d2}(t) - r_3(t) \end{bmatrix}, \quad \text{(2–17)}$$

where $L(t) \in \mathbb{R}$ is defined as

$$L(t) \triangleq \left(\cos \left(\hat{\theta}(t) \right) r_1(t) + \sin \left(\hat{\theta}(t) \right) r_2(t) \right).$$

(2–18)

To facilitate the subsequent development, let $\tilde{z}(t) \in \mathbb{R}^2$ be defined as

$$\tilde{z}(t) \triangleq z_d(t) - z(t),$$

(2–19)

where $z_d(t) \in \mathbb{R}^2$. Based on the open-loop error system in (2–12) and utilizing (2–13)-(2–16), the auxiliary controller in [60] can be used to show $\tilde{z}(t)$, $w(t)$ are globally exponentially stable, and hence, $e_1(t)$ is globally uniformly ultimately bounded. Specifically, the auxiliary controller in [60] is designed as

$$u(t) \triangleq u_a(t) - k_2 z(t). \tag{2–20}$$

The auxiliary control term $u_a(t) \in \mathbb{R}^2$ is defined as

$$u_a(t) \triangleq \left(\frac{k_1 w(t) + f(t)}{\delta_d^2(t)} \right) J z_d(t) + \Omega_1(t) z_d(t), \tag{2–21}$$

where $\dot{z}_d(t)$ is defined as

$$\dot{z}_d(t) \triangleq \frac{\dot{\delta}_d(t)}{\delta_d(t)} z_d(t) + \left(\frac{k_1 w(t) + f(t)}{\delta_d^2(t)} + w(t) \Omega_1(t) \right) J z_d(t), \ z_d^T(0) z_d(0) = \delta_d^2(0), \tag{2–22}$$

and $\Omega_1(t) \in \mathbb{R}$ and $\delta_d(t) \in \mathbb{R}$ are defined as

$$\Omega_1(t) \triangleq k_2 + \frac{\dot{\delta}_d(t)}{\delta_d(t)} + w(t) \left(\frac{k_1 w(t) + f(t)}{\delta_d^2(t)} \right), \tag{2–23}$$

$$\delta_d(t) \triangleq \alpha_0 \exp(-\alpha_1 t) + \varepsilon_1, \tag{2–24}$$

where k_1, k_2, α_0, α_1, $\varepsilon_1 \in \mathbb{R}$ are positive, constant control gains. It was shown in [60] that $z_d(t)^T z_d(t) = \delta_d^2(t)$. Substituting in (2–20) and (2–21) into (2–12), the closed-loop tracking error can be expressed as

$$\begin{bmatrix} \dot{w}(t) \\ \dot{\tilde{z}}(t) \end{bmatrix} = \begin{bmatrix} u_a^T(t) J \tilde{z}(t) - k_1 w(t) \\ -k_2 \tilde{z}(t) + w(t) J u_a(t) \end{bmatrix}. \tag{2–25}$$

2.2.2 State Estimate

Consider the family of systems

$$\dot{e}_2(t) \triangleq f_p\left(t, q(t), \hat{q}(t)\right), \tag{2–26}$$

where $f_p : [0, \infty) \times \mathbb{R}^3 \times \mathbb{R}^3 \to \mathbb{R}^3, \ p \in \{a, u\}$, a is an index referring to when the features are visible and u is an index referring to the conditions when features are not visible. After taking the time derivative of (2–11) and substituting in (2–7) and (2–8) for the periods with and without state feedback, respectively, the family of systems in (2–26) can be expressed as

$$
f_p\left(t, q(t), \hat{q}(t)\right) = \begin{cases} S(q(t))v(t) + d(t) - S(\hat{q}(t))v(t) - R(t), & p = a, \\ S(q(t))v(t) + d(t) - proj(S(\hat{q}(t))v(t)), & p = u. \end{cases} \tag{2–27}
$$

When features are visible, $R(t)$ is designed as

$$
R(t) = k_3 e_2(t) + \bar{d}sgn(e_2(t)). \tag{2–28}
$$

Substituting (2–28) into (2–27), the family of systems described in (2–26) can be expressed as

$$
\dot{e}_2(t) = \begin{cases} -k_3 e_2(t) + d(t) - \bar{d}sgn(e_2(t)), & p = a, \\ S(q(t))v(t) - proj\left(S(\hat{q}(t))v(t)\right) + d(t), & p = u. \end{cases} \tag{2–29}
$$

2.3 Stability Analysis

To facilitate further analysis for the switched systems, let $t_i^a \in \mathbb{R}_{>0}$ denote the time of the ith instance at which features are visible, and $t_i^u \in \mathbb{R}_{>0}$ denotes the time of the ith instance when the features are not visible, where $n \in \mathbb{N}$. The dwell-time in the ith activation of the subsystem a and u is then defined as $\Delta t_i^a \triangleq t_i^u - t_i^a \in \mathbb{R}_{>0}$ and $\Delta t_i^u \triangleq t_{i+1}^a - t_i^u \in \mathbb{R}_{>0}$, respectively. Additionally, consider two candidate Lyapunov functions for the tracking error and the estimation error, respectively as

$$
V_1(w(t), \tilde{z}(t)) \triangleq \frac{1}{2}w^2(t) + \frac{1}{2}\tilde{z}^T(t)\tilde{z}(t), \tag{2–30}
$$

24

$$V_2(e_2(t)) \triangleq \frac{1}{2}e_2^T(t) e_2(t), \tag{2-31}$$

and a switched Lyapunov function for the switched subsystems is designed to capture both the estimation and control objective as

$$V_\sigma(\zeta(t)) \triangleq V_1(w(t), \tilde{z}(t)) + V_2(e_2(t)), \tag{2-32}$$

where $\zeta(t) \triangleq \left[w(t), \tilde{z}^T(t), e_2^T(t)\right]^T$. To derive the stabilizing dwell-time conditions, a maximum bound $V_M \in \mathbb{R}$ can be arbitrarily selected based on the desired tolerance for $V_\sigma(\zeta(t))$ in the worst case, such that

$$V_\sigma(\zeta(t)) \leq V_M, \ \forall t \in [t_i^u, t_{i+1}^a), \ \forall i, \tag{2-33}$$

and an arbitrary lower threshold on $V_\sigma(\zeta(t))$, $V_T \in \mathbb{R}$ where $V_T < V_M$ such that

$$V_\sigma(\zeta(t_i^u)) \leq V_T, \ \forall i. \tag{2-34}$$

Theorem 2.1. *The switched system generated by the family of systems described by (2–25), (2–29), and a piece-wise constant, right continuous switching signal $\sigma : [0, \infty) \to p \in \{a, u\}$ is globally uniformly ultimately bounded provided that the switching signal, controlled by a desired trajectory, satisfies the minimum visibility dwell-time condition*

$$\Delta t_i^a \geq \frac{-1}{\lambda_s} \ln\left(\min\left(\frac{V_T}{V_\sigma(\zeta(t_i^a))}, 1\right)\right), \tag{2-35}$$

and the maximum loss of visibility dwell-time condition

$$\Delta t_i^u \leq \frac{1}{\lambda_u} \ln\left(\frac{V_M + \frac{\varepsilon}{\lambda_u}}{V_\sigma(\zeta(t_i^u)) + \frac{\varepsilon}{\lambda_u}}\right), \tag{2-36}$$

where $\lambda_s, \ \lambda_u \in \mathbb{R}$ are subsequently defined, known positive constants.

Proof. From [60], the Lyapunov function in (2–30) can be used to show $\tilde{z}(t), \ w(t)$ are globally exponentially stable, regardless of the visibility of the landmark. Specifically,

$$\dot{V}_1(w\,(t)\,,\tilde{z}\,(t)) \le -\lambda V_1(w\,(t)\,,\tilde{z}\,(t)), \ \forall t, \qquad (2\text{--}37)$$

where $\lambda \triangleq 2min\,(k_1,\ k_2) \in \mathbb{R}_{>0}$. Similar to the analysis in [58], the Lyapunov function in (2–31) can be used to show $e_2\,(t)$ is globally exponentially stable when the landmark is visible and exhibits an exponential growth rate otherwise. Specifically,

$$\dot{V}_2(e_2\,(t)) \le \begin{cases} -2k_3 V_2((e_2\,(t))), & t \in [t_i^a, t_i^u), \\ \lambda_u V_2((e_2\,(t))) + \varepsilon, & t \in [t_i^u, t_{i+1}^a), \end{cases} \quad \forall i, \qquad (2\text{--}38)$$

where $\lambda_u \triangleq 2c + 1 \in \mathbb{R}_{>0}$, $\varepsilon \triangleq \frac{1}{2}\bar{d}^2 \in \mathbb{R}_{>0}$ is a constant, and $c \in \mathbb{R}_{>0}$ is a positive constant bound.

Taking the time derivative of (2–32) and substituting in (2–25) and (2–29) yield

$$\dot{V}_\sigma(\zeta\,(t)) \le \begin{cases} -\lambda_s V_\sigma(\zeta\,(t)), & t \in [t_i^a, t_i^u), \\ \lambda_u V_\sigma(\zeta\,(t)) + \varepsilon, & t \in [t_i^u, t_{i+1}^a), \end{cases} \quad \forall i \in \mathbb{N}, \qquad (2\text{--}39)$$

where $\lambda_s \triangleq 2min\,(k_1,\ k_2,\ k_3) \in \mathbb{R}_{>0}$. The solutions to (2–39) for the two subsystems are given as

$$V_\sigma(\zeta\,(t)) \le V_\sigma(\zeta\,(t_i^a))e^{-\lambda_s\left(t-t_i^a\right)},\ t \in [t_i^a, t_i^u),$$

$$V_\sigma(\zeta\,(t)) \le V_\sigma(\zeta\,(t_i^u))e^{\lambda_u\left(t-t_i^u\right)} - \frac{\varepsilon}{\lambda_u}\left(1 - e^{\lambda_u\left(t-t_i^u\right)}\right),\ t \in [t_i^u, t_{i+1}^a), \qquad (2\text{--}40)$$

for all i.

Clearly, when the landmark is visible, the bound on the switched Lyapunov function, containing states $w\,(t)$ and $\tilde{z}\,(t)$ is globally exponentially stable, therefore $e_1(t)$ is globally uniformly ultimately bounded. Since $e_2(t)$ is globally exponentially stable, the tracking error between the true state and the desired trajectory, $q\,(t) - q_d\,(t) = e_1\,(t) + e_2\,(t)$, is also globally uniformly ultimately bounded. From (2–33), the maximum dwell-time condition

for each of the i unobservable periods is $\left(V_\sigma(\zeta(t_i^u)) + \frac{\varepsilon}{\lambda_u} \right) e^{\lambda_u \Delta t_i^u} - \frac{\varepsilon}{\lambda_u} \leq V_M$, and hence,

$$\Delta t_i^u \leq \frac{1}{\lambda_u} \ln \left(\frac{V_M + \frac{\varepsilon}{\lambda_u}}{V_\sigma(\zeta(t_i^u)) + \frac{\varepsilon}{\lambda_u}} \right),$$

and from (2–34),

$$\Delta t_i^a \geq \frac{-1}{\lambda_s} \ln \left(\min \left(\frac{V_T}{V_\sigma(\zeta(t_i^a))}, 1 \right) \right).$$

Since $V_\sigma(\zeta(t)) \leq V_\sigma(\zeta(t_i^a)) e^{-\lambda_s (t - t_1^a)}$ when $i = 1$ implies exponential convergence, and that $V_\sigma(\zeta(t)) \leq V_\sigma(\zeta(t_i^a)) e^{-\lambda_s (t - t_i^a)} \leq V_\sigma(\zeta(t_i^a)) \leq V_M$, $p = a$ and $V_\sigma(\zeta(t)) \leq V_\sigma(\zeta(t_i^u)) e^{\lambda_u (t - t_i^u)} - \frac{\varepsilon}{\lambda_u} \left(1 - e^{\lambda_u (t - t_i^u)} \right) \leq V_\sigma(\zeta(t_{i+1}^a)) \leq V_M$, $p = u$ for all $i > 1$, then

$$V_\sigma(t) \leq V_M, \ \forall t > t_1^u. \tag{2–41}$$

Hence the switched system generated by (2–25) and (2–29) is globally uniformly ultimately bounded as depicted in Figure 2-1. □

Remark 2.1. A lower threshold on $V_\sigma(\zeta(t))$ enforces the convergence of $\|e_2(t)\|$ to an arbitrary small value. The threshold can be selected arbitrarily small, but the resulting minimum dwell-time condition in (2–35) becomes larger as V_T approaches zero. By choosing a V_T very close to V_M, the landmark is allowed to leave the FOV almost immediately upon entering the FOV, which implies that $V_\sigma(\zeta(t))$ can potentially be very close to V_M and result in a very small maximum dwell-time condition in (2–36). Hence, the selection on V_T varies depending on the application.

2.4 Simulation

A simulation is performed to verify the robustness of the controller design to the loss of state feedback from the imaging signal. The initial and the desired ending states are selected as

$$q_{initial} = \begin{bmatrix} 0 & 0 & 0 \end{bmatrix}^T, \ q_{desired} = \begin{bmatrix} 3 & 1.0 & -\pi \end{bmatrix}^T.$$

The initial state and state estimate for the WMR is
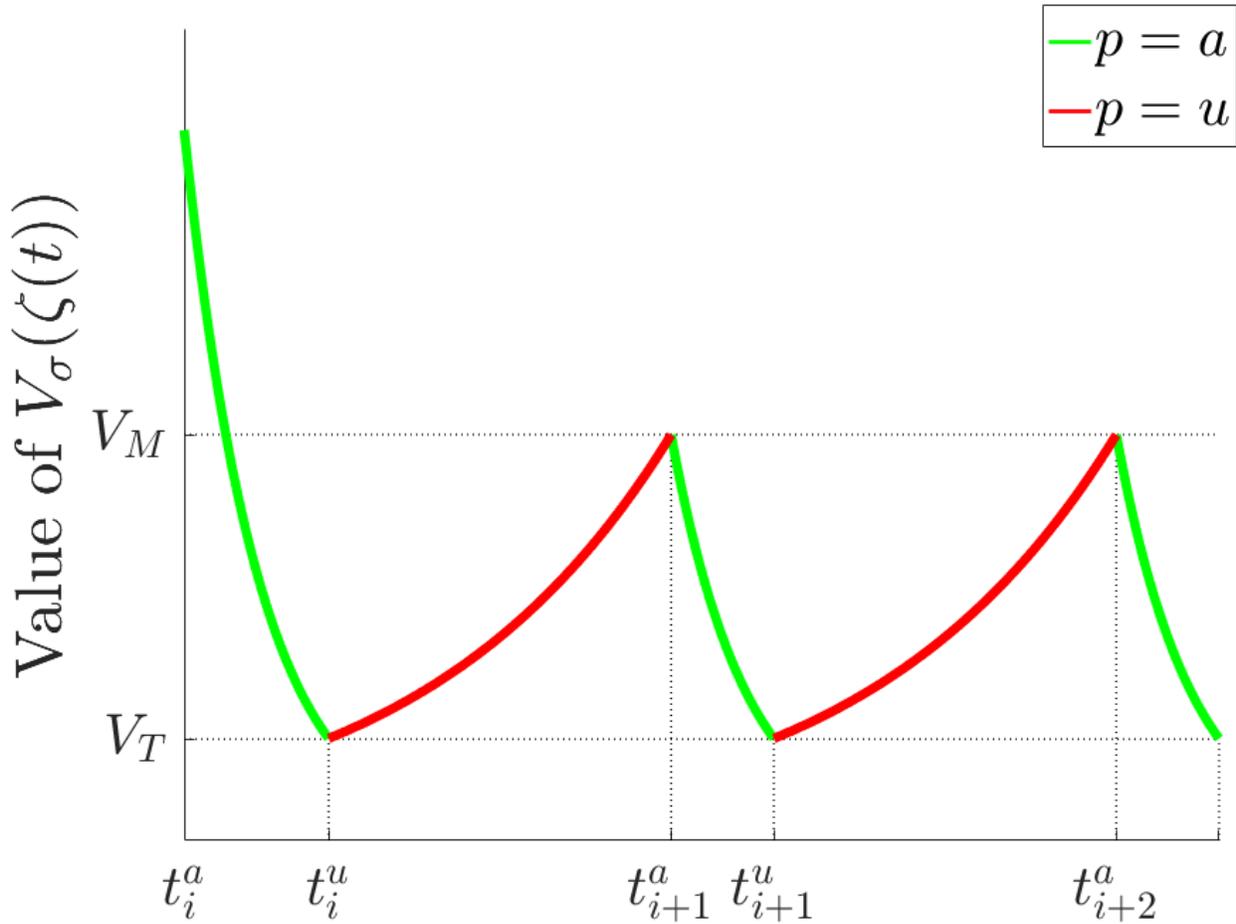
Figure 2-1. Representative illustration for the evolution of $V_\sigma\left(\zeta\left(t\right)\right)$ during the interval $\left[t_i^a, t_{i+2}^a\right]$.

$$q\left(0\right) = \begin{bmatrix} 0 & 0 & 0 \end{bmatrix}^{T}, \ \hat{q}\left(0\right) = \begin{bmatrix} 0 & 0.3 & 0 \end{bmatrix}^{T}.$$

The disturbance introduced to the system is a 0 mean normal distribution with variance 0.5 and a cut-off at ± 1.5, and the viewing angle of the camera is $\frac{\pi}{3}$ radians, centered about the x-axis of the WMR. A cubic Bézier curve is utilized as the desired trajectory because Bézier curves are continuously differentiable, can specify initial and final position and orientation through control points, and can be parameterized with respect to the dwell-time conditions. The gains for the observer and the controller are selected as

$$k_1 = 10, \ k_2 = 10, \ k_3 = 20, \ \alpha_0 = 2, \ \alpha_1 = 1, \ \varepsilon_1 = 0.01.$$

The initial values for $z_d\left(t\right)$ are selected as

$$z_d\left(0\right) = \begin{bmatrix} 0.01 & 0.01 \end{bmatrix}^{T}.$$

Based on the simulation, the system enters the unstable region when the landmark leaves the simulated FOV and re-enters the stable region once the landmark returns to the FOV. Figure 2-4 indicates that, the state estimation error $\|e_2\left(t\right)\|$ converges exponentially to zero when the landmark is visible, and the tracking error $\|e_1\left(t\right)\|$ is globally uniformly ultimately bounded between the state estimate and the desired trajectory, as shown in Figure 2-3. When the landmark is not visible, $\|e_1\left(t\right)\|$ remains globally uniformly ultimately bounded since the controller in (2–17) is enforcing the state estimate $\hat{q}\left(t\right)$ to track the desired trajectory $q_d\left(t\right)$. However, $\|e_2\left(t\right)\|$ grows when state feedback is not available. As the landmark reappears in the FOV, $\|e_2\left(t\right)\|$ converges to zero exponentially, implying that $\hat{q}\left(t\right) - q\left(t\right) \to 0$ exponentially. Since q deviated from $q_d\left(t\right)$ during the period without state feedback, $\|e_1\left(t\right)\|$ increases as $\hat{q}\left(t\right) - q\left(t\right) \to 0$ and converges as the controller drives $\hat{q}\left(t\right)$ to $q_d\left(t\right)$. From the simulation, it is clear that

the switched systems approach presented in this chapter is robust to intermittent state feedback and disturbances from the system kinematics, and thus a smooth trajectory can be designed to navigate the WMR without keeping the landmark in the FOV at all times, as depicted in Figure 2-2.

2.5   Experimental Results

An experimental is performed to demonstrate the control scheme. For the experiment, a Clearpath Robotics Turtlebot 2 with a Kobuki base is used. A landmark is created by a pentagon prism with fiducial markers, developed by [72], to the sides, and placed at the origin. A Bézier spline joint by six cubic Bézier curves has a initial position at $(-2, 0)$ and a final position at $(2, 0)$. The goal of this experiment is to regulate the WMR to the final position by viewing the landmark and updating the pose information while tracking the Bézier spline. The gains for the observer and the controller are selected as

$$k_1 = 0.2, \ k_2 = 0.8, \ k_3 = 1.2, \ \alpha_0 = 0.3, \ \alpha_1 = 0.2, \ \varepsilon_1 = 0.1.$$

The initial values for $z_d(t)$ are selected as

$$z_d(0) = \left[\begin{array}{cc} 0.2828 & 0.2828 \end{array} \right]^T.$$

Figure 2-5 represents the tracking result of this experiment, and Figures 2-6 and 2-7 shows evolution of $e_1(t)$ and $e_2(t)$ over time, respectively. In Figure 2-5, large tracking error is apparent when the predictor is active. An explanation for this behavior is that there exists a mismatch between the commanded and actual system velocities due to slip conditions and the controller board's ability to track the reference velocities. However, when the WMR senses the landmark between 18 to 21 seconds and 38 to 43 seconds, the state estimate is regulated towards the true state as indicated by Figure 2-7. As a result, the WMR is able to correct the tracking error and drive in reverse towards the desired trajectory. In Figure 2-6 and 2-7, predictor is activated for short periods of
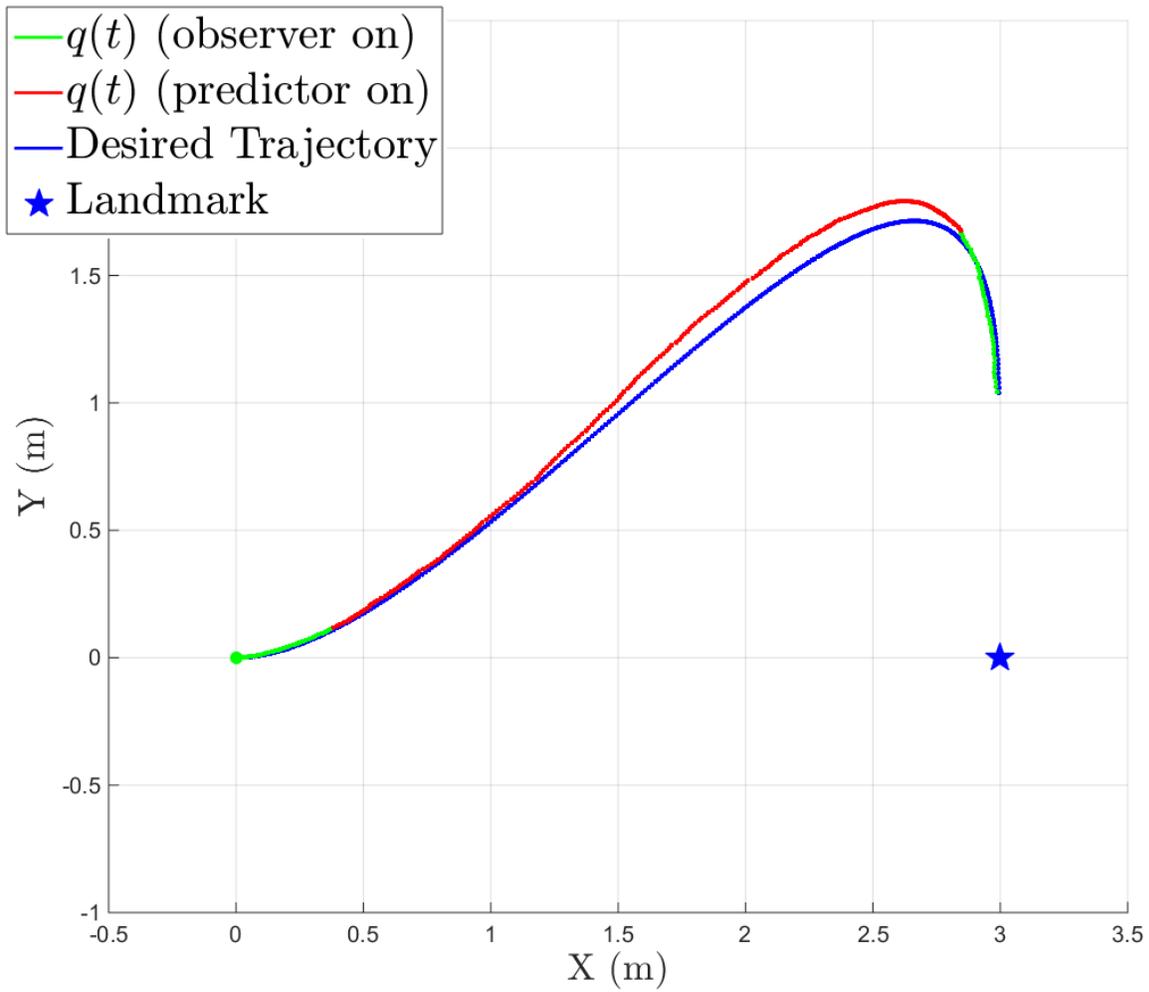
Figure 2-2. The trajectory tracking result. The green and red trajectories indicate whenever the observer and predictor are activated, respectively. When the predictor is active, the WMR diverges from the desired trajectory because of the disturbance. However, when the landmark returns to the FOV, regulation of the tracking error is achieved.
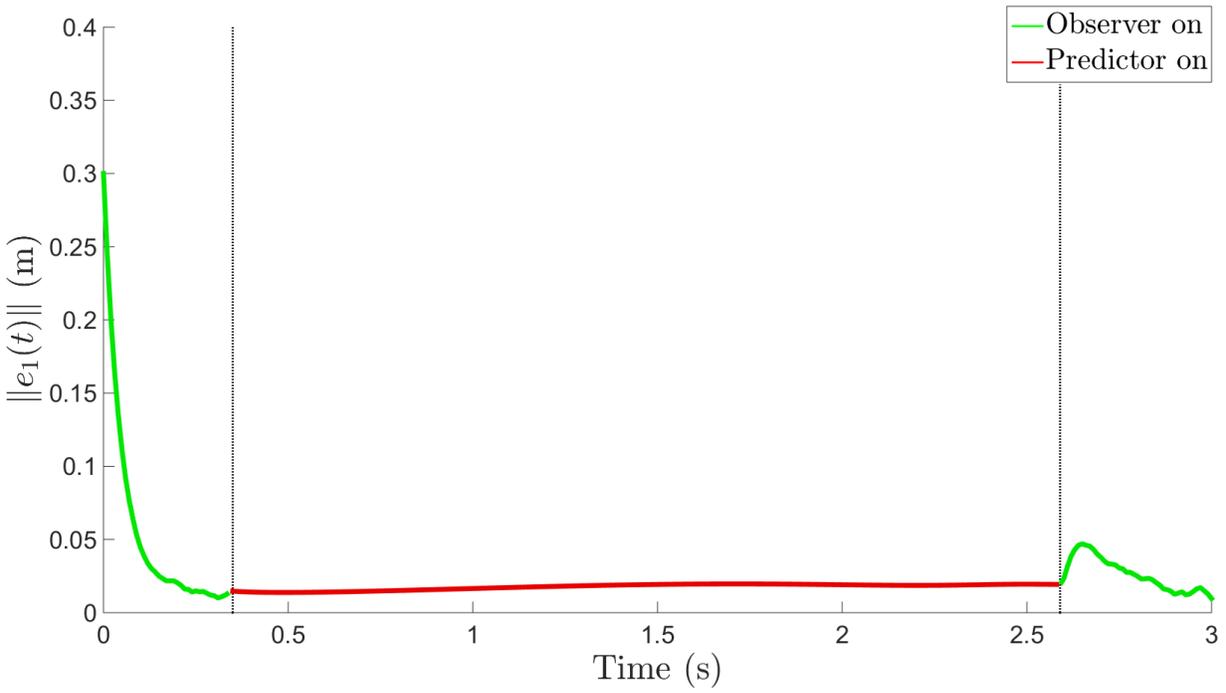
Figure 2-3. State estimate tracking error. The estimate tracking error is regulated when the predictor is activated because the update law propagates the state estimate using a model of the WMR. When the observer is activated at 2.6 secs, the estimate initially converges towards the true state and eventually converges to the desired trajectory along with the true state.
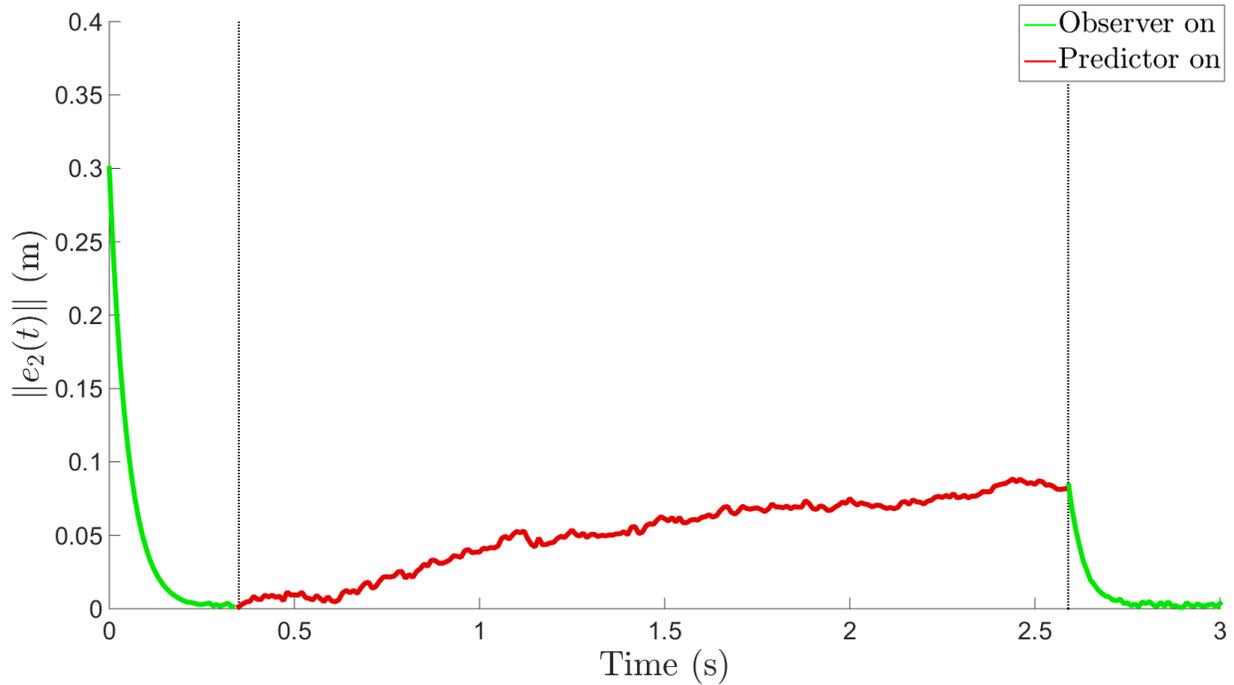
Figure 2-4. State estimation error. The estimate is exponentially regulated to the true state whenever the observer is active and diverges whenever the predictor is active.

time during 18 to 21 seconds and 38 to 43 seconds because the fiducial markers are lost to image blurring despite being in the camera's FOV.

2.6 Summary

A set of maximum and minimum dwell-time conditions is developed from a Lyapunov-based, switched systems analysis to ensure a globally uniformly ultimately bounded error of trajectory tracking for WMR's despite intermittent state feedback. The dwell-time conditions allow for a more flexible trajectory design, which can purposefully turn away from the landmark in order to achieve a smoother path and wider range of operation. A simulation utilizing a Bézier splines trajectory that satisfies the dwell-time conditions is performed to illustrate the robustness of the approach.
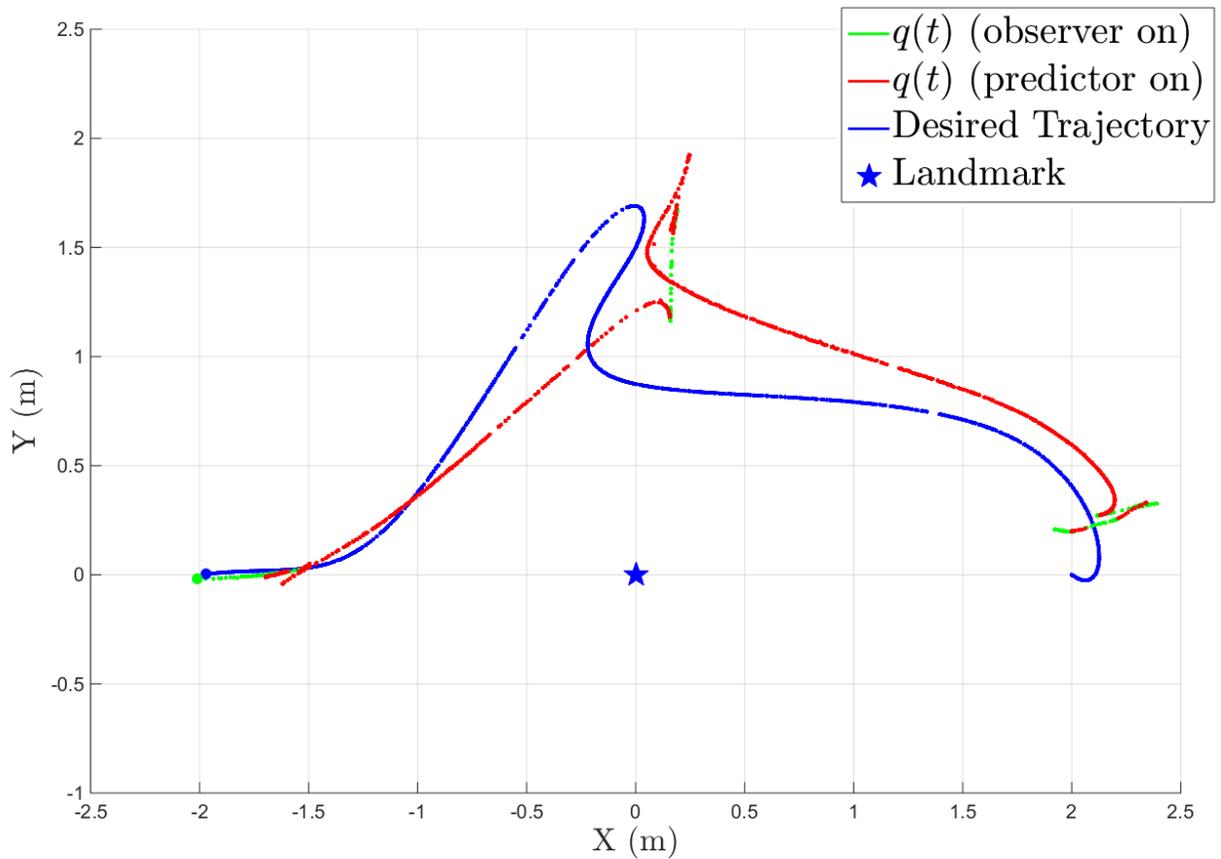
Figure 2-5. The trajectory tracking result. The green and red trajectories indicate whenever the observer and predictor are activated, respectively. When the predictor is active, the WMR diverges from the desired trajectory because of the disturbance. However, when the landmark returns to the FOV, the WMR adjusts its course to compensate for the accumulated error.
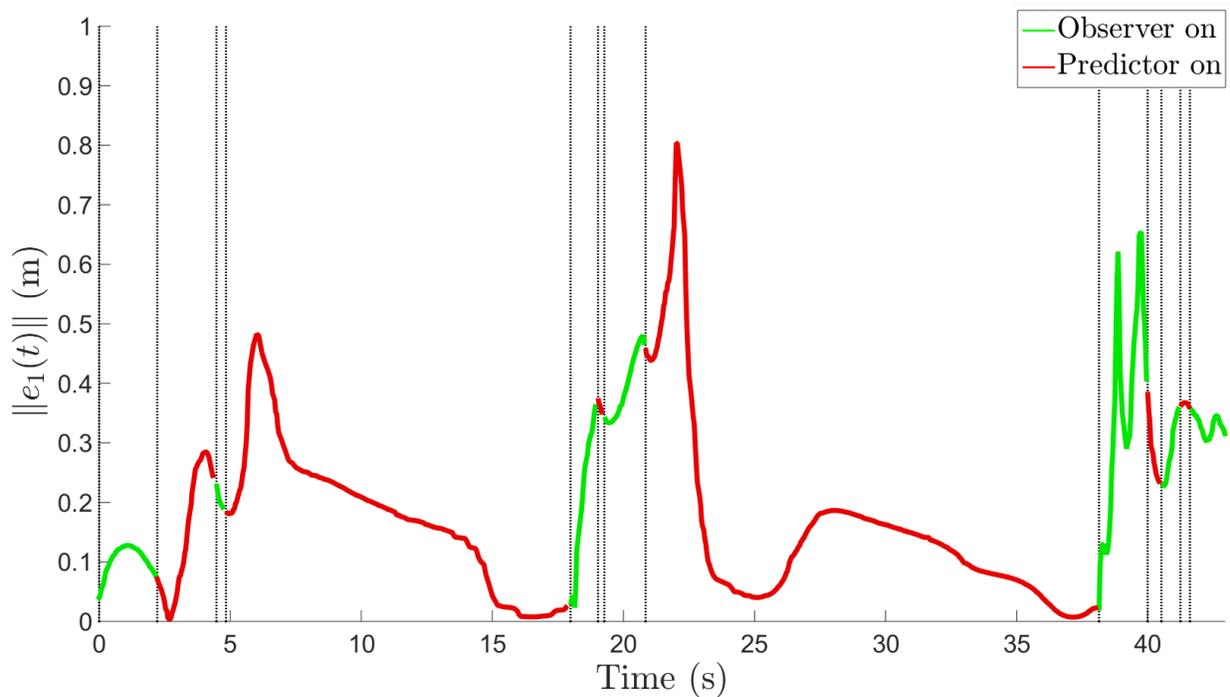
Figure 2-6. State estimate tracking error. During the periods of time between 5 to 18 seconds and 21 to 38 seconds, the estimate tracking error is regulated because the predictor update law propagates the state estimate using a model of the WMR. When the observer is active, the state estimate is regulated towards the true state, and hence, the estimate tracking error may increase.
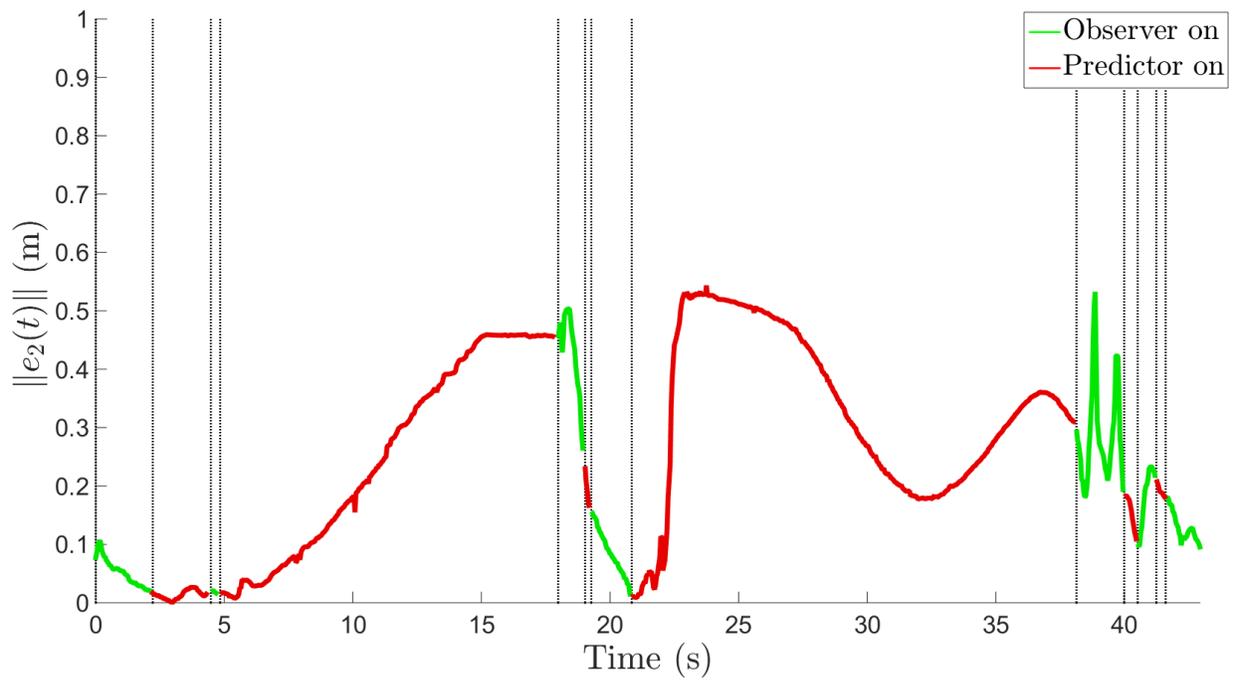
Figure 2-7. State estimation error. When the predictor is active for a prolonged period of time, the stability of the estimation error is not guaranteed. When the observer is active, estimation error is regulated.

CHAPTER 3
A SWITCHED SYSTEMS APPROACH TO PATH-FOLLOWING WITH INTERMITTENT STATE FEEDBACK

In this chapter, a novel control method is provided for a holonomic system that exhibits temporary loss of state feedback. Unlike the previous chapter, the problem considered in this chapter involves a desired (primary) trajectory completely outside the feedback region. Based on the development in [65], an observer is used while state feedback is available to reduce estimation error, and a predictor is utilized to propagate the estimates while state feedback is unavailable. Based on the resulting subsystems, maximum and minimum dwell time conditions are developed via a Lyapunov-based switched systems analysis to relax the constraint of maintaining constant feedback. The dwell times assist in designing a switching trajectory that ensures overall system stability while tracking a desired primary trajectory outside a feedback region. A scheme for designing a switching trajectory with smoother-step transition functions is provided, and simulation results are presented to demonstrate the performance of control design.

3.1 System Model

Consider a dynamic system subject to an exogenous disturbance as

$$\dot{x}(t) = f(x(t), t) + v(t) + d(t), \tag{3–1}$$

where $x(t), \dot{x}(t) \in \mathbb{R}^n$ denote a generalized state and its time derivative, $f : \mathbb{R}^n \times \mathbb{R} \to \mathbb{R}^n$ denotes the locally Lipschitz drift dynamics, $v(t) \in \mathbb{R}^n$ is the control input, and $d(t) \in \mathbb{R}^n$ is the exogenous disturbance where the Euclidean norm is bounded as $\|d(t)\| \leq \bar{d} \in \mathbb{R}_{\geq 0}$ with $n \in \mathbb{N}$ and $t \in \mathbb{R}_{\geq 0}$.

3.2 State Estimate and Control Objective

The overall objective is to achieve path following under intermittent loss of feedback. Specifically, a known feedback region is denoted as a closed set $\mathcal{F} \subset \mathbb{R}^n$, where the complement region where feedback is unavailable is denoted by $\mathcal{F}^c$. That is, feedback is available when $x(t) \in \mathcal{F}$ and unavailable when $x(t) \in \mathcal{F}^c$.

A desired path is denoted as $x_d \subset \mathcal{F}^c$. It is clear that state feedback is unavailable while attempting to follow x_d, and hence the system must return to the feedback region $\mathcal{F}$ intermittently to maintain stability. Therefore, a switching trajectory, denoted by $\bar{x}_d(t) \in \mathbb{R}^n$, is designed to overlay x_d while adhering to the subsequently developed dwell time constraints. To quantify the ability of the controller to track the switching trajectory, the tracking error $e(t) \in \mathbb{R}^n$ is defined as

$$e(t) \triangleq e_1(t) + e_2(t), \qquad (3\text{--}2)$$

where the estimate tracking error $e_1(t) \in \mathbb{R}^n$ is defined as

$$e_1(t) \triangleq \hat{x}(t) - \bar{x}_d(t), \qquad (3\text{--}3)$$

and the state estimation error $e_2(t) \in \mathbb{R}^n$ is defined as

$$e_2(t) \triangleq x(t) - \hat{x}(t), \qquad (3\text{--}4)$$

where $\hat{x}(t) \in \mathbb{R}^n$ is the state estimate.

Based on (3–3) and (3–4), the control objective is to ensure that $e_1(t)$ and $e_2(t)$ converge, and therefore $e(t)$ will converge. To facilitate the subsequent development, let the composite error vector be defined as $z(t) \triangleq \begin{bmatrix} e_1^T(t) & e_2^T(t) \end{bmatrix}^T$.

Assumption 3.1. The system is initialized in a feedback region.

3.3 Controller and Update Law Designs

To facilitate the subsequent analysis, two subsystems are defined to indicate when the states are inside or outside the feedback region. When $x(t) \in \mathcal{F}$, an exponentially stable observer can be designed using various approaches (e.g., observers such

as [58, 74, 75] could be used). The subsequent development is based on an observer update law designed as

$$\dot{\hat{x}}(t) = f(\hat{x}(t), t) + v(t) + v_r(t), \tag{3–5}$$

where $v_r(t) \in \mathbb{R}^n$ is a high-frequency sliding-mode term designed as [1]

$$v_r(t) = k_2 e_2(t) + \bar{d} sgn(e_2(t)), \tag{3–6}$$

where $k_2 \in \mathbb{R}^{n \times n}$ is a constant, positive definite gain matrix. When $x(t) \in \mathcal{F}^c$, the state estimate is updated by a predictor designed as

$$\dot{\hat{x}}(t) = f(\hat{x}(t), t) + v(t). \tag{3–7}$$

Since the state is required to transition between $\mathcal{F}$ and $\mathcal{F}^c$, a switched systems analysis is used to investigate the stability of the overall switched system. To facilitate this analysis, the error systems for $e_1(t)$ and $e_2(t)$ are expressed as

$$\dot{e}_1(t) = f_{1p}\left(\bar{x}_d(t), \hat{x}(t), t\right), \tag{3–8}$$

$$\dot{e}_2(t) = f_{2p}\left(x(t), \hat{x}(t), t\right), \tag{3–9}$$

where $f_{1p}, \ f_{2p} : \mathbb{R}^n \times \mathbb{R}^n \times \mathbb{R}_{\geq 0} \rightarrow \mathbb{R}^n, \ p \in \{a, u\}$, a is an index for subsystems with available feedback, and u is an index for subsystems when feedback is unavailable. Based on (3–8) and the subsequent stability analysis, the controller is designed as

---

[1] In cases where a piece wise-continuous controller is required, the robustifying term in (3–5) may be designed as $v_r(t) = k_2 e_2 + \frac{\bar{d}^2}{\epsilon} e_2$, where $\epsilon \in \mathbb{R}_{>0}$ is a design parameter.

$$v(t) = \begin{cases} \dot{\bar{x}}_d(t) - f(\hat{x}(t), t) - k_1 e_1(t) - v_r(t), & p = a, \\ \\ \dot{\bar{x}}_d(t) - f(\hat{x}(t), t) - k_1 e_1(t), & p = u, \end{cases} \qquad (3\text{--}10)$$

where $\dot{\bar{x}}_d(t) \in \mathbb{R}^n$, and $k_1 \in \mathbb{R}^{n \times n}$ is a constant, positive definite gain matrix. By taking the time derivative of (3–3) and substituting (3–5), (3–7) and (3–10) into the resulting expression, (3–8) can be expressed as

$$\dot{e}_1(t) = -k_1 e_1(t), \ \forall p. \qquad (3\text{--}11)$$

After taking the time derivative of (3–4) and substituting (3–1), (3–5) and (3–7) into the resulting expression, the family of systems in (3–9) can be expressed as

$$\dot{e}_2(t) = \begin{cases} f(x(t), t) - f(\hat{x}(t), t) + d(t) \\ \\ -\bar{d} sgn(e_2(t)) - k_2 e_2(t), & p = a, \\ \\ f(x(t), t) - f(\hat{x}(t), t) + d(t), & p = u. \end{cases} \qquad (3\text{--}12)$$

3.4   Stability Analysis

To further facilitate the analysis for the switched system, let $t_i^a \in \mathbb{R}_{\geq 0}$ denote the time of the ith instance when $x(t)$ transitions from $\mathcal{F}^c$ to $\mathcal{F}$, and $t_i^u \in \mathbb{R}_{>0}$ denote the time of the ith instance when $x(t)$ transitions from $\mathcal{F}$ to $\mathcal{F}^c$, for $i \in \mathbb{N}$. The dwell time in the ith activation of the subsystems a and u is defined as $\Delta t_i^a \triangleq t_i^u - t_i^a \in \mathbb{R}_{>0}$ and $\Delta t_i^u \triangleq t_{i+1}^a - t_i^u \in \mathbb{R}_{>0}$, respectively. By Assumption 3.2 subsystem a is activated when $t = 0$, and consequently $t_i^u > t_i^a, \ \forall i \in \mathbb{N}$.

Assumption 3.2. The system is initialized in a feedback region (i.e. $x(0) \in \mathcal{F}$).

To analyze the switched system, a common Lyapunov-like function is designed as

$$V_\sigma(z(t)) = V_1(e_1(t)) + V_2(e_2(t)), \qquad (3\text{--}13)$$

where the candidate Lyapunov functions for the tracking error and the estimation error are selected as

$$
\begin{aligned}
V_1(e_1(t)) &= \frac{1}{2}e_1^T(t)e_1(t), &\text{(3–14)}\\
V_2(e_2(t)) &= \frac{1}{2}e_2^T(t)e_2(t), &\text{(3–15)}
\end{aligned}
$$

respectively. The common Lyapunov-like function $V_\sigma(z(t))$ globally exponentially converges while $x(t) \in \mathcal{F}$ and exhibits an exponential growth when $x(t) \in \mathcal{F}^c$. Hence, a desired maximum bound V_M and a minimum threshold V_T on $V_\sigma(z(t))$ may be imposed such that $V_\sigma(z(t)) \leq V_M$ and $V_\sigma(z(t_i^u)) \leq V_T$. A representative illustration for the evolution of $V_\sigma(z(t))$ is shown in Figure 2-1. A lower threshold, V_T, enforces the convergence of $\|z(t)\|$ to an arbitrary small value. When implementing a high-frequency controller, V_T may be selected arbitrarily close to zero. However, the closer V_T is selected to zero, the longer $x(t)$ is required to remain in $\mathcal{F}$, and therefore the selection of V_T is dependent on the individual application tolerance. When a high-gain controller (e.g., $v_r(t) = k_2 e_2(t) + \frac{d^2}{\epsilon}e_2(t)$) is implemented, V_T should be selected such that $V_T \geq \epsilon$, where ϵ is a design parameter.

Theorem 3.1. *The composite error system trajectories of the switched system generated by the family of subsystems described by (3–11), (3–12), and a piece-wise constant, right continuous switching signal $\sigma : [0, \infty) \to p \in \{a, u\}$ are globally uniformly ultimately bounded provided the switching signal satisfies the minimum feedback availability dwell time condition*

$$
\Delta t_i^a \geq \frac{-1}{\lambda_s} \ln\left(\min\left(\frac{V_T}{V_\sigma(z(t_i^a))}, 1\right)\right) \tag{3–16}
$$

and the maximum loss of feedback dwell time condition

$$\Delta t_i^u \leq \frac{1}{\lambda_u} \ln \left(\frac{V_M + \frac{\bar{d}^2}{2\lambda_u}}{V_\sigma(z(t_i^u)) + \frac{\bar{d}^2}{2\lambda_u}} \right), \tag{3–17}$$

where λ_s and λ_u are subsequently defined known positive constants.

Proof. By taking the time derivative of (3–14) and substituting for (3–11) yields

$$\dot{V}_1(e_1(t)) \leq -2\underline{k}_1 V_1(e_1(t)), \; \forall t, \tag{3–18}$$

where $\underline{k}_1$ is the minimum eigenvalue of k_1. By using (3–12), the time derivative of (3–15) can be expressed as

$$\dot{V}_2(e_2(t)) \leq \begin{cases} -2(\underline{k}_2 - c)V_2(e_2(t)), & t \in [t_i^a, t_i^u), \\ \lambda_u V_2(e_2(t)) + \frac{1}{2}\bar{d}^2, & t \in [t_i^u, t_{i+1}^a), \end{cases} \tag{3–19}$$

where $c \in \mathbb{R}_{>0}$ is a Lipschitz constant, $\underline{k}_2 > c \in \mathbb{R}$ is the minimum eigenvalue of k_2, and $\lambda_u \triangleq 2c + 1 \in \mathbb{R}_{>0}$.

From (3–18) and (3–19), the time derivative of the common Lyapunov-like function can be expressed as

$$\dot{V}_\sigma(z(t)) \leq \begin{cases} -\lambda_s V_\sigma(z(t)), & t \in [t_i^a, t_i^u), \\ \lambda_u V_\sigma(z(t)) + \frac{1}{2}\bar{d}^2, & t \in [t_i^u, t_{i+1}^a), \end{cases} \quad \forall i \in \mathbb{N}, \tag{3–20}$$

where $\lambda_s = 2min\left(\underline{k}_1, (\underline{k}_2 - c)\right) \in \mathbb{R}_{>0}$. The solutions to (3–20) for the two subsystems are

$$V_\sigma(z(t)) \leq V_\sigma(z(t_i^a))e^{-\lambda_s\left(t - t_i^a\right)}, \; t \in [t_i^a, t_i^u), \tag{3–21}$$

$$V_\sigma(z(t)) \leq V_\sigma(z(t_i^u))e^{\lambda_u\left(t - t_i^u\right)}$$
$$- \frac{\bar{d}^2}{2\lambda_u}\left(1 - e^{\lambda_u\left(t - t_i^u\right)}\right), \; t \in [t_i^u, t_{i+1}^a). \tag{3–22}$$

The inequality in (3–21) indicates that $\|z(t)\| \leq \|z(t_i^a)\|e^{-\frac{1}{2}\lambda_s\left(t - t_i^a\right)}, \; t \in [t_i^a, t_i^u)$. The minimum threshold V_T is selected to enforce the convergence of $\|z(t)\|$ to desired

threshold before allowing $x(t)$ to transition into $\mathcal{F}^c$. This condition can be expressed as $V_\sigma(z(t_i^a))e^{-\lambda_s \Delta t_i^a} \leq V_T$, and therefore the condition in (3–16) is obtained after algebraic manipulation. If $\frac{V_T}{V_\sigma(t_i^a)} > 1$, the value of $V_\sigma(t_i^a)$ is already below the threshold and thus no minimum dwell time is required for the subsystem.

When $t \in [t_i^u, t_{i+1}^a)$, the inequality in (3–22) indicates that $\|z\| \leq \sqrt{\|z(t_i^u)\|^2 e^{\lambda_u (t - t_i^u)} - \frac{\bar{d}^2}{2\lambda_u} \left(1 - e^{\lambda_u \left(t - t_i^u\right)}\right)}$, and hence, the maximum bound V_M is selected to limit the growth of errors, where $V_M > V_T$. The maximum dwell time condition for each of the ith unstable periods is expressed as $V_\sigma(z(t_i^u))e^{\lambda_u \Delta t_i^u} - \frac{\bar{d}^2}{2\lambda_u} \left(1 - e^{\lambda_u \Delta t_i^u}\right) \leq V_M$, and therefore the condition in (3–17) can be obtained.

Therefore, the composite error system trajectories generated by (3–11) and (3–12) are globally uniformly ultimately bounded. $\qquad\qquad\qquad\qquad\qquad\qquad\qquad\qquad\qquad\square$

Remark 3.1. When using single integrator dynamics, $\dot{x}(t) = u + d(t)$, the resulting estimation error dynamics for the unstable subsystem is $\|\dot{e}_2(t)\| \leq \bar{d}$, and the corresponding Lyapunov-like function derivative is $\dot{V}_\sigma(t) \leq \bar{d}\|e_2(t)\|$. By solving the ordinary differential equation for $\dot{e}_2(t)$, the estimation error $e_2(t)$ exhibits a linear growth that can be bounded as $e_2(t) \leq e_2(t_i^u) + \bar{d}(t - t_i^u)$. After substituting in the linear bound on $e_2(t)$, it follows that $\dot{V}_\sigma(t) \leq \bar{d}\|e_2(t_i^u)\| + \bar{d}^2(t - t_i^u)$, and solving the ordinary differential equation yields $V_\sigma(t) \leq \frac{1}{2}\bar{d}^2 (t - t_i^u)^2 + \bar{d}\|e_2(t_i^u)\| (t - t_i^u) + V_\sigma(z(t_i^u))$. After imposing $V_\sigma(t) \leq V_M$ as the upper bound constraint, the maximum dwell time can be derived by solving the quadratic equation and taking the positive root as

$$\Delta t_i^u \leq \frac{\left(\sqrt{\|e_2(t_i^u)\|^2 - 2\left(V_\sigma(z(t_i^u)) - V_M\right)} - \|e_2(t_i^u)\|\right)}{\bar{d}}.$$

3.5 Switching Trajectory Design

Since x_d lies outside the feedback region, i.e. $x_d \subset \mathcal{F}^c$, $\forall t$, and cannot be followed for all time, the switching trajectory $\bar{x}_d(t)$ is designed to enable $x(t)$ to follow x_d to the extent possible given the dwell time conditions in (3–16) and (3–17). A design challenge

for $\bar{x}_d(t)$ is to ensure $x(t)$ re-enters $\mathcal{F}$ to satisfy the sufficient condition in (3–17). While $x(t)$ transitions through $\mathcal{F}^c$, $e(t)$ may grow as indicated by (3–22), and this growth must be accounted for when designing $\bar{x}_d(t)$. To facilitate the development of the switching trajectory $\bar{x}_d(t)$, $x_b(t) \in \mathbb{R}^n$ is defined as the closest orthogonal projection of $\bar{x}_d(t)$ on the boundary of $\mathcal{F}$.

When the maximum dwell time condition is reached, $\|e(t)\| \leq 2\sqrt{V_M}$. This bound implies there exist a set $\mathcal{B} = \left\{ y \in \mathbb{R}^n | \|y - \bar{x}_d(t)\| \leq 2\sqrt{V_M} \right\}$ such that $x(t) \in \mathcal{B}$, $\forall t$. Therefore, the switching trajectory must penetrate a sufficient distance into $\mathcal{F}$ to compensate for the error accumulation. The distance to compensate for error growth motivates the design of a cushion that ensures the re-entry of the actual states when the maximum dwell time is reached. To compensate for the potential accumulation of error, $\bar{x}_d(t)$ must penetrate a sufficient distance into $\mathcal{F}$, motivating the design of a cushion state $x_\epsilon(t) \in \mathbb{R}^n$ as

$$x_\epsilon(t) \triangleq x_b(t) + \Phi(t),$$

where $\Phi(t) \in \mathbb{R}^n$, such that $\|\Phi(t)\| \geq 2\sqrt{V_M}$ and there exist a compact set $\mathcal{A} = \left\{ y \in \mathbb{R}^n | \|y - x_\epsilon(t)\| \leq \|\Phi(t)\| \right\}$ such that $\mathcal{A}$ is less than or equal to the inscribed ball of $\mathcal{F}$ in $\mathbb{R}^n$. Therefore, the requirement of $x(t) \in \mathcal{B} \subseteq \mathcal{A} \subseteq \mathcal{F}$ can be satisfied if $x_\sigma(t)$ coincides with $x_\epsilon(t)$ when the maximum dwell-time is reached.

An example switching trajectory $\bar{x}_d(t)$ can be developed utilizing a smoother-step function described in [76] to transition smoothly between x_d and $x_\epsilon(t)$ while meeting the dwell time conditions (see Remark 3.2). The smoother-step function is defined in [76] as

$$S(\rho) = 6\rho^5 - 15\rho^4 + 10\rho^3 \qquad (3\text{–}23)$$

where $\rho \in [0, 1]$ is the input parameter. Given the transition function in (3–23), the switching trajectory is designed as

$$\bar{x}_d(t) \triangleq \begin{cases} H\Big(S(\rho_i^a), x_b(t), x_\epsilon(t)\Big), & t_i^a \leq t < t_i^u, \\ H\Big(S(\rho_i^{u1}), g\left(x_d, t\right), x_b(t)\Big), & t_i^u \leq t < t_i^{u1}, \\ H\Big(S(\rho_i^{u2}), g\left(x_d, t\right), g\left(x_d, t\right)\Big), & t_i^{u1} \leq t < t_i^{u2}, \\ H\Big(S(\rho_i^{u3}), x_\epsilon(t), g\left(x_d, t\right)\Big), & t_i^{u2} \leq t < t_i^{u3}, \end{cases}$$ (3–24)

where $H\left(S(\cdot), q\left(t\right), r\left(t\right)\right) \triangleq S(\cdot)q\left(t\right) + \left[1 - S(\cdot)\right] r\left(t\right)$ for $q(t),\ r(t) \in \mathbb{R}^n$, $g : x_d \times \mathbb{R} \to \mathbb{R}^n$ gives the desired state on x_d at time t, ρ_i^a, ρ_i^{u1} ρ_i^{u2}, and ρ_i^{u3} are designed as $\rho_i^a \triangleq \frac{t - t_i^a}{\Delta t_i^a}$ and $\rho_i^{uj+1} \triangleq \frac{t - \left(t_i^u + \sum_{k=0}^j p_k \Delta t_i^u\right)}{p_{j+1} \Delta t_i^u}$, $j \in \{0, 1, 2\}$, the weights used to partition the maximum dwell time are denoted by $p_k \in [0, 1)$, and the corresponding partitions are denoted by t_i^{uj+1}. The final partition, t_i^{u3}, coincides with t_{i+1}^a. To avoid a singularity in ρ_i^a and to ensure a smooth and continuous switching trajectory, Δt_i^a must be arbitrarily lower bounded above zero (see Remark 3.3).

Remark 3.2. Other trajectories satisfying the dwell time conditions in Theorem 3.1 may also be implemented, such as the work in [59].

Remark 3.3. Lower bounding Δt_i^a by an arbitrary value, $\alpha \in \mathbb{R}_{>0}$, does not violate Theorem 3.1 since the system is allowed to remain in the feedback region longer than the minimum dwell time, implying that $\Delta t_i^a \leq \alpha \leq (t - t_i^a)$ holds. Other trajectory designs may not require Δt_i^a to be lower bounded.

3.6 Simulation

A simulation is performed to illustrate the performance of the controller given intermittent loss of state feedback. Based on the system model given in (3–1), $f(x(t), t)$ is selected as $f(x(t), t) = Ax$ where $A = 0.5I_3$, and $d(t)$ is drawn from a uniform distribution between $[0,\ 0.06]$ meters per second. The initial states and estimates are selected as $x(0) = \begin{bmatrix} 0.1\text{m} & 0.2\text{m} & 0\text{rads} \end{bmatrix}$ and $\hat{x}(0) = \begin{bmatrix} 0.2\text{m} & 0.3\text{m} & \frac{\pi}{6}\text{rads} \end{bmatrix}$. The observer and the controller gains were selected as $k_1 = 3I_3$ and $k_2 = 3I_3$, respectively. The desired upper bound and lower threshold for the composite error

$\|z(t)\|$ are selected as 0.9 and 0.02 meters, respectively. Based on the desired error bound and threshold, the Lyapunov function bound and threshold are determined as $V_M = 0.2025$ and $V_T = 1 \times 10^{-4}$.

The desired path x_d is selected as a circular trajectory with a radius of 2 meters centered at the origin. The boundary of the feedback region is selected as a circle with a 1-meter radius about the origin. The switching trajectory $\bar{x}_d(t)$ were designed as described in Section 3.5 and follows x_d at $\frac{\pi}{5}$ radians per second, where the partition weights are selected as $p_0 = 0, \quad p_1 = 0.3, \quad p_2 = 0.4, \quad p_3 = 0.3$.

Figure 3-1 depicts the agent's planar trajectory and shows that when the agent was inside the region with state feedback, both the estimation and tracking errors, $\|e_1(t)\|$ and $\|e_2(t)\|$, exponentially converged. When the agent was outside the feedback region, the tracking error converged while the predictor error exhibited exponential divergence.

The average maximum and minimum dwell times between switches are 2.16 and 0.26 seconds, respectively. Based on the simulation result, the system is allowed to remain 8.23 times longer outside the feedback region than inside on average. Furthermore, 40% of the maximum dwell time is dedicated to following the desired path, which translates to 36% of the combined duration of the maximum and minimum dwell times per cycle.

In Figure 3-2, the composite error $\|z(t)\|$ is shown. Figure 3-2 indicates that $\|z(t)\|$ remained below 0.9 meters for all time and less than or equal to 0.02 (indicated by the black dashed line) by the end of each stable period, which demonstrates the robustness of the presented control design under the dwell time condition constraints and disturbances. Since an exact model of the system was used in this simulation, the resulting tracking error is bounded well below the maximum bound, and hence emphasizing the conservative nature of the Lyapunov analysis method.
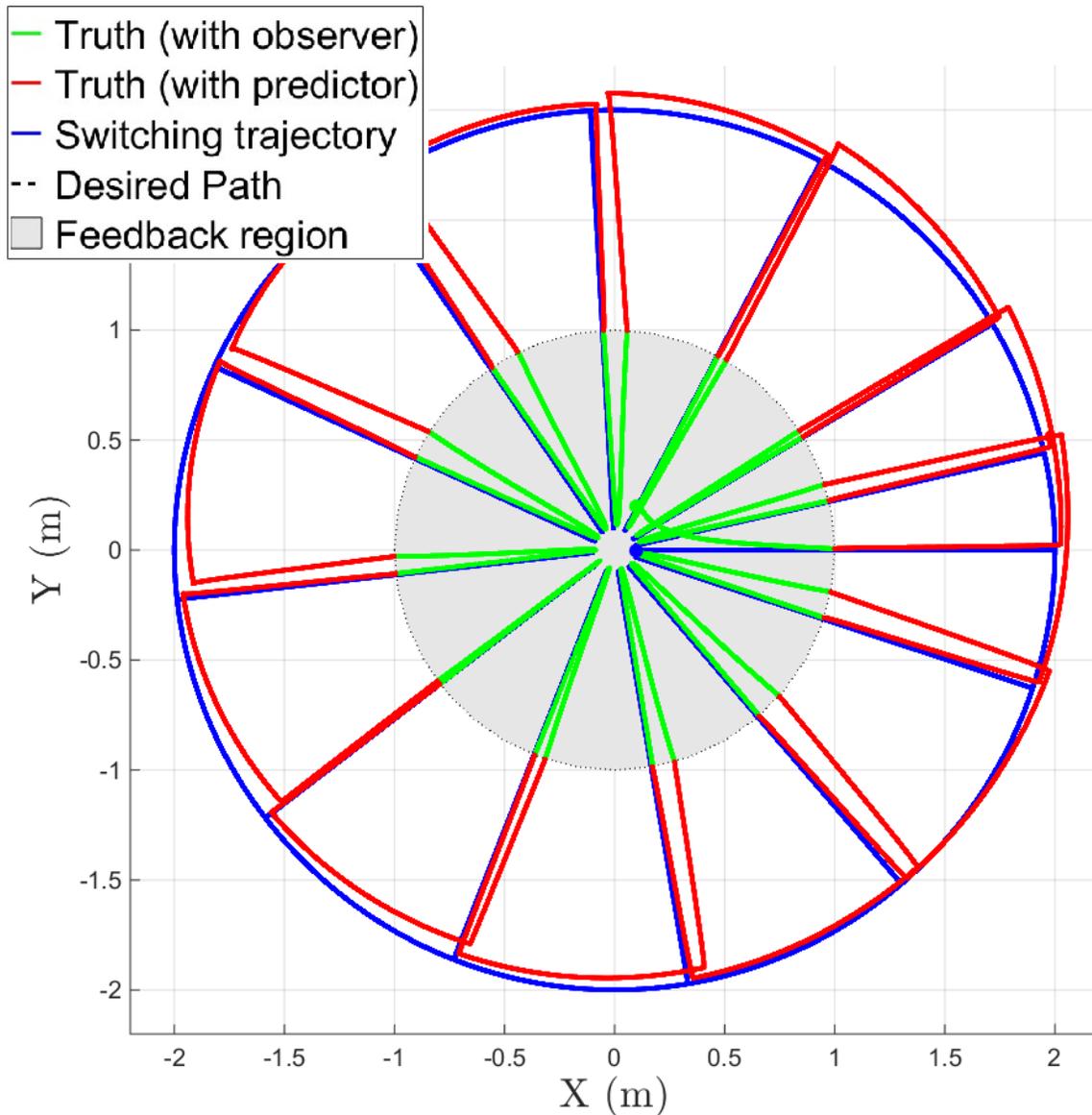
Figure 3-1. Simulation result for 30 seconds. Both system state $x(t)$ and switching trajectory $\bar{x}_d(t)$ are initialized in the feedback region (gray). During the minimum dwell time, $x(t)$ converges to $\bar{x}_d(t)$ exponentially with the observer activated. When $x(t)$ transitions into the feedback-denied region (white), the predictor is activated, and $x(t)$ gradually diverges from $\bar{x}_d(t)$ due to disturbances. Before the maximum dwell time is reached, $x(t)$ re-enters the feedback region and the observer is re-activated. Hence, $x(t)$ is able to converge to $\bar{x}_d(t)$.
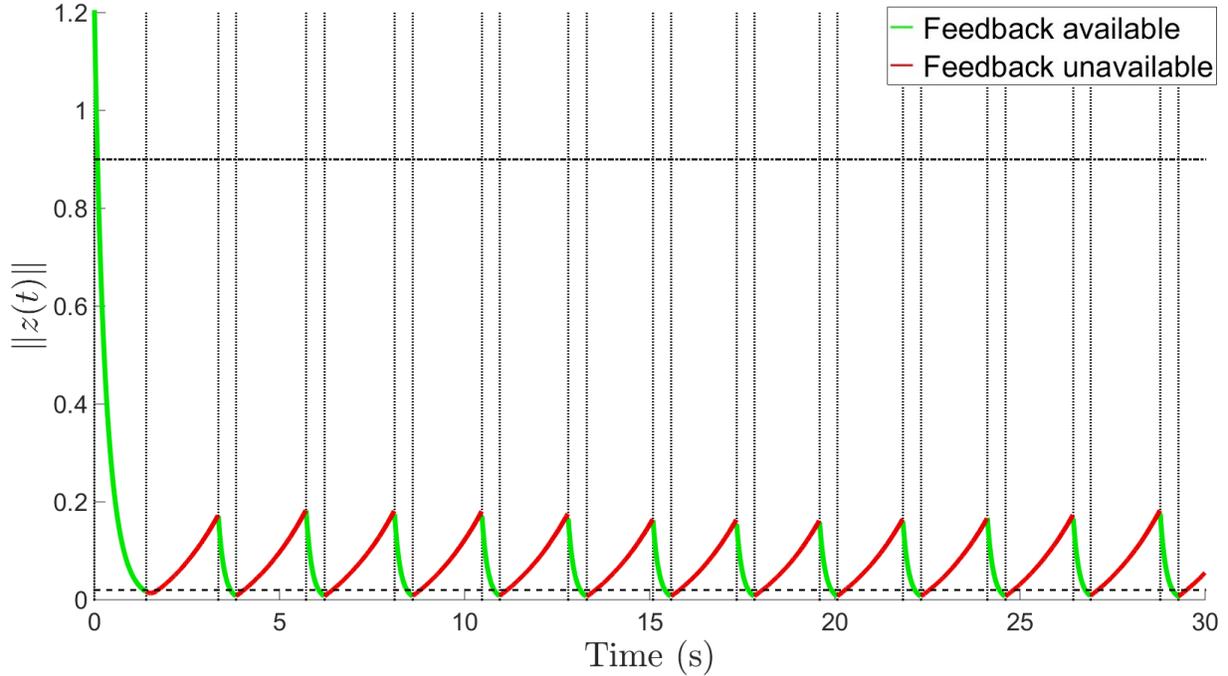
Figure 3-2. Evolution of $\|z(t)\|$. The top dashed line denotes V_M and the bottom dashed line denotes V_T.

3.7 Experimental Results

In Section 3.7, an experiment is performed to verify the theoretical results where a single integrator dynamic is used instead of the exact system model. The overall goal of the experiment is to represent a scenario where an unmanned air vehicle is tasked with following a path where feedback is not available (e.g., inside an urban canyon). Specifically, the objective is to demonstrate the boundedness of the tracking error $e(t)$ through multiple cycles of switching between the feedback-available and unavailable regions based on the dwell time constraints established in Section 3.4. A Parrot Bebop 2.0 quadcopter is used as the unmanned air vehicle. The quadcopter is equipped with a 3-axis gyroscope, a 3-axis accelerometer, an ultrasound sensor, and an optical-flow sensor. The on-board sensors provide an estimate of the linear and angular velocities of the quadcopter at 5Hz. To control the quadcopter, the *bebop_autonomy* package developed by [77] is utilized to send velocity commands generated from an off-board computer running Robotic Operating System (ROS) Kinetic in Ubuntu 16.04. The

48

communication link between the computer and the quadcopter is established through a WiFi channel at 5GHz.

A NaturalPoint, Inc. OptiTrack motion capture system is used to simulate a feedback signal and record the ground truth pose of the quadcopter at a rate of 120Hz. While the quadcopter is inside the feedback region, pose information from the motion capture system is directly used as feedback in the controller and update laws designed in Section 3.3. When the quadcopter operated outside of the feedback region, the pose feedback is discarded. During these times, the on-board velocity measurements are used to feed-forward the state estimate. Although the OptiTrack system continue to record the pose of the quadcopter, the pose information is only used as ground truth for illustration purposes.

Utilizing the motion capture system, a circular region of available feedback is centered at the origin of the Euclidean world frame with a radius of 1 meter. Since torque level control authority is not available, single integrator dynamics, $\dot{q}(t) = u(t) + d(t)$, are assumed for the quadcopter where $q(t) = \begin{bmatrix} x(t) & y(t) & z(t) & \alpha(t) \end{bmatrix}^T$, and $x(t),\ y(t),\ z(t),\ \alpha(t) \in \mathbb{R}$ are the 3-D Euclidean coordinates and yaw rotation of the quadcopter with respect to the inertial frame. The disturbance is assumed to be upper bounded as $\bar{d} = 0.035$. To compensate for the disturbance, a high-gain robust controller is implemented to ensure a continuous control command. The controller and update law gains are selected as $k_1 = 0.4I_4,\ k_2 = 0.6I_4,$ and $\epsilon = 0.1$. To regulate and match the actual velocity output to the control command, a low level PID controller is implemented.

The desired upper bound and lower threshold on $\|z(t)\|$ are selected as 0.9 and 0.14 meters, respectively. Since single integrator dynamics are assumed for the quadcopter dynamic, a less conservative minimum dwell time condition can be derived (details are given in Remark 3.1). The desired path is defined as a circular path centered at the origin with a radius of 1.5 meters as depicted by Figure 3-3. Following the design method outlined in Section 3.5, a switching trajectory is designed to follow

49

x_d with an angular velocity of $\frac{\pi}{15}$ radians per second. To prevent the quadcopter from drifting out of the feedback region prematurely, a intermediate trajectory is design to be $x_{int}(t) = 0.7x_b(t)$ to replace $x_b(t)$ in (3–24) as a safety measure. The partitions for the maximum dwell time are selected as $p_0 = 0,\ p_1 = 0.4,\ p_2 = 0.2,\ p_3 = 0.4$.

Initially, the quadcopter is launched inside $\mathcal{F}$ along with the switching trajectory, which transitions between $\mathcal{F}$ and x_d over the prescribed time span. The experimental results demonstrate that the quadcopter is capable of intermittently leaving $\mathcal{F}$ to follow x_d for some period of time and then return to $\mathcal{F}$ consistently. The supplementary video accompanying [65], available for viewing at https://www.youtube.com/user/NCRatUF, gives a recording of the experiment with the motion of the quadcopter and the switching trajectory projected on the floor. The overall path following plot, including the desired path, switching trajectory and actual states, is shown in Figure 3-4, where a total of 8 cycles of leaving and re-entering $\mathcal{F}$ occurred. During the periods when the quadcopter is outside the feedback region, large odometry drifts are apparent and the actual tracking error diverges as the dynamic models in Section 3.4 indicate. Table 3-1 indicates the maximum and minimum dwell times for each cycle. On average, the quadcopter was allowed to reside approximately 6 times longer in $\mathcal{F}^c$ than $\mathcal{F}$, and 20% of which is dedicated to following x_d. Specifically, the quadcopter is allowed 19.85 seconds in $\mathcal{F}^c$ and is required to remain in $\mathcal{F}$ for 3.31 seconds on average. Based on the partition weights of the maximum dwell time, Table 3-2 describes the partitions and the duration for each partition. During partition 1, $\bar{x}_d(t)$ transitions from the $x_b(t)$ to x_d where the partition weight was set to 50%. The relatively large partition allots more time in transition to yield a slower velocity profile, which produces less overshoot in the tracking performance. The distance between x_d and $\mathcal{F}$ is also a major factor in distributing partition weights in the sense that the closer x_d is to $\mathcal{F}$, the less time is required for transition and more time can be allocated to follow x_d.
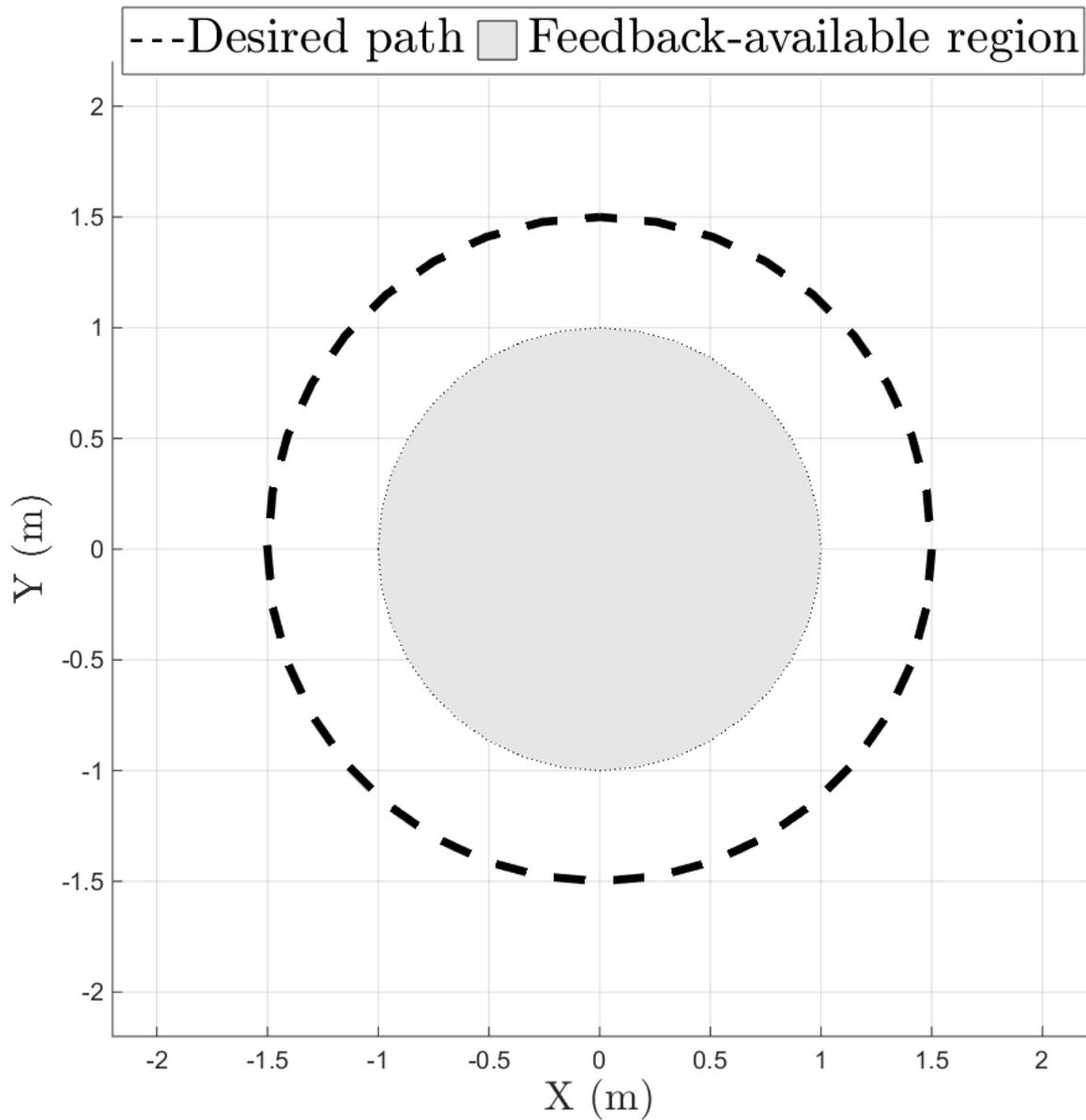
Figure 3-3. A representation of the feedback-available region and the desired path. The gray region denotes the feedback-available region, which is 1.0 meter in radius, and the black dotted line denotes x_d, which is a circular path with a radius of 1.5 meters.
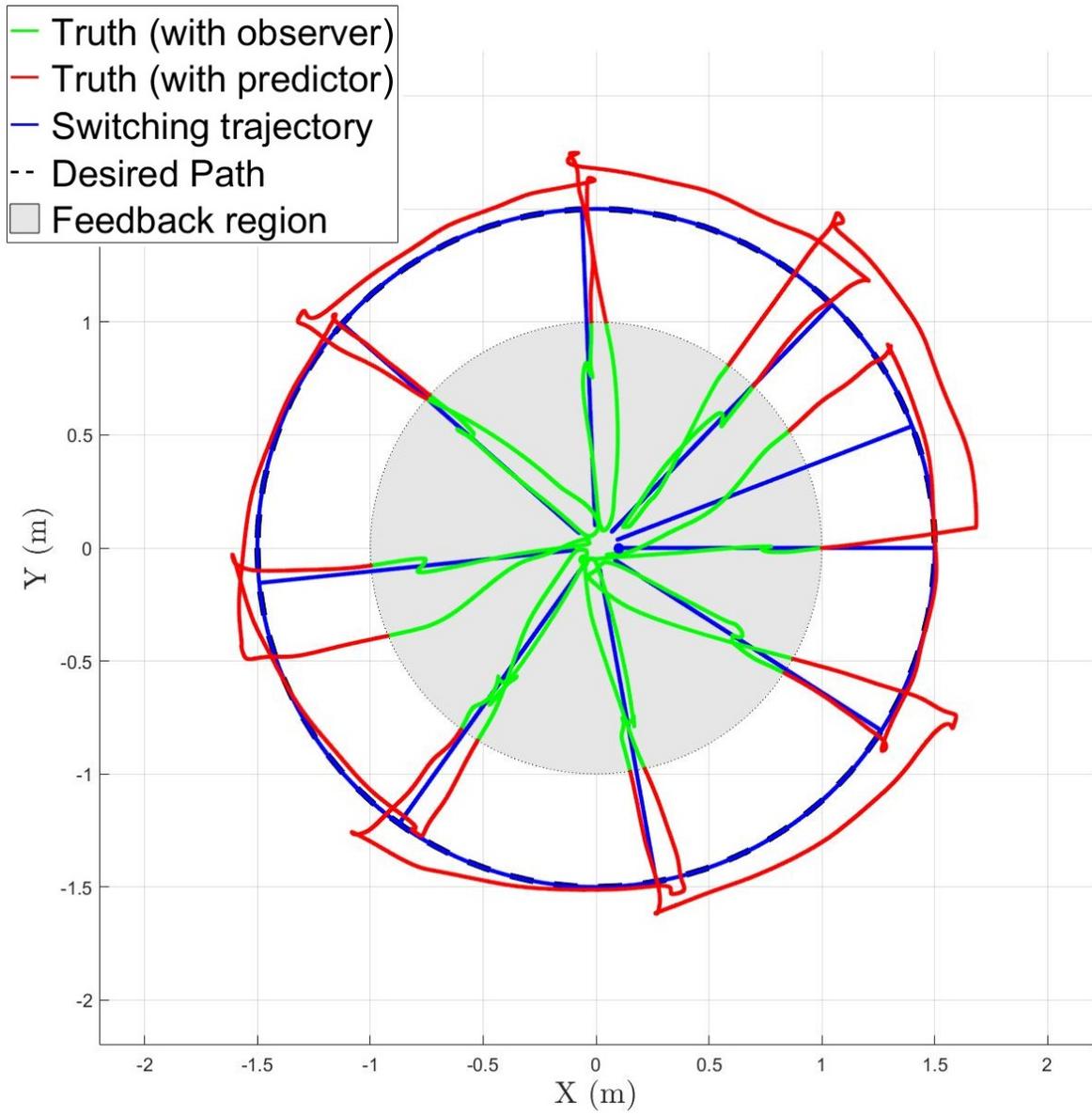
Figure 3-4. Actual and switching trajectory over 185 seconds.

Table 3-1. Minimum and Maximum Dwell Times.

Cycle	Max. D. T. (s)	Min. D. T. (s)
0	-	3.50
1	19.12	4.55
2	19.38	4.09
3	19.25	3.20
4	19.72	3.34
5	20.21	1.67
6	19.08	2.55
7	19.65	3.73
8	22.35	3.16
Avg	19.85	3.31

Table 3-2. Maximum Dwell Time Partitions.

Cycle	Maximum dwell times (s)		
	Part. 1 (40%)	Part. 2 (20%)	Part. 3 (40%)
1	7.65	3.82	7.65
2	7.75	3.88	7.75
3	7.70	3.85	7.70
4	7.89	3.94	7.89
5	8.08	4.04	8.08
6	7.63	3.82	7.63
7	7.86	3.93	7.86
8	8.94	4.47	8.94

To illustrate the stability of the controller, the Euclidean norm of the estimate tracking error, $e_1(t)$, and the estimation error, $e_2(t)$, are displayed in Figure 3-5 and 3-6. The estimate tracking error exponentially converges, reflecting the analysis in (3–18). The estimation error exhibits growth when $x(t) \in \mathcal{F}^c$. For a better illustration, the norm of the composite and actual tracking error are shown in Figure 3-7 and 3-8, respectively, where the dwell time duration is indicated by vertical dash-dot lines and the upper bound and lower threshold on the actual tracking error are indicated by horizontal dashed lines. Over the 8 cycles, $\|z(t)\|$ is upper bounded by 0.9 meters at all times, and converges to below 0.14 meters within the minimum dwell time when $x(t) \in \mathcal{F}$. The plots also indicate that $x(t)$ is able to return to $\mathcal{F}$ within the maximum dwell times. This can be verified by the activation of the observer before the maximum dwell time is reached for every cycle. In Figure 3-9, the evolution of V_σ is shown along with the calculated V_M and V_T as indicated by the horizontal dashed lines. As expected, the Lyapunov-like function V_σ is upper bounded below V_M for all times and converges below V_T within the minimum dwell times. Based on Figure 3-8 and 3-9, the controller and update laws developed in Section 3.3 demonstrate robustness towards disturbances and a simple assumed dynamic model. Hence, the trajectory design scheme provided in Section 3.5 is able to generate a switching signal $\sigma(t)$ that satisfied the dwell time conditions developed in Section 3.4 and, therefore, verifying the claim in Theorem 3.1.

3.8 Summary

A novel method that utilizes a switched systems approach to ensure path following stability under intermittent state feedback is presented. The developed method relieves the requirement of state feedback at all times. State estimates are used in the tracking control to compensate for the intermittence of state feedback. A Lyapunov-based, switched systems analysis is used to develop maximum and minimum dwell time conditions to guarantee stability of the overall system. The dwell time conditions allow the desired path to be completely outside of the feedback region, and a switching
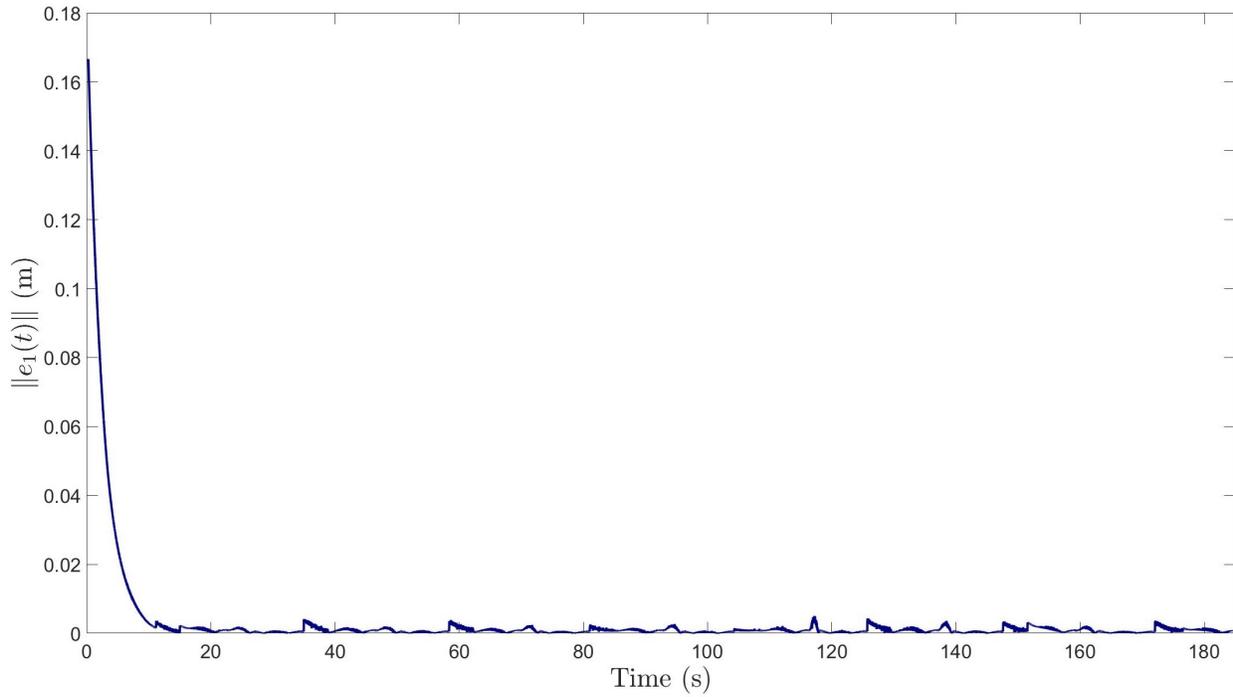
Figure 3-5. Estimate tracking error $\|e_1(t)\|$. As indicated by the analysis, the estimate tracking error exhibits exponential stability regardless of feedback availability.
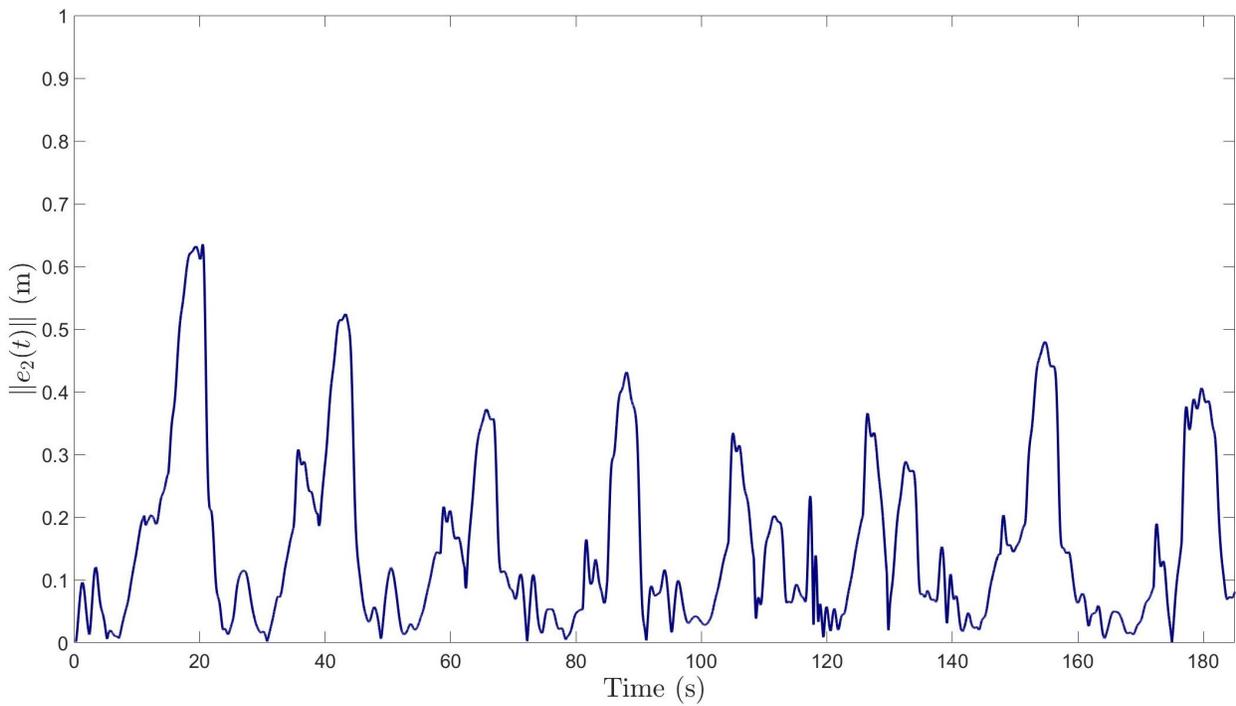
Figure 3-6. Estimation error $\|e_2(t)\|$. As indicated by the analysis, the estimation error converges when $x(t) \in \mathcal{F}$ and diverges when $x(t) \in \mathcal{F}^c$.
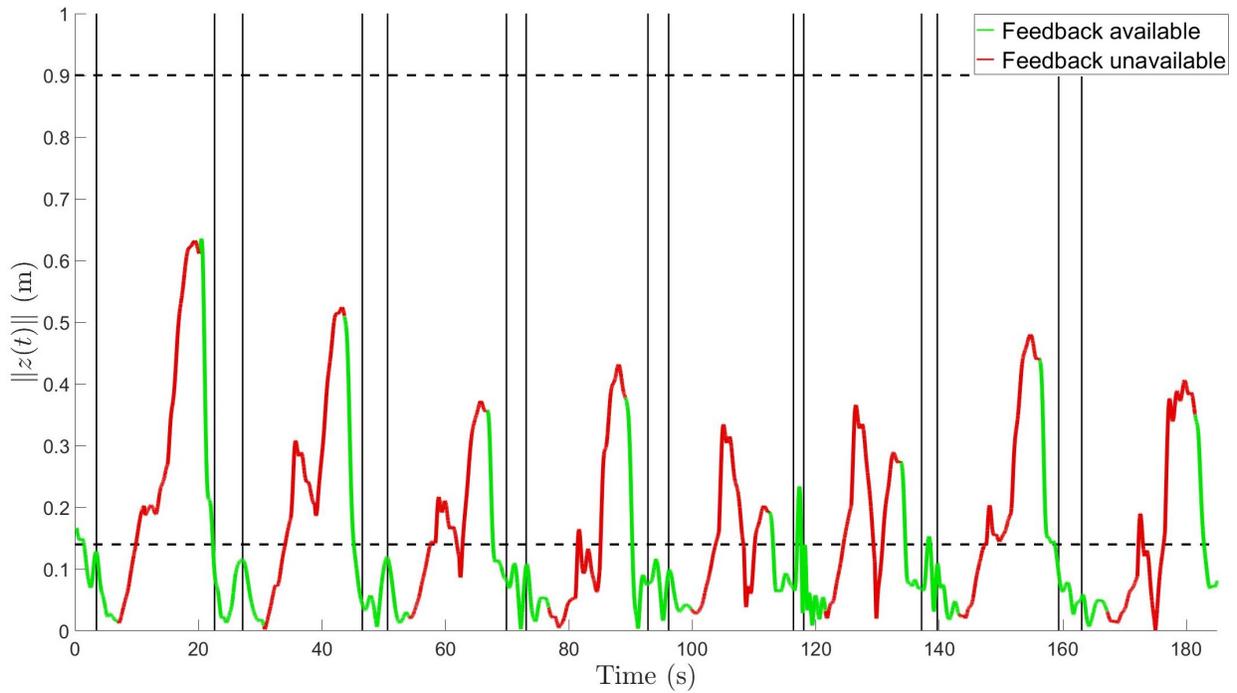
Figure 3-7. Evolution of $\|z(t)\|$. The dash-dot (vertical) lines indicate the switching interface of minimum and maximum dwell times, and the dashed (horizontal) lines indicate the prescribed upper bound and lower threshold.
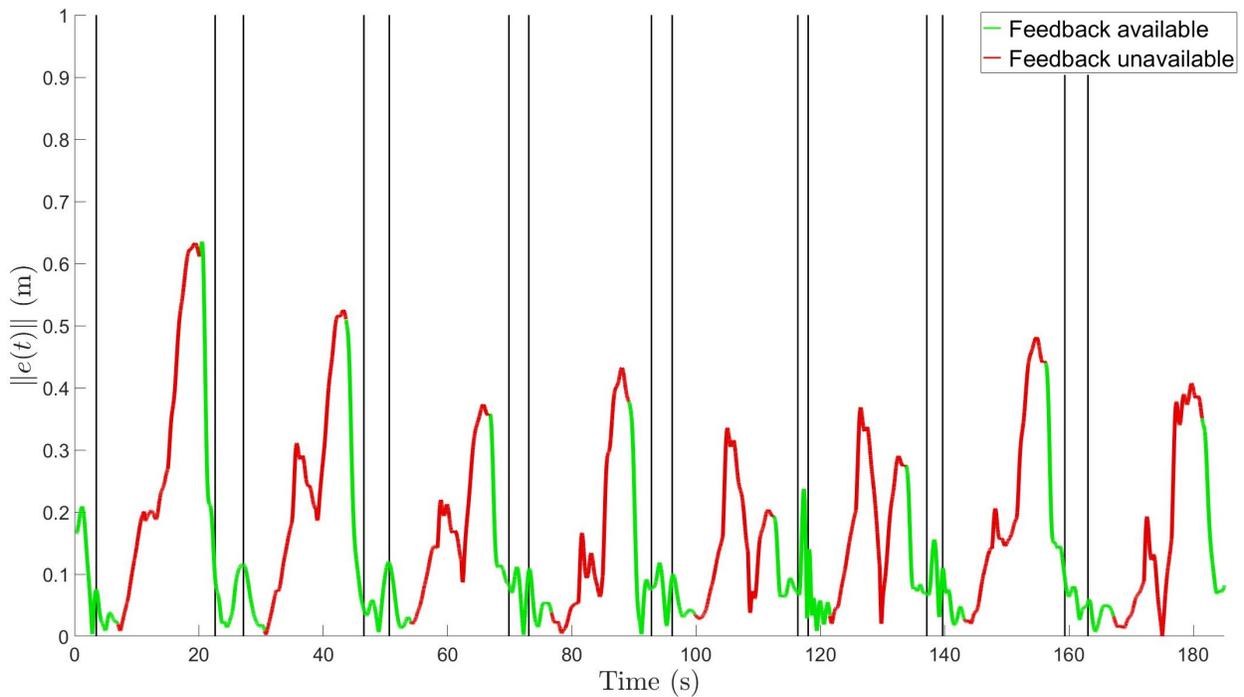
Figure 3-8. Actual tracking error $\|e(t)\|$. The dash-dot lines indicate the switching interface of minimum and maximum dwell times.
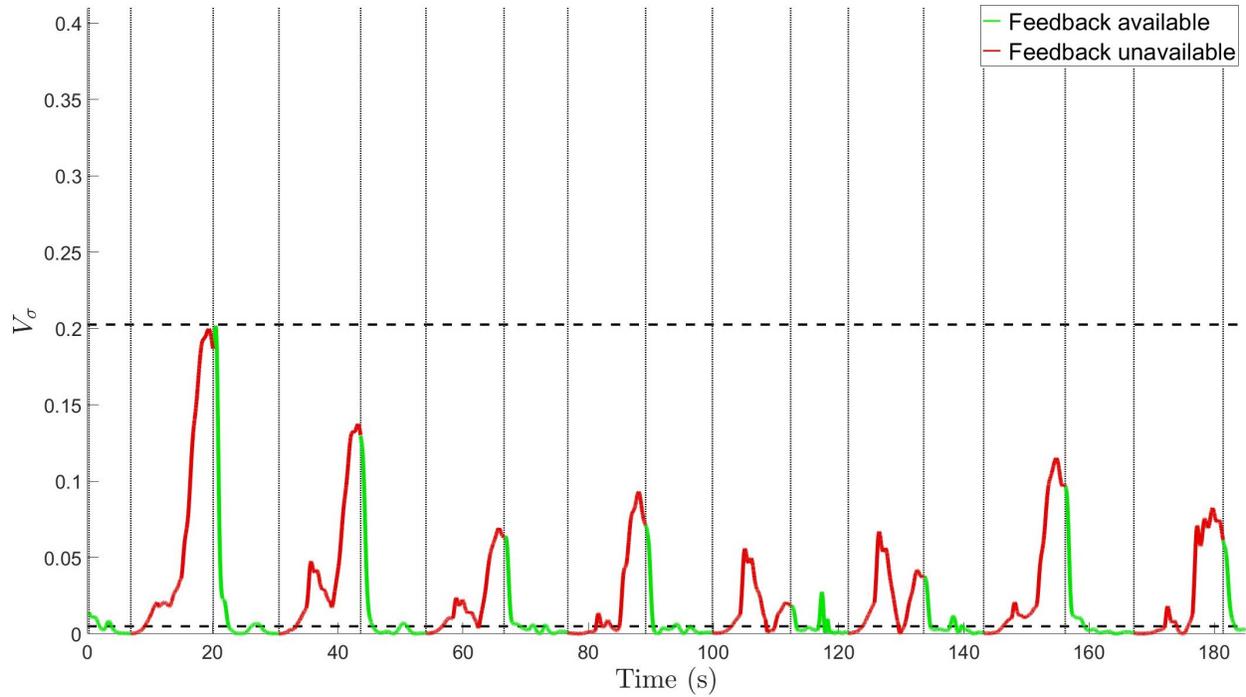
Figure 3-9. Evolution of $V_\sigma(t)$. The dotted (vertical) lines indicate the time instants when the quadcopter crossed the feedback region boundary. The dashed (horizontal) lines indicate the prescribed V_M and V_T for V_σ.

trajectory is designed to bring the states back into the feedback region before the error growth exceeds a defined threshold. The candidate switching trajectory switches between the desired path and the feedback region using smoother-step transition functions. A simulation and an experiment were performed to illustrate the robustness of the control and trajectory design. Future research will focus on development of an approximate optimal control approach using adaptive dynamic programming concepts to yield approximately optimal results.

CHAPTER 4
A GENERALIZED FRAMEWORK FOR SYSTEMS TO INTERMITTENTLY OPERATE IN A FEEDBACK-DENIED ENVIRONMENT

This chapter focuses on a generalized switched systems framework for path-following with intermittent state feedback. The analytical approach in previous chapters places constraints in the controller and update law designs, and upon closer examination, a more generalized approach is explained in this chapter. In addition, analysis under this approach may support the extension of this framework to include the use of true states in the controller or reset maps when the system is inside a feedback-available region, which are not admissible in the previous chapters.

4.1   System Model

Extending from Chapter 3, consider a nonlinear dynamic system subjected to an exogenous disturbance as described in (3–1), where $x(t)$, $\dot{x}(t) \in \mathbb{R}^n$ denote a generalized state and its time derivative, $f : \mathbb{R}^n \times \mathbb{R} \to \mathbb{R}^n$ denotes the locally Lipschitz dynamics, $v(x(t), t) \in \mathbb{R}^n$ is the control input, and $d(t) \in \mathbb{R}^n$ is a bounded exogenous disturbance, where $\|d(t)\| \leq \bar{d} \in \mathbb{R}_{>0}$ with $n \in \mathbb{N}$ and $t \in \mathbb{R}_{\geq 0}$.

4.2   State Estimation and Control Objective

The objective is to enable an agent to follow a desired path, denoted by x_d, that lies completely outside of a region where feedback is available. Similar to Chapter 3, the feedback-available and -denied regions are denoted by $\mathcal{F} \subset \mathbb{R}^n$ and $\mathcal{F}^c \subset \mathbb{R}^n$, respectively. Since the agent is required to intermittently depart from following x_d to obtain feedback, an auxiliary trajectory, denoted by $x_\sigma(t) \in \mathbb{R}^n$, is developed to guide the agent between $\mathcal{F}$ and x_d. The design of $x_\sigma(t)$ is motivated by the desire to maximize the time $x(t)$ follows x_d, while adhering to subsequently developed dwell-time conditions. However, in contrast to Chapter 3, three error systems are defined as

$$e(t) \triangleq x(t) - x_\sigma(t), \tag{4–1}$$

$$\hat{e}(t) \triangleq \hat{x}(t) - x_\sigma(t), \tag{4–2}$$

$$\tilde{e}(t) \triangleq x(t) - \hat{x}(t), \tag{4–3}$$

where $e(t)$ is the actual tracking error, $\hat{e}(t)$ is the estimate tracking error, and $\tilde{e}(t)$ is the state estimation error. When $x(t) \in \mathcal{F}$, the objective is to regulate all three error systems. When $x(t) \in \mathcal{F}^c$, state feedback is no longer available, and the objective is to regulate $\hat{e}(t)$; however, $\tilde{e}(t)$ may become unstable due to the lack of state feedback, and therefore, $e(t)$ may become unstable. As a result of potential instabilities when $x(t) \in \mathcal{F}^c$, another challenge in this chapter is to ensure $e(t)$ does not grow beyond an application-based, desired bound while simultaneously maximizing the time $x(t) \in \mathcal{F}^c$ where $x(t)$ follows x_d. To facilitate the subsequent development, let $p \in \mathscr{P} \triangleq \{a, u\}$, where a is an index for the subsystem with available state feedback, and u is an index for the subsystem without state feedback.

4.3 Stability Analysis

To illustrate framework development, consider any design of nonlinear controllers, observers (when $p = a$) and predictors (when $p = u$) that yield a family of closed-loop error dynamics of the forms

$$\dot{e}(t) = \begin{cases} g_{e,p}\left(v(x,t),t\right), & p = a, \\ \\ g_{e,p}\left(v(\hat{x},t),t\right), & p = u, \end{cases} \tag{4–4}$$

$$\dot{\hat{e}}(t) = \begin{cases} g_{\hat{e},p}\left(v(x,t),t\right), & p = a, \\ \\ g_{\hat{e},p}\left(v(\hat{x},t),t\right), & p = u, \end{cases} \tag{4–5}$$

$$\dot{\tilde{e}}(t) = g_{\tilde{e},p}\left(x,\hat{x},t\right), \ \forall p, \tag{4–6}$$

where $g_{e,p}$, $g_{\hat{e},p} : \mathbb{R}^n \times [0,\infty) \to \mathbb{R}^n$ are nonlinear functions that depend on the controller, $g_{\tilde{e},p} : \mathbb{R}^n \times \mathbb{R}^n \times [0,\infty) \to \mathbb{R}^n$ is a nonlinear function that depends on the observer and predictor, and satisfy the following assumption.

Assumption 4.1. The origins of the error systems $e(t) = \tilde{e}(t) = 0$ are exponentially stable when $p = a$, and the origin of the error system $\hat{e}(t) = 0$ is exponentially stable when $p = u$. Furthermore, there exist three first-order differentiable, positive-definite candidate Lyapunov-like functions $V_e(e(t)),\ V_{\hat{e}}(\hat{e}(t)),\ V_{\tilde{e}}(\tilde{e}(t)) : \mathbb{R}^n \to \mathbb{R}$ such that

$$\dot{V}_e(e(t)) \leq -2\lambda_s V_e(e(t)),\ p = a, \tag{4–7}$$

$$\dot{V}_{\hat{e}}(\hat{e}(t)) \leq -2\lambda_s V_{\hat{e}}(\hat{e}(t)),\ p = u, \tag{4–8}$$

$$\dot{V}_{\tilde{e}}(\tilde{e}(t)) \leq \begin{cases} -2\lambda_{\tilde{e}} V_{\tilde{e}}(\tilde{e}(t)), & p = a, \\ 2\lambda_u V_{\tilde{e}}(\tilde{e}(t)) + \delta, & p = u, \end{cases} \tag{4–9}$$

where $\lambda_s,\ \lambda_{\tilde{e}},\ \lambda_u,\ \delta \in \mathbb{R}_{>0}$ are known, positive constants.

To further facilitate the analysis for the switched system, let the time of the ith instance when $x(t)$ transitions from $\mathcal{F}^c$ to $\mathcal{F}$ and from $\mathcal{F}^c$ to $\mathcal{F}$ be denoted by $t_i^a \in \mathbb{R}_{\geq 0}$ and $t_i^u \in \mathbb{R}_{>0}$, respectively, for $i \in \mathbb{N}$. Based on the switching instants, dwell-time of the ith activation of the subsystems a and u are defined as $\Delta t_i^a \triangleq t_i^u - t_i^a \in \mathbb{R}_{>0}$ and $\Delta t_i^u \triangleq t_{i+1}^a - t_i^u \in \mathbb{R}_{>0}$, respectively. To ensure the tracking error is bounded, a minimum threshold $\hat{e}_T \in \mathbb{R}_{>0}$ on $\|\hat{e}(t)\|$ and a desired maximum bound $e_M \geq 2\hat{e}_T$ on $\|e(t)\|$ may be imposed such that $V_e(e(t_i^a)) \leq V_M$ and $V_{\hat{e}}(\hat{e}(t_i^u)) \leq V_T$, where $V_M,\ V_T \in \mathbb{R}_{>0}$ are the respective maximum bound and minimum threshold. The selection on e_M is also dictated by the size of $\mathcal{F}$, where the compact ball of radius e_M must be less than or equal to the inscribed ball of $\mathcal{F}$ in $\mathbb{R}^n$.

Theorem 4.1. *The trajectories of the switched systems generated by the family of subsystems described by (4–4)-(4–6), and a piecewise constant, right-continuous switching signal $\sigma : [0, \infty) \to p \in \{a, u\}$ are globally uniformly ultimately bounded provided the switching signal satisfies the minimum feedback availability dwell-time condition*

$$\Delta t_i^a \geq \frac{-1}{\min(\lambda_s, \lambda_{\tilde{e}})} \ln\left(\min\left(\frac{\hat{e}_T}{(\|e(t_i^a)\| + \|\tilde{e}(t_i^a)\|)}, 1\right)\right), \tag{4–10}$$

and the maximum loss of feedback dwell-time condition

$$\Delta t_i^u \leq \ln\left(X_{min}\right), \tag{4--11}$$

where X_{min} is a subsequently defined positive constant.

Proof. While $p = a$, it can be shown from (4–7)-(4–9) that $e(t)$ and $\tilde{e}(t)$ are globally exponentially stable with the bounds

$$\|e(t)\| \leq \|e(t_i^a)\|e^{-\lambda_s \Delta t_i^a}, \tag{4--12}$$

$$\|\tilde{e}(t)\| \leq \|\tilde{e}(t_i^a)\|e^{-\lambda_{\tilde{e}} \Delta t_i^a}. \tag{4--13}$$

Utilizing the relationship $\hat{e}(t) = e(t) - \tilde{e}(t) \implies \|\hat{e}(t)\| \leq \|e(t)\| + \|\tilde{e}(t)\| \implies \|\hat{e}(t)\| \leq \|e(t_i^a)\|e^{-\lambda_s \Delta t_i^a} + \|\tilde{e}(t_i^a)\|e^{-\lambda_{\tilde{e}} \Delta t_i^a} \leq \|e(t_i^a)\|e^{-\min(\lambda_s,\lambda_{\tilde{e}})\Delta t_i^a} + \|\tilde{e}(t_i^a)\|e^{-\min(\lambda_s,\lambda_{\tilde{e}})\Delta t_i^a} \implies \|\hat{e}(t)\| \leq (\|e(t_i^a)\| + \|\tilde{e}(t_i^a)\|) e^{-\min(\lambda_s,\lambda_{\tilde{e}})\Delta t_i^a}$. Based on the convergence rate of $\|\hat{e}(t)\|$, the minimum dwell-time condition can be derived as $\|\hat{e}(t_i^u)\| \leq \hat{e}_T \implies (\|e(t_i^a)\| + \|\tilde{e}(t_i^a)\|) e^{-\min(\lambda_s,\lambda_{\tilde{e}})\Delta t_i^a} \leq \hat{e}_T$, and therefore the minimum dwell-time condition in (4–10) can be obtained by solving the inequality.

While $p = u$, it can be shown from (4–7)-(4–9) that the evolution of $\hat{e}(t)$ and $\tilde{e}(t)$ are bounded by

$$\|\hat{e}(t)\| \leq \|\hat{e}(t_i^u)\|e^{-\lambda_s \Delta t_i^u}, \tag{4--14}$$

$$\|\tilde{e}(t)\| \leq \sqrt{\|\tilde{e}(t_i^u)\|^2 e^{2\lambda_u \Delta t_i^u} - \frac{\delta}{2\lambda_u}(1 - e^{2\lambda_u \Delta t_i^u})}. \tag{4--15}$$

Utilizing the relationship $e(t) = \hat{e} + \tilde{e}(t)$, $\|e(t)\| \leq \|\hat{e}(t)\| + \|\tilde{e}(t)\| \implies \|e(t)\| \leq \|\hat{e}(t_i^u)\|e^{-\lambda_s \Delta t_i^u} + \sqrt{\|\tilde{e}(t_i^u)\|^2 e^{2\lambda_u \Delta t_i^u} - \frac{\delta}{\lambda_u}(1 - e^{2\lambda_u \Delta t_i^u})}$. Substituting in the desired error bound of $e\left(t_{i+1}^a\right) \leq e_M$ and performing algebraic manipulations yields $\|\hat{e}(t_i^u)\|^2 X^{-2\lambda_s} - 2e_M\|\hat{e}(t_i^u)\|X^{-\lambda_s} - \|\tilde{e}(t_i^u)\|^2 X^{2\lambda_u} - \frac{\delta}{2\lambda_u}X^{2\lambda_u} + e_M^2 + \frac{\delta}{2\lambda_u} \geq 0$, where $X = e^{\Delta t_i^u}$. Numerical

solutions for X can be computed, and by taking the natural logarithm on the minimum positive, real solution $X_{min} \in \mathbb{R}_{\geq 1}$, the maximum dwell-time condition can be derived.

□

Remark 4.1. A more conservative bound on the maximum dwell-time condition in (4–11) for continuous state estimates can be derived by upper bounding $\|\hat{e}(t)\|$ by $\|\hat{e}(t)\| \leq \|\hat{e}(t_i^u)\| e^{-\lambda_s \Delta t_i^u} \leq \|\hat{e}(t_i^u)\|$ to yield $\Delta t_i^u \leq \frac{1}{2\lambda_u} \ln \left(\frac{\left(e_M - \|\hat{e}(t_i^u)\|\right)^2 + \frac{\delta}{2\lambda_u}}{\|\tilde{e}(t_i^u)\|^2 + \frac{\delta}{2\lambda_u}} \right)$.

Remark 4.2. With single integrator dynamics, the estimation error dynamics are upper bounded by $\dot{\tilde{e}}(t) \leq \bar{d}$ when $p = u$, and therefore $\tilde{e}(t)$ exhibits a linear growth that can be bounded by $\|\tilde{e}(t)\| \leq \|\tilde{e}(t_i^u)\| + \bar{d}(\Delta t_i^u)$. Following the development, the maximum dwell-time can be derived by solving the inequality as $\|\hat{e}(t_i^u)\| e^{-\lambda_s \Delta t_i^u} + \|\tilde{e}(t_i^u)\| + \bar{d}(\Delta t_i^u) \leq e_M$, $\|\hat{e}(t_i^u)\| + \|\tilde{e}(t_i^u)\| + \bar{d}(\Delta t_i^u) \leq e_M$, and therefore $\Delta t_i^u \leq \frac{e_M - \|\hat{e}(t_i^u)\| - \|\tilde{e}(t_i^u)\|}{\bar{d}}$.

Utilizing Reset Maps

The result in Theorem 4.1 relies on an observer to provide state estimates when $x(t) \in \mathcal{F}$, which results in a minimum dwell-time condition. However, the minimum dwell-time condition can be eliminated by using reset maps. Specifically, it is possible to exploit reset maps to reset $x_{\sigma,i}$ to a new path $x_{\sigma,i+1}$ and $\hat{x}(t)$ to coincide $x(t)$ at t_i^a, i.e., upon every instance of re-entry to $\mathcal{F}$. However, imposing reset maps on x_σ and $\hat{x}(t)$ introduces a discontinuity in the error dynamics; hence, a switched hybrid system analysis is required. To facilitate the development, let $E \subset \mathscr{P} \times \mathscr{P}$ represent a one-way transition from $p = u$ to $p = a$. Let the reset maps for x_σ and $\hat{x}(t)$ be denoted as $\phi_\sigma : E \times x_{\sigma,i} \to \mathbb{R}^n$ and $\hat{\phi} : E \times \mathbb{R}^n \to \mathbb{R}^n$, respectively, and be designed as $\phi_\sigma(E, x_{\sigma,i}(t)) \triangleq x_{\sigma,i+1}$ and $\hat{\phi}(E, \hat{x}(t)) \triangleq x(t)$.

When x_{σ_i} and $\hat{x}(t)$ are reset at t_i^a, $e(t) = \tilde{e}(t) = 0$, and hence, $\hat{e}(t) = 0$. It can be shown that the switches satisfy the *sequence non-increasing condition* described in [78], such that $V_e(e(t_i^{a-})) \geq V_e(e(t_i^a))$, $V_{\hat{e}}(\hat{e}(t_i^{a-})) \geq V_{\hat{e}}(\hat{e}(t_i^a))$ and $V_{\tilde{e}}(\tilde{e}(t_i^{a-})) \geq V_{\tilde{e}}(\tilde{e}(t_i^a))$, where $t_i^{a-} \triangleq \lim t \to t_i^a$ from the left. Following a similar proof for Theorem 4.1, with the exception that $e(t) = \hat{e}(t) = \tilde{e}(t) = 0$ when $p = a$, the same stability conditions can be

obtained. Since $e_T > e(t) = 0$, the minimum tracking error condition is automatically and instantaneously satisfied, indicating that $x(t)$ may leave $\mathcal{F}$ immediately upon entry, i.e. $\Delta t_i^a \geq 0$. Utilizing $\|\hat{e}(t_i^u)\| = 0$, the maximum dwell-time condition can then be solved analytically as $\|\tilde{e}(t_i^u)\|^2 e^{2\lambda_u \Delta t_i^u} - \frac{\delta}{2\lambda_u} e^{2\lambda_u \Delta t_i^u} + e_M^2 + \frac{\delta}{2\lambda_u} \geq 0$, and therefore $\Delta t_i^u \leq \frac{1}{2\lambda_u} \ln \left(\frac{e_M^2 + \frac{\delta}{2\lambda_u}}{\|\tilde{e}(t_i^u)\|^2 + \frac{\delta}{2\lambda_u}} \right)$.

4.4 Auxiliary Trajectory Design

Since x_d denotes a path that lies outside the feedback region, i.e. $x_d \subset \mathcal{F}^c$, $x(t)$ must leave $\mathcal{F}$ while following x_d, resulting in the loss of feedback. Therefore, an auxiliary trajectory $x_\sigma(t)$ is designed for the agent to track so that $x(t)$ follows x_d to the extent possible given the dwell-time conditions in (4–10) and (4–11). To facilitate the development of $x_\sigma(t)$, let the closest orthogonal projection of $x_\sigma(t)$ on the boundary of $\mathcal{F}$ be denoted as $x_b(t) \in \mathbb{R}^n$.

While $x(t) \in \mathcal{F}^c$, $\|e(t)\|$ can be upper bounded by e_M when the maximum dwell-time is reached, implying that there exist a compact set $\mathcal{B} = \{y \in \mathbb{R}^n | \|y - x_\sigma(t)\| \leq e_M\}$ such that $x(t) \in \mathcal{B}, \forall t$. To compensate for the potential accumulation of error, $x_\sigma(t)$ must penetrate a sufficient distance into $\mathcal{F}$, motivating the design of a cushion state $x_\epsilon(t) \in \mathbb{R}^n$ as

$$x_\epsilon(t) \triangleq x_b(t) + \Phi(t), \tag{4–16}$$

where $\Phi(t) \in \mathbb{R}^n$, such that $\|\Phi(t)\| \geq e_M$ and there exist a compact set $\mathcal{A} = \{y \in \mathbb{R}^n | \|y - x_\epsilon(t)\| \leq \|\Phi(t)\|\}$ such that $\mathcal{A}$ is less than or equal to the inscribed ball of $\mathcal{F}$ in $\mathbb{R}^n$. Therefore, the requirement of $x(t) \in \mathcal{B} \subseteq \mathcal{A} \subseteq \mathcal{F}$ can be satisfied if $x_\sigma(t)$ coincides with $x_\epsilon(t)$ when the maximum dwell-time is reached.

4.5 Design Example

To illustrate the developed framework, consider an example controller designed as

$$v\left(x_p\left(t\right), t\right) \triangleq \dot{x}_\sigma\left(t\right) - \left(k + \frac{\bar{d}^2}{\varepsilon} I_n\right)\left(x_p\left(t\right) - x_\sigma\left(t\right)\right) - f\left(x_p\left(t\right), t\right), \tag{4–17}$$

where $x_p(t) = x(t)$ when $p = a$ and $x_p(t) = \hat{x}(t)$ when $p = u$, $k \in \mathbb{R}^{n \times n}$ is a constant, positive-definite gain matrix, and $\varepsilon \in \mathbb{R}_{>0}$ a design parameter. In (4–17), the design structure remains the same for all p, where only the input signal switches between using $x(t)$ or $\hat{x}(t)$.

Examples of the state estimate update laws for the observer and predictor are given as

$$\dot{\hat{x}}(t) \triangleq \begin{cases} f(\hat{x}(t), t) + v(x(t), t) + v_r(\tilde{e}(t)), & p = a, \\ f(\hat{x}(t), t) + v(\hat{x}(t), t), & p = u, \end{cases} \tag{4–18}$$

where $v_r(\tilde{e}(t)) \in \mathbb{R}^n$ contains a high-frequency sliding-mode term to compensate for disturbances and is designed as

$$v_r(\tilde{e}(t)) \triangleq k_{\tilde{e}}\tilde{e}(t) + \bar{d}sgn(\tilde{e}(t)), \tag{4–19}$$

where $k_{\tilde{e}} \in \mathbb{R}^{n \times n}$ is a constant, positive-definite gain matrix. Unlike the development in [59] and [65], the controller does not require canceling terms since the controller receives $x(t)$ as feedback when $p = a$ and the robustifying term is not added to the predictor when $p = u$. Additionally, the controller and observer designs are decoupled and can be designed independently under the framework developed in Section 4.3.

After taking the time derivative of (4–1) - (4–3), substituting in (3–1) and (4–17) - (4–19) and selecting the candidate Lyapunov-like functions as $V_e(e(t)) \triangleq \frac{1}{2}e^T(t)e(t)$, $V_{\hat{e}}(\hat{e}(t)) \triangleq \frac{1}{2}\hat{e}^T(t)\hat{e}(t)$ and $V_{\tilde{e}}(\tilde{e}(t)) \triangleq \frac{1}{2}\tilde{e}^T(t)\tilde{e}(t)$, the known, positive constants in (4–7) - (4–9) are determined as $\lambda_s = \underline{k}$, $\lambda_{\tilde{e}} = \underline{k}_{\tilde{e}} - c$, $\lambda_u = c + \frac{1}{2}$, $\lambda_s > 0$, and $\delta = \frac{1}{2}\bar{d}^2$, where $\underline{k} > 0$ and $\underline{k}_{\tilde{e}} > c$ are the minimum eigenvalues of k and $k_{\tilde{e}}$, respectively, and $c \in \mathbb{R}_{>0}$ is a Lipschitz constant. The tracking error $\|e(t)\|$ is shown to exponentially converge $\forall \|e(t)\| > \sqrt{\frac{\varepsilon}{4\lambda_s}}$. Hence, the dwell-time conditions can be derived accordingly, where $\hat{e}_T > \sqrt{\frac{\varepsilon}{4\lambda_s}}$.

To illustrate the design of the auxiliary trajectory, an example of $x_\sigma(t)$ using an observer is given as

$$x_{\sigma,i}(t) \triangleq \begin{cases} \rho_i^a x_\epsilon(t) + (1 - \rho_i^a) x_b(t), & t_i^a \leq t < t_i^u, \\ \rho_i^{u1} x_b(t) + (1 - \rho_i^{u1}) g(x_d, t), & t_i^u \leq t < t_i^{u1}, \\ g(x_d, t), & t_i^{u1} \leq t < t_i^{u2}, \\ \rho_i^{u3} g(x_d, t) + (1 - \rho_i^{u3}) x_\epsilon(t), & t_i^{u2} \leq t < t_i^{u3}, \end{cases} \quad (4\text{--}20)$$

where $g : x_d \times \mathbb{R} \to \mathbb{R}^n$ maps t to the desired state in x_d, ρ_i^a, ρ_i^{u1}, ρ_i^{u2} and ρ_i^{u3} are time-based ratios designed as $\rho_i^a \triangleq \frac{t - t_i^a}{\Delta t_i^a}$ and $\rho_i^{u(j+1)} \triangleq \frac{t - \left(t_i^u + \sum_{k=0}^{j} p_k \Delta t_i^u\right)}{p_{j+1} \Delta t_i^u}$, $j \in \{0, 1, 2\}$, the weights used to partition the maximum dwell-time are denoted by $p_k \in [0, 1)$, and the corresponding partitions are denoted by $t_i^{u(j+1)}$. In addition, t_i^{u3} coincides with t_{i+1}^a, and Δt_i^a must be arbitrarily lower bounded above zero to avoid a singularity in ρ_i^a.

If a reset map is used instead of the observer, the auxiliary trajectory can be designed as

$$x_{\sigma,i}(t) \triangleq \begin{cases} \rho_i^{u1} x(t) + (1 - \rho_i^{u1}) g(x_d, t), & t_i^u \leq t < t_i^{u1}, \\ g(x_d, t), & t_i^{u1} \leq t < t_i^{u2}, \\ \rho_i^{u3} g(x_d, t) + (1 - \rho_i^{u3}) x_\epsilon(t), & t_i^{u2} \leq t < t_i^{u3}. \end{cases} \quad (4\text{--}21)$$

4.6 Experimental Results

Two experiments are conducted to demonstrate the ability of an unmanned air vehicle to follow a path that lies outside a feedback region. Specifically, the objective is to examine the boundedness of the tracking error $e(t)$, and therefore stability of the system, throughout multiple revisits to the feedback region based on the dwell-time constraints established in Theorem 4.1. Both experiments use the example controller and predictor in (4–17) and (4–18), respectively. One experiment uses the observer in (4–18) and (4–19) with $x_\sigma(t)$ given in (4–20). The other experiment uses a reset map with $x_\sigma(t)$ given in (4–21).

For both experiments, the same experimental setup described in Section 3.7 is utilized, where the feedback available region $\mathcal{F}$ is defined as a region inside a 1-meter circle, and x_d is a 1.5-meter circle with the same origin as $\mathcal{F}$. Pose information obtained from the motion capture system is used as feedback only when the quadcopter is inside $\mathcal{F}$. Even though the OptiTrack system continues to record pose information when the quadcopter is outside the feedback region, the information is only used as ground truth for comparison purposes. For both experiments, on-board velocity measurements are utilized to match the velocity commands generated by the ground station.

Simplified dynamics of the quadcopter are represented by $\dot{x}(t) = u(t) + d(t)$, where $x(t)$ is the composite vector of the Euclidean coordinates of the quadcopter with respect to the inertial frame. For both experiments, the upper bound of the disturbance is assumed to be $\bar{d} = 0.05$, and the controller and update law are designed as described in Section 4.5, where $f(x,t) = f(\hat{x},t) = \begin{bmatrix} 0 & 0 & 0 \end{bmatrix}^T$, $k = 0.4I_3$, $k_{\tilde{e}} = 4I_3$, and $\varepsilon = 0.02$.

The auxiliary trajectory $x_\sigma(t)$ is designed to follow x_d with an angular velocity of $\frac{\pi}{15}$ radians per second during $t_i^{u1} \leq t < t_i^{u2}$, and the partitions for the maximum dwell-time are selected as $p_0 = 0$, $p_1 = 0.4$, $p_2 = 0.3$, $p_3 = 0.3$. The desired error bound and threshold are selected as $e_M = 0.9$ meters and $\hat{e}_T = 0.14$ meters. Since single integrator dynamics are used for the quadcopter, Remark 4.2 provides a less conservative minimum dwell-time condition that is implemented for both experiments.

Figures 4-1-4-4 illustrate the experimental results using the observer and reset map, respectively. When using the observer, the quadcopter is allowed to remain in $\mathcal{F}^c$ for 16.10 seconds and is required to remain in $\mathcal{F}$ for 3.59 seconds on average. When using the reset map, the quadcopter is allowed 18.00 seconds in $\mathcal{F}^c$ and no minimum dwell-times are required. In both experiments, the tracking error converges exponentially when $x(t) \in \mathcal{F}$ and exhibits growth when $x(t) \in \mathcal{F}^c$, reflecting the analysis in Section 4.3. The growth of $\|e(t)\|$ can be attributed to the open-loop tracking performance, and various techniques (e.g., the use of inertial measurement units or visual odometry)
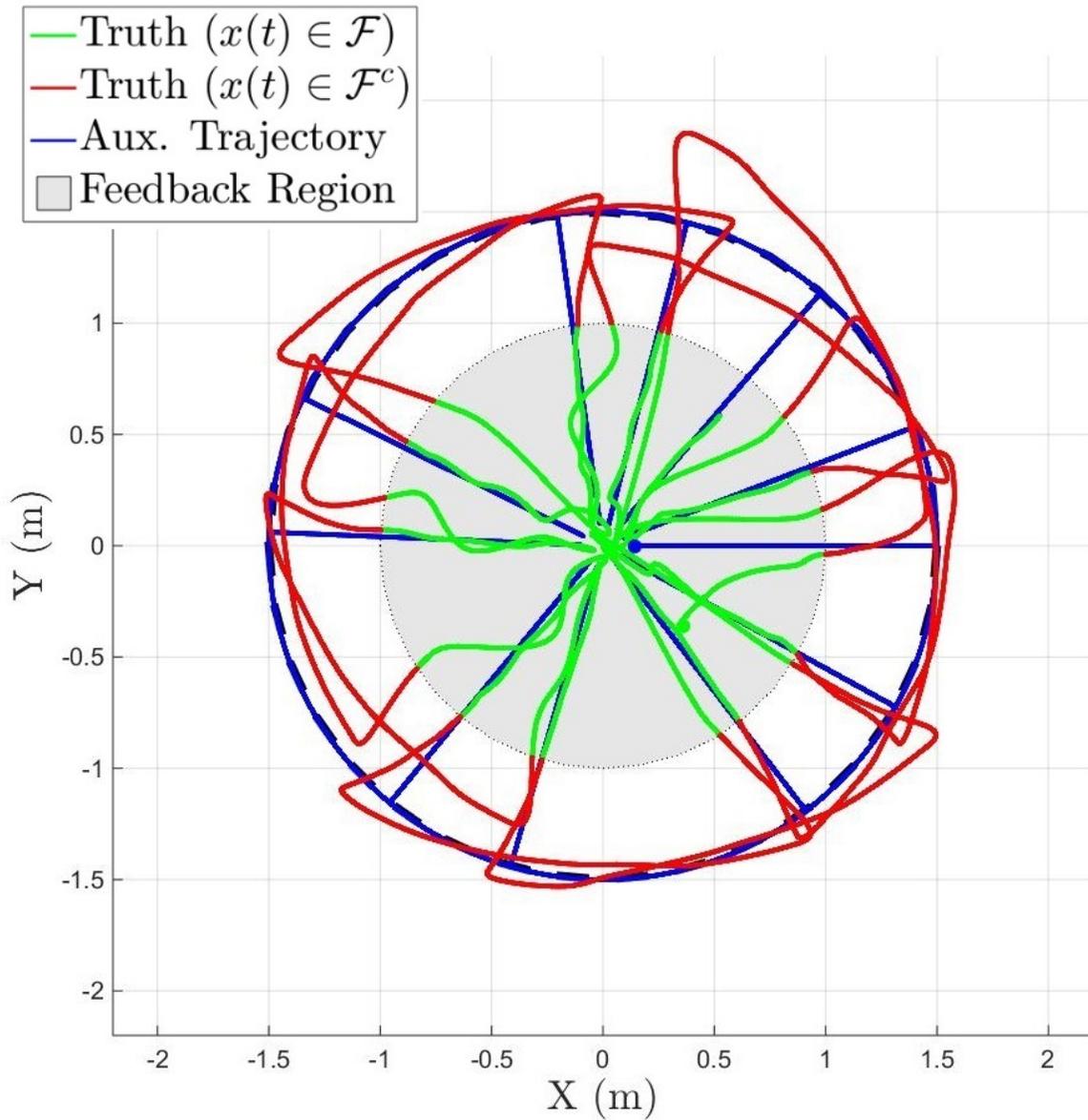
Figure 4-1. Overall path following result using an observer for the state estimate. The agent is required to remain inside the feedback-available region for periods of time as indicated by the green line.
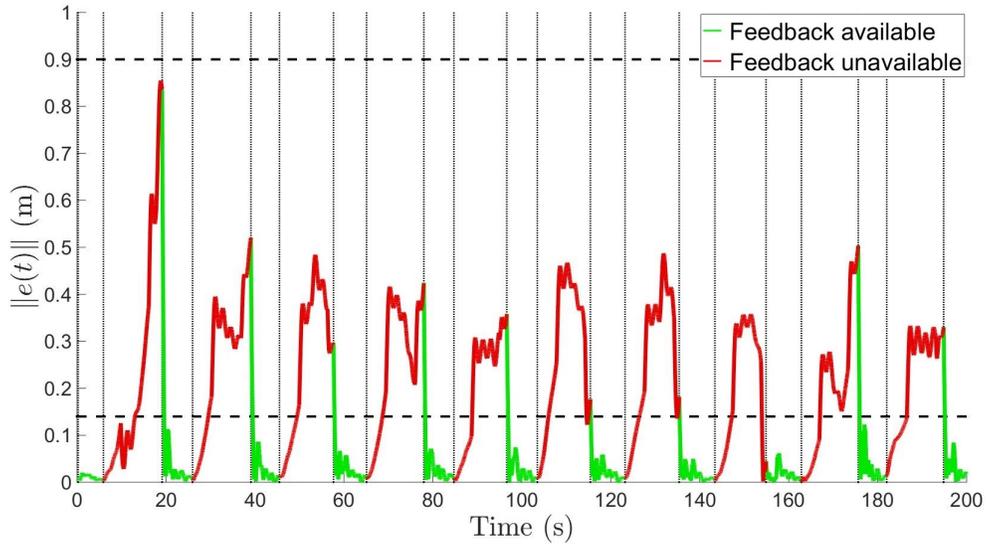
Figure 4-2. The evolution of $\|e(t)\|$ for continuous state estimates. The tracking error is regulated below $\hat{e}_T$ (bottom dotted line) before leaving $\mathcal{F}$ and remains under e_M (top dotted line) for all times when outside of $\mathcal{F}$. The vertical lines denote the instants when $x(t)$ enters and leaves $\mathcal{F}$.

can be applied to minimize the open-loop tracking error when $x(t) \in \mathcal{F}^c$. The goal for both experiments is to demonstrate the developed switching framework that allows the quadcopter to compensate for the lack of feedback and achieve timely loop-closures such that the tracking error growth stays bounded. As shown in Figures 4-2 and 4-4, $\|e(t)\|$ is upper bounded by e_M, and converges to below $\hat{e}_T$ before leaving $\mathcal{F}$. Therefore, these experiments demonstrate that the switching signal $\sigma(t)$ generated by $x_\sigma(t)$ satisfies the dwell-time conditions developed in Section 4.3 and stabilizes the overall system.

4.7 Summary

A novel method that establishes a switched systems framework for path following under an intermittent state feedback constraint is presented. Specifically, the presented method relieves the requirement of uninterrupted state feedback, and allows the system to dwell in a feedback-denied region for periods of time. In comparison to Chapter 3, applicable controllers and observers from existing literature can be directly implemented
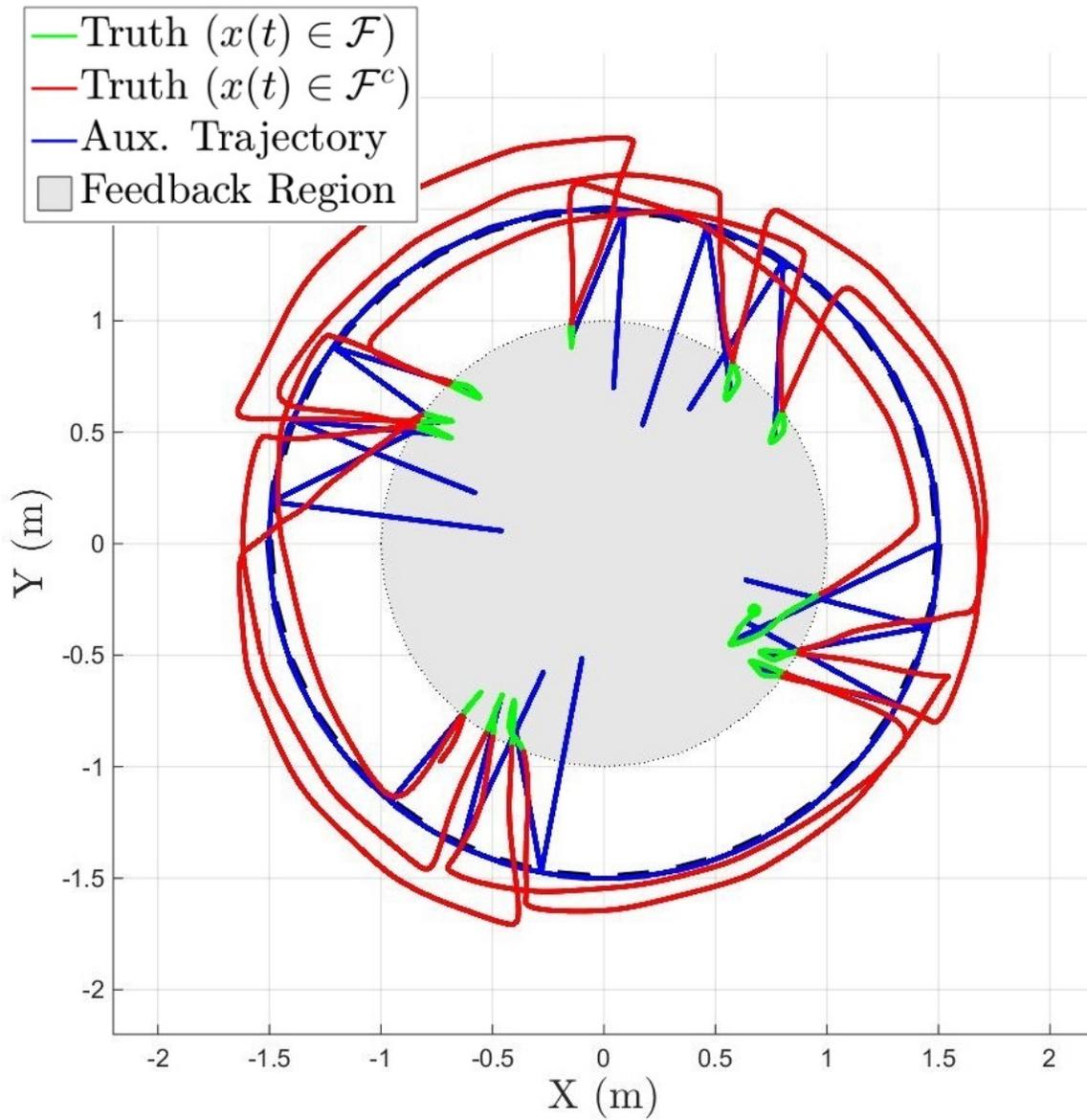
Figure 4-3. Overall path following result using reset maps. The agent is allowed to leave the feedback-available region immediately as indicated by the green line.
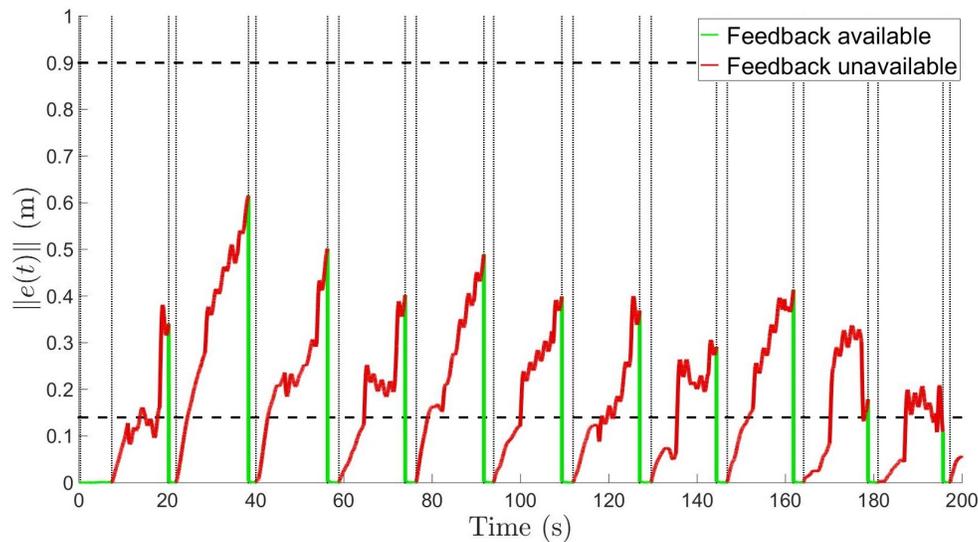
Figure 4-4. The evolution of $\|e(t)\|$ for discrete state estimates using a reset map. The tracking error is regulated below $\hat{e}_T$ (bottom dotted line) before leaving $\mathcal{F}$ and remains under e_M (top dotted line) for all times when outside of $\mathcal{F}$. The vertical lines denote the instants when $x(t)$ enters and leaves $\mathcal{F}$.

without altering the design structure, stability analysis, or gain selection. Maximum and minimum dwell-time conditions are developed via a Lyapunov-based, switched systems analysis to guarantee stability of the overall system. Alternatively, the analysis indicates that reset maps can also be utilized to eliminate the requirement of minimum dwell-time conditions, which is not previously achievable in Chapter 3. An auxiliary trajectory is designed based on the dwell-time conditions to regulate the states into the feedback region before the tracking error exceeds a defined threshold. Two experiments were performed to illustrate the control development and trajectory design with and without using reset maps. The results are indicate that using reset maps allows the agent to spend more time in the feedback denied region and that the agent is not required to remain in the feedback-available region as it is in Chapter 3.

CHAPTER 5
ASSISTED PATH-FOLLOWING FOR AGENTS IN A STATE-FEEDBACK-DENIED REGION

This chapter presents a novel approach to allow an agent to follow a path in a feedback-denied region with the assist from another agent that intermittently visits the feedback-available region. In Chapters 3 and 4, the agent is allowed no more than 50% of the time tracking the desired path, and hence, motivating the development of this chapter to allow the agent to follow the desired path at all times. The focus of this chapter also includes the development of a switched systems framework for controlling systems with uncertainty in the dynamics under intermittent state feedback, as opposed to assuming exact model knowledge in previous chapters.

5.1 System Model

Consider a general nonlinear dynamic system for an exploring agent described as

$$\dot{x}_e\left(t\right) \;\; = \;\; f_e(x_e\left(t\right), v_e(x_e\left(t\right), t)) + d_e\left(t\right), \tag{5–1}$$

where $x_e\left(t\right),\ \dot{x}_e\left(t\right)\ \in\ \mathbb{R}^n$ denote the generalized states and its time derivative, $f_e\ :$ $\mathbb{R}^n \times \mathbb{R}^m \times \mathbb{R} \to \mathbb{R}^n$ denotes the known general dynamics, $v_e(x_e\left(t\right), t) \in \mathbb{R}^m$ is the control inputs, and $d_e\left(t\right) \in \mathbb{R}^n$ is a bounded exogenous disturbance, with $n,\ m \in \mathbb{N}$ and $t \in \mathbb{R}_{\geq 0}$.

Consider a control-affine nonlinear dynamic system for a relay agent described as

$$\dot{x}_r\left(t\right) \;\; = \;\; f_r(x_r\left(t\right)) + v_r(x_r\left(t\right), t) + d_r\left(t\right), \tag{5–2}$$

where $x_r\left(t\right),\ \dot{x}_r\left(t\right)\ \in\ \mathbb{R}^n$ denote the generalized states and its time derivative, and $f_r :\ \mathbb{R}^n \times \mathbb{R} \to \mathbb{R}^n$ denotes unknown continuous dynamics, $v_r(x_r\left(t\right), t) \in \mathbb{R}^n$ is the control inputs, and $d_r\left(t\right) \in \mathbb{R}^n$ is a bounded exogenous disturbance.

Assumption 5.1. The exogenous disturbances $d_e\left(t\right)$ and $d_r\left(t\right)$ are bounded such that $\|d_e\left(t\right)\| \leq \bar{d}_e$ and $\|d_r\left(t\right)\| \leq \bar{d}_r$.

Assumption 5.2. The unknown drift dynamics f_r is at least a class C^0 function and is bounded such that $\|f_r\left(x_r\left(t\right)\right)\| \leq \bar{f}_r \in \mathbb{R}^n$

5.2 State Estimation and Control Objective

Similar to Chapters 3 and 4, the feedback-available and -denied regions are defined as $\mathcal{F} \subset \mathbb{R}^n$ and $\mathcal{F}^c \subset \mathbb{R}^n$, respectively. The objective is to enable the exploring agent to follow a desired path, $x_d \subset \mathcal{F}^c$, while the relay agent updates $\hat{x}_e(t)$ for the exploring agent by visiting $\mathcal{F}$ intermittently. The state estimates, $\hat{x}_r(t)$ and $\hat{x}_e(t)$, are reset using subsequently designed reset maps when $x_r(t) \in \mathcal{F}$ and when $\|x_r(t) - x_e(t)\|$ is less than a subsequently defined communication radius.

Assumption 5.3. The exploring and relay agents are initialized at $t = t_0 \in \mathbb{R}_{\geq 0}$ in a feedback-available region (i.e. $x_e(t_0), \ x_r(t_0) \in \mathcal{F} \subset \mathbb{R}^n$), where $\mathcal{F}$ is a compact set.

Assumption 5.4. The communication range of the relay agent is defined as $R_{com} \in \mathbb{R}_{>0}$, and the relationship between $x_e(t)$ and $x_r(t)$ may be measured and communicated directly from the relay to the exploring agent when $\|x_e(t) - x_r(t)\| \leq R_{com}$.

By Assumption 5.4, $\hat{x}_e(t)$ may be updated whenever $\|x_e(t) - x_r(t)\| \leq R_{com}$. To facilitate the subsequent development, let $p_e \in \mathscr{S}_e \triangleq \{a_e, u_e\}$, where a_e and u_e are the indices for the exploring agent's subsystems when $\|x_e(t) - x_r(t)\| \leq R_{com}$ and $\|x_e(t) - x_r(t)\| > R_{com}$, respectively. Let $p_r \in \mathscr{S}_r \triangleq \{a_r, u_r\}$, where a_r and u_r are the indices for the relay agent's subsystems when $x_r(t) \in \mathcal{F}$ and $x_r(t) \in \mathcal{F}^c$, respectively.

Based on the objectives, three error systems are defined for the exploring agent as

$$e_e(t) \triangleq x_e(t) - x_{ref}(t), \tag{5--3}$$

$$\hat{e}_e(t) \triangleq \hat{x}_e(t) - x_{ref}(t), \tag{5--4}$$

$$\tilde{e}_e(t) \triangleq x_e(t) - \hat{x}_e(t), \tag{5--5}$$

where $x_{ref}(t) \in \mathbb{R}^n$ is a reference trajectory generated by a reference model that follows the desired path x_d.

Similarly, four error systems are defined for the relay agent as

72

$$e_r\left(t\right) \triangleq x_r\left(t\right) - x_{aux}\left(t\right), \tag{5--6}$$

$$\hat{e}_r\left(t\right) \triangleq \hat{x}_r\left(t\right) - x_{aux}\left(t\right), \tag{5--7}$$

$$\tilde{e}_r\left(t\right) \triangleq x_r\left(t\right) - \hat{x}_r\left(t\right), \tag{5--8}$$

$$\tilde{f}_r(x_r\left(t\right)) \triangleq f_r(x_r\left(t\right)) - \hat{f}_r(\hat{x}_r\left(t\right)) \tag{5--9}$$

where $x_{aux}\left(t\right)$ is a subsequently designed auxiliary trajectory for the relay agent, $e_r\left(t\right)$ is the actual tracking error, $\hat{e}_r\left(t\right)$ is the estimated tracking error, and $\tilde{e}_r\left(t\right)$ is the state estimation error, and let $\zeta_r\left(t\right) \triangleq \left[e_r^T\left(t\right), \tilde{f}_r^T\left(t\right)\right]^T$.

Assumption 5.5. There exist a set of nonlinear controllers, update laws for $\hat{f}_r\left(\hat{x}_r\left(t\right)\right)$, and reset maps for $\hat{x}_r(t)$ and $\hat{x}_e\left(t\right)$ that exponentially stabilizes the origins of the error systems described by (5--3)-(5--5) when $p_e = a_e$, (5--6)-(5--9) when $p_r = a_r$, (5--4) when $p_e = u_e$, and (5--8) when $p_r = u_r$. Specifically, there exists first-order differentiable, positive-definite candidate Lyapunov-like functionals $V_\zeta^a\left(\zeta_r\left(t\right)\right)$, $V_{\hat{r}}^u\left(\hat{e}_r\left(t\right)\right)$ and $V_{\hat{e}}^u\left(\hat{e}_e\left(t\right)\right)$, such that, by utilizing the control designs, the respective time derivatives yield

$$\dot{V}_\zeta^a\left(\zeta_r\left(t\right)\right) \leq -\lambda_r^a V_\zeta^a\left(\zeta_r\left(t\right)\right) + \delta_r^a, \ p_r = a_r, \tag{5--10}$$

$$\dot{V}_{\hat{r}}^u\left(\hat{e}_r\left(t\right)\right) \leq -\lambda_r^a V_{\hat{r}}^u\left(\hat{e}_r\left(t\right)\right), \ p_r = u_r, \tag{5--11}$$

$$\dot{V}_{\hat{e}}^u\left(\hat{e}_e\left(t\right)\right) \leq -\lambda_e^a V_{\hat{e}}^u\left(\hat{e}_e\left(t\right)\right), \ p_e = u_e, \tag{5--12}$$

where $\lambda_r^a, \ \lambda_e^a, \ \delta_r^a \in \mathbb{R}$ are known, positive constants. Furthermore, there exists first-order differentiable, positive-definite candidate Lyapunov-like functionals $V_{\tilde{r}}^u\left(\tilde{e}_r\left(t\right)\right)$ and $V_{\tilde{e}}^u\left(\tilde{e}_e\left(t\right)\right)$ for the state estimates of both agents with exact structures (i.e., $V_{\tilde{r}}^u\left(\tilde{e}_r\left(t\right)\right) = V_{\tilde{e}}^u\left(\tilde{e}_r\left(t\right)\right)$ and $V_{\tilde{e}}^u\left(\tilde{e}_e\left(t\right)\right) = V_{\tilde{r}}^u\left(\tilde{e}_e\left(t\right)\right)$), where the time derivatives of $V_{\tilde{r}}^u\left(\tilde{e}_r\left(t\right)\right)$ and $V_{\tilde{e}}^u\left(\tilde{e}_e\left(t\right)\right)$ take the forms of

$$\dot{V}_{\tilde{r}}^u \left(\tilde{e}_r \left(t \right) \right) \le \lambda_r^u V_{\tilde{r}}^u \left(\tilde{e}_r \left(t \right) \right) + \delta_r^u, \; p_r = u_r, \tag{5--13}$$

$$\dot{V}_{\tilde{e}}^u \left(\tilde{e}_e \left(t \right) \right) \le \lambda_e^u V_{\tilde{e}}^u \left(\tilde{e}_e \left(t \right) \right) + \delta_e^u, \; p_e = u_e, \tag{5--14}$$

where $\lambda_r^u, \; \lambda_e^u, \; \delta_r^u, \; \delta_e^u \in \mathbb{R}$ are known, positive constants.

5.3   Stability Analysis

In this section, the stability of the switched systems for both the exploring and relay agent are examined. When $x_r \left(t \right) \in \mathcal{F}$, the objective is to regulate the error systems in (5--6)-(5--8) and (5--9). Most importantly, the regulation of (5--8) and (5--9) ensures a better estimate of the dynamics described in (5--2). When $x_r \left(t \right) \in \mathcal{F}^c$, state feedback is no longer available, and the relay agent must rely on the estimated dynamics to navigate towards the exploring agent. Therefore, the objective is to regulate (5--7) when $x_r \left(t \right) \in \mathcal{F}^c$. Inevitably, the stability of (5--8) cannot be guaranteed during this phase because state feedback is not available to generate a stabilizing update law, and consequently, the stability of (5--6) is potentially voided. To compensate for the potential instabilities, one challenge in this chapter is to determine the bound on the growth rate of $e_r \left(t \right)$ and $e_e \left(t \right)$ during the feedback-denied time-frame and develop stabilizing conditions via a switched systems approach to ensure (5--6) remains within an application-based, user-defined bound while under the influence of unknown drift dynamics. For the exploring agent, the objective is for (5--3) to be bounded by a user-defined threshold, implying the regulation of (5--4) and bounding of (5--5). Similar to the dynamics of the relay agent, since $x_e \left(t \right) \in \mathcal{F}^c$, the stability of (5--3) and (5--5) depends on stabilizing conditions to ensure boundedness.

To further facilitate the development for the switched systems, let the time of the ith instance when $x_r \left(t \right)$ transitions from $\mathcal{F}^c$ to $\mathcal{F}$ and from $\mathcal{F}$ to $\mathcal{F}^c$ be denoted by $t_{r,i}^a \in \mathbb{R}_{\ge 0}$ and $t_{r,i}^u \in \mathbb{R}_{>0}$, for $i \in \mathbb{N}$, respectively. Additionally, let $t_{r,i}^{a-} \triangleq \lim_{\Delta t \to 0} t_{r,i}^a - \Delta t$. Based on the switching instants, dwell-time of the ith activation of the subsystems a_r and u_r

are defined as $\Delta t_{r,i}^a \triangleq t_{r,i}^u - t_{r,i}^a \in \mathbb{R}_{\geq 0}$ and $\Delta t_{r,i}^u \triangleq t_{r,i+1}^a - t_{r,i}^u \in \mathbb{R}_{\geq 0}$, respectively.

Similarly, let the time of the jth instance when $\hat{x}_e(t)$ is updated (i.e., the time when $\|x_r(t) - x_e(t)\| \leq R_{com}$ becomes valid) be denoted by $t_{e,j}^a \in \mathbb{R}_{\geq 0}$ for $j \in \mathbb{N}$, and $t_{e,j}^{a-} \triangleq \lim_{\Delta t \to 0} t_{e,j}^a - \Delta t$. Then the dwell-time of the jth activation of subsystem u_e is defined as $\Delta t_{e,j}^u \triangleq t_{e,j+1}^a - t_{e,j}^a \in \mathbb{R}_{\geq 0}$.

Inspired by the approach in [66], reset maps are utilized to update $\hat{x}_e(t)$ and $\hat{x}_r(t)$ at $t_{e,j}^a$ and $t_{r,i}^a$, respectively. Specifically, it is possible to exploit reset maps to reset $\hat{x}_e(t)$ to $\hat{x}_r(t) + (x_e(t) - x_r(t))$ and $\hat{x}_r(t)$ to $x_r(t)$, where the difference, $x_e(t) - x_r(t)$, is measurable by Assumption 5.4. To facilitate the analysis, let $E_r \subset \mathscr{S}_r \times \mathscr{S}_r$ and $E_e \subset \mathscr{S}_s \times \mathscr{S}_s$ represent a one-way transition from $p_r = u_r$ to $p_r = a_r$ and from $p_e = u_e$ to $p_e = a_e$, respectively. Let the reset maps for $\hat{x}_e(t)$, $\hat{x}_r(t)$ and $x_{aux}(t)$ be denoted as $\phi_e : E_e \times \mathbb{R}^n \to \mathbb{R}^n$, $\phi_r : E_r \times \mathbb{R}^n \to \mathbb{R}^n$ and $\phi_{aux} : E_r \times \mathbb{R}^n \to \mathbb{R}^n$ and be designed as $\phi_e(E_e, \hat{x}_e(t)) \triangleq \hat{x}_r(t) + (x_e(t) - x_r(t))$, $\phi_r(E_r, \hat{x}_r(t)) \triangleq x_r(t)$ and $\phi_{aux}(E_r, x_{aux}(t)) \triangleq x_r(t)$, respectively.

5.3.1 Relay Agent

First, the stability of the system of the relay agent is examined. Given Assumption 5.5 and a desired threshold $\|\tilde{e}_r(t)\| \leq \tilde{e}_{r,T} \in \mathbb{R}_{>0}$, such that $V_{\tilde{r},T}^u \triangleq V_{\tilde{r}}^u(\tilde{e}_{r,T}) \in \mathbb{R}_{>0}$ and $V_{\tilde{r}}^u(\tilde{e}_r(t)) \leq V_{\tilde{r},T}^u$, the stabilizing dwell-time condition is presented in the following theorem.

Theorem 5.1. *Controllers and update laws satisfying Assumption 5.5 and a piece-wise constant, right-continuous switching signal $\sigma_r : [0, \infty) \to p_r \in \{a_r, u_r\}$ satisfying the maximum loss of feedback dwell-time condition for the relay agent,*

$$\Delta t_{r,i}^u \leq \frac{1}{\lambda_r^u} \ln \left(\frac{V_{\tilde{r},T}^u + \frac{\delta_r^u}{\lambda_r^u}}{\frac{\delta_r^u}{\lambda_r^u}} \right), \tag{5–15}$$

ensures $\|e_r(t)\|$ is globally uniformly ultimately bounded by a design parameter, $\tilde{e}_{r,T}$.

Proof. First, the stability over every discrete reset is examined. When reset maps are invoked at $t_{r,i}^a$, it can be shown that $V_\zeta^a\left(\zeta_r\left(t\right)\right)$ satisfy the *sequence non-increasing condition* described in [78, 79], such that $V_\zeta^a(\zeta(t_{r,i}^{a-})) \le V_\zeta^a(\zeta_r(t_{r,i}^a))$, and hence, is stable over each switch. By solving (5–10), it is shown that $V_\zeta^a\left(\zeta_r\left(t\right)\right)$ is bounded by

$$V_\zeta^a\left(\zeta_r\left(t\right)\right) \le \left(V_\zeta^a\left(\zeta_r\left(t_{r,i}^a\right)\right) - \frac{\delta_r^a}{\lambda_r^a}\right)e^{-\lambda_r^a\left(t-t_{r,i}^a\right)} + \frac{\delta_r^a}{\lambda_r^a},$$

$\forall i \in \mathbb{N},\ t \in [t_{r,i}^a, t_{r,i}^u)$. Therefore, $V_\zeta^a\left(\zeta_r\left(t\right)\right) \le V_\zeta^a\left(\zeta_r\left(t_{r,i}^a\right)\right)$ and thus $\|e_r\left(t\right)\| \le \|e_r\left(t_{r,i}^a\right)\|, \forall i \in \mathbb{N},\ t \in [t_{r,i}^a, t_{r,i}^u)$. Next, the proof for the maximum loss of feedback dwell-time condition in (5–15) is presented. Solving for (5–11) and (5–13) yields

$$V_{\hat{r}}^u(\hat{e}_r\left(t\right)) \le V_{\hat{r}}^u(\hat{e}_r(t_{r,i}^u))e^{-\lambda_r^a\Delta t_{r,i}^u}, \tag{5–16}$$

$$V_{\tilde{r}}^u(\tilde{e}_r\left(t\right)) \le V_{\tilde{r}}^u(\tilde{e}_r(t_{r,i}^u))e^{\lambda_r^u\Delta t_{r,i}^u} - \frac{\delta_r^u}{\lambda_r^u}\left(1 - e^{\lambda_r^u\Delta t_{r,i}^u}\right). \tag{5–17}$$

By the virtue of reset maps, $V_{\hat{r}}^u(\hat{e}_r(t_{r,i}^u)) = V_{\tilde{r}}^u(\tilde{e}_r(t_{r,i}^u)) = 0$, and therefore $V_{\hat{r}}^u(\hat{e}_r\left(t\right)) = 0$ and $V_{\tilde{r}}^u(\tilde{e}_r\left(t\right)) \le \frac{\delta_r^u}{\lambda_r^u}\left(e^{\lambda_r^u\Delta t_{r,i}^u} - 1\right)$. After imposing an arbitrarily user-defined constraint, $V_{\tilde{r}}^u\left(\tilde{e}_r\left(t\right)\right) \le V_{\tilde{r},T}^u$, the dwell-time condition in (5–15) for $p_r = u_r$ is obtained. Therefore, when the dwell-time condition is satisfied, $V_{\tilde{r}}^u\left(\tilde{e}_r\left(t\right)\right) \le V_{\tilde{r},T}^u$, and thus $\|\tilde{e}_r\left(t\right)\|$ is bounded by definition. Since $i \in \mathbb{N}$ and the dwell-time interval is arbitrary, the result holds for all i and dwell-time intervals. Since $\|e_r\left(t_0\right)\| = 0$ by Assumption 5.3, $\|e_r\left(t\right)\| \le \|\hat{e}_r\left(t\right)\| + \|\tilde{e}_r\left(t\right)\|$ and $\|\hat{e}_r\left(t\right)\| = 0$ by definition, it can be shown that $\|e_r\left(t\right)\|$ is bounded by $\tilde{e}_{r,T}$ given the dwell-time condition is satisfied. $\qquad\square$

Theorem 5.1 implies that given any desired bound on $V_{\tilde{r}}^u\left(\tilde{e}_r\left(t\right)\right)$, a maximum dwell-time condition can be derived to satisfy this constraint. Let $V_{\tilde{r},I}^u \triangleq V_{\tilde{r}}^u\left(\tilde{e}_{r,I}\right) \in \mathbb{R}$ and $V_{\tilde{r},M}^u \triangleq V_{\tilde{r}}^u\left(\tilde{e}_{r,M}\right) \in \mathbb{R}$ denote the desired bounds for $V_{\tilde{r}}^u\left(\tilde{e}_r\left(t\right)\right)$, where $\tilde{e}_{r,I} \in \mathbb{R}$ and $\tilde{e}_{r,M} \in \mathbb{R}$ are the desired bounds for $\|\tilde{e}_r\left(t_{e,j}^a\right)\|$ and $\|\tilde{e}_r\left(t_{r,i}^a\right)\|, \forall i,\ j \in \mathbb{N}$, respectively. Then, the maximum dwell-time condition for both constraints can be derived by substituting $V_{\tilde{r},T}^u$ for $V_{\tilde{r},I}^u$ and $V_{\tilde{r},M}^u$, respectively.

5.3.2 Exploring Agent

A stabilizing dwell-time condition is now investigated for the exploring agent. Similar to Theorem 5.1, a design parameter $V_{\tilde{e},M}^u \triangleq V_{\tilde{e}}^u(\tilde{e}_{e,M}) \in \mathbb{R}_{>0}$ is introduced for deriving a stabilizing condition, where $\tilde{e}_{e,M} \in \mathbb{R}_{>0}$ is a desired bound on $\|\tilde{e}_e(t)\|$.

Theorem 5.2. *Update laws for $\dot{\hat{x}}_e(t)$ satisfying Assumption 5.5 and a piece-wise constant, right-continuous switching signal $\sigma_e : [0,\infty) \to p_e \in \{a_e, u_e\}$ that triggers the reset map $\phi_e(E_e, \hat{x}_e(t)) \triangleq \hat{x}_r(t) + (x_e(t) - x_r(t))$ while satisfying the maximum loss of feedback dwell-time condition for the exploring agent given by,*

$$\Delta t_{e,j}^u \leq \frac{1}{\lambda_e^u} \ln\left(\frac{V_{\tilde{e},M}^u + \frac{\delta_e^u}{\lambda_e^u}}{V_{\tilde{r},I}^u + \frac{\delta_e^u}{\lambda_e^u}}\right), \tag{5–18}$$

ensure $\|\tilde{e}_e(t)\|$ is globally uniformly ultimately bounded by a design parameter, $\tilde{e}_{e,M}$.

Proof. The generalized solution to (5–14) is given as

$$V_{\tilde{e}}^u(\tilde{e}_e(t)) \leq V_{\tilde{e}}^u(\tilde{e}_e(t_{e,j}^u)) e^{\lambda_e^u(t - t_{e,j}^a)} - \frac{\delta_e^u}{\lambda_e^u}\left(1 - e^{\lambda_e^u(t - t_{e,j}^a)}\right), \tag{5–19}$$

$\forall j \in \mathbb{N}, \forall t \in [t_{e,j}^a, t_{e,j+1}^a)$. Since $\|\tilde{e}_e(t_{e,j}^a)\| = \|\hat{x}_r(t_{e,j}^a) + (x_e(t_{e,j}^a) - x_r(t_{e,j}^a)) - x_e(t_{e,j}^a)\| = \|\tilde{e}_r(t_{e,j}^a)\|$, $V_{\tilde{e}}^u(\tilde{e}_e(t_{e,j}^a)) = V_{\tilde{r}}^u(\tilde{e}_r(t_{e,j}^a)) \leq V_{\tilde{r},I}^u$ by Assumption 5.5. By enforcing the stabilizing constraint, $V_{\tilde{e}}^u(\tilde{e}_e(t_{e,j+1}^a)) \leq V_{\tilde{e},M}^u$, the stabilizing condition described by (5–18) can be obtained. Therefore, $\|\tilde{e}_e(t)\| \leq \tilde{e}_{e,M}$ whenever the dwell-time condition is satisfied. $\square$

Naturally, $V_{\tilde{e},M}^u$ is selected to be greater than $V_{\tilde{r},I}^u$ because $V_{\tilde{e},M}^u$ is the maximum tolerance for $V_{\tilde{e}}^u(\tilde{e}_e(t))$ and $V_{\tilde{r},I}^u$ is the maximum value $V_{\tilde{e}}^u(\tilde{e}_e(t))$ is reset to. Given the same sets of closed-loop dynamics, the selection on both parameters ultimately depends on the communication radius R_{com} as discussed subsequently.

Remark 5.1. If the drift dynamic is not present, i.e., $f_r \equiv 0_{n\times 1}$ and the constant $\lambda_e^u \equiv 0$, the condition in (5–18) may be further simplified. Utilizing L'Hôpital's Rule, (5–19) can be

rewritten when λ_e^u approaches zero as

$$
\begin{aligned}
\lim_{\lambda_e^u \to 0} V_{\tilde{e}}^u(\tilde{e}_e(t)) &\leq \lim_{\lambda_e^u \to 0} V_{\tilde{e}}^u(\tilde{e}_e(t_{e,j}^a)) e^{\lambda_e^u \Delta t_{e,j}^u} - \lim_{\lambda_e^u \to 0} \frac{\delta_e^u}{\lambda_e^u} \left(1 - e^{\lambda_e^u \Delta t_{e,j}^u}\right), \\
&\leq V_{\tilde{e}}^u(\tilde{e}_e(t_{e,j}^a)) + \delta_e^u \Delta t_{e,j}^a.
\end{aligned}
$$

Then, $V_{\tilde{e}}^u(\tilde{e}_e(t)) \leq V_{\tilde{r},I}^u + \delta_e^u \Delta t_{e,j}^a$, and hence $\Delta t_{e,j}^u \leq \frac{V_{\tilde{e},M}^u - V_{\tilde{r},I}^u}{\delta_e^u}$.

Based on the dwell-time condition in (5–18), it can then be shown that $e_e(t)$ is upper bounded by a constant.

Theorem 5.3. *The piece-wise constant, right-continuous switching signal $\sigma_e : [0, \infty) \to p_e \in \{a_e, u_e\}$ abiding by the maximum loss of feedback dwell-time condition in Theorem 5.2 ensures $\|e_e(t)\|$ is globally uniformly ultimately bounded.*

Proof. Consider a single cycle of the jth activation of $p_e = u_e$, where $j \in \mathbb{N}$. By solving the general solution to (5–13),

$$
V_{\hat{e}}^u(\hat{e}_e(t)) \leq V_{\hat{e}}^u(\hat{e}_e(t_{e,j}^a)) e^{-\lambda_e^a(t - t_{e,j}^a)}, \ \forall t \in [t_{e,j}^a, t_{e,j+1}^a). \tag{5–20}
$$

Let a composite candidate Lyapunov-like functional be defined as

$$
V_e^u(\hat{e}_e(t), \tilde{e}_e(t)) \triangleq V_{\hat{e}}^u(\hat{e}_e(t)) + V_{\tilde{e}}^u(\tilde{e}_e(t)). \tag{5–21}
$$

Then, the upper bound of (5–21) may be written as $V_e^u(e_e(t)) \leq$ $V_{\hat{e}}^u(\hat{e}_e(t_{e,j}^a)) e^{-\lambda_e^a(t - t_{e,j}^a)} + \left(V_{\tilde{e}}^u(\tilde{e}_e(t_{e,j}^a)) + \frac{\delta_e^u}{\lambda_e^u}\right) e^{\lambda_e^u(t - t_{e,j}^a)} - \frac{\delta_e^u}{\lambda_e^u}, \ \forall t \in [t_{e,j}^a, t_{e,j+1}^a).$ Utilizing the fact that $\left(V_{\tilde{e}}^u(\tilde{e}_e(t_{e,j}^a)) + \frac{\delta_e^u}{\lambda_e^u}\right) e^{\lambda_e^u(t - t_{e,j}^a)} - \frac{\delta_e^u}{\lambda_e^u} \leq V_{\tilde{e},M}^u, \ V_e^u(e_e(t)) \leq$ $V_{\hat{e}}^u(\hat{e}_e(t_{e,j}^a)) e^{-\lambda_e^a(t - t_{e,j}^a)} + V_{\tilde{e},M}^u.$ The change in $V_e^u(e_e(t))$ over the cycle is derived as $V_e^u(e_e(t_{e,j+1}^{a-})) - V_e^u(e_e(t_{e,j}^a)) \leq V_{\hat{e}}^u(\hat{e}_e(t_{e,j}^a)) \left(e^{-\lambda_e^a \Delta t_{e,j}^a} - 1\right) + V_{\tilde{e},M}^u - V_{\tilde{r},I}^u.$ Therefore, $V_e^u(e_e(t))$ proportionally decreases over a single cycle if $V_{\hat{e}}^u(\hat{e}_e(t_{e,j}^a)) > \frac{V_{\tilde{r},I}^u - V_{\tilde{e},M}^u}{1 - \exp(-\lambda_e^a \Delta t_{e,j}^u)}$, increases if $V_{\hat{e}}^u(\hat{e}_e(t_{e,j}^a)) < \frac{V_{\tilde{r},I}^u - V_{\tilde{e},M}^u}{1 - \exp(-\lambda_e^a \Delta t_{e,j}^u)}$, and remains constant if $V_{\hat{e}}^u(\hat{e}_e(t_{e,j}^a)) = \frac{V_{\tilde{r},I}^u - V_{\tilde{e},M}^u}{1 - \exp(-\lambda_e^a \Delta t_{e,j}^u)}$. Since $j \in \mathbb{N}$ and the dwell-time interval is arbitrary, the result holds for all j and dwell-time intervals. Therefore, it can be shown that $V_{\hat{e}}^u(\hat{e}_e(t_{e,j}^a))$ approaches

$\frac{V_{\tilde{r},I}^u - V_{\tilde{e},M}^u}{1 - \exp\left(-\lambda_e^a \Delta t_{e,j}^u\right)}$ as $t \to \infty$ and that $\|\hat{e}_e(t)\|$ is bounded. Combined with the result from Theorem 5.2, it can be shown that $\|e_e(t)\| \leq \|\hat{e}_e(t)\| + \|\tilde{e}_e(t)\|$ is also bounded. $\quad\square$

In Theorem 5.3, the norm of the tracking error $\|e_e(t)\|$ is proven to be bounded. However, the bound may be large. For most applications, it is desirable to allow the user to prescribe an upper bound such that $\|e_e(t)\| \leq \|\hat{e}_e(t)\| + \|\tilde{e}_e(t)\| \leq e_{e,M} \in \mathbb{R}_{>0}$. Therefore, a controller gain selection rule is provided in the following theorem.

Theorem 5.4. *The piece-wise constant, right-continuous switching signal $\sigma_e : [0, \infty) \to p_e \in \{a_e, u_e\}$ abiding by the maximum loss of feedback dwell-time condition in Theorem 5.2 ensures $\|e_e(t)\|$ is globally uniformly ultimately bounded by $e_{e,M}$, provided the controller gains are selected such that*

$$\lambda_e^a \geq -\frac{1}{\Delta t_{e,j}^u} \ln\left(\frac{V_{\hat{e}}^u(e_{e,M} - \tilde{e}_{e,M}) + V_{\tilde{r},I}^u - V_{\tilde{e},M}^u}{V_{\hat{e}}^u(e_{e,M} - \tilde{e}_{e,M})}\right), \tag{5–22}$$

where $e_{e,M}$ is selected such that $V_{\hat{e}}^u(e_{e,M} - \tilde{e}_{e,M}) \geq V_{\tilde{r},I} - V_{\tilde{e},M}^u$.

Proof. By combining (5–19) with (5–20), $V_e^u(e_e(t))$ defined in (5–21) may be upper bounded by $V_e^u(e_e(t)) \leq V_{\hat{e}}^u\left(\hat{e}_e\left(t_{e,j}^a\right)\right) e^{-\lambda_e^a\left(t - t_{e,j}^a\right)} + \left(V_{\tilde{e}}^u\left(\tilde{e}_e\left(t_{e,j}^a\right)\right) + \frac{\delta_e^u}{\lambda_e^u}\right) e^{\lambda_e^u\left(t - t_{e,j}^a\right)} - \frac{\delta_e^u}{\lambda_e^u}$, $\forall j \in \mathbb{N}$, $\forall t \in [t_{e,j}^a, t_{e,j+1}^a)$. After substituting in (5–18) and (5–22), the bound on $V_e^u(e_e(t_{e,j+1}^a))$ becomes $V_e^u\left(e_e\left(t_{e,j+1}^a\right)\right) \leq V_{\hat{e}}^u\left(\hat{e}_e\left(t_{e,j}^a\right)\right) \left(\frac{V_{e,M}^u - V_{\tilde{e},M}^u}{V_{\hat{e}}^u(e_{e,M} - \tilde{e}_{e,M})}\right) + V_{\tilde{e},M}^u$, $\forall j \in \mathbb{N}$. Utilizing the fact that $V_e^u\left(e_e\left(t_{e,j}^a\right)\right) \leq V_{\hat{e}}^u\left(\hat{e}_e\left(t_{e,j}^a\right)\right) + V_{\tilde{r},I}^u$, the change in $V_e^u(e_e(t))$ over a single cycle is bounded by $V_e^u\left(e_e\left(t_{e,j+1}^{a-}\right)\right) - V_e^u\left(e_e\left(t_{e,j}^a\right)\right) \leq \frac{V_{\hat{e}}^u(e_{e,M} - \tilde{e}_{e,M}) + V_{\tilde{r},I}^u - V_{\tilde{e},M}^u}{V_{\hat{e}}^u(e_{e,M} - \tilde{e}_{e,M})} \left(V_{\hat{e}}^u\left(\hat{e}_e\left(t_{e,j}^a\right)\right)\right) + V_{\tilde{e},M}^u - \left(V_{\hat{e}}^u\left(\hat{e}_e\left(t_{e,j}^a\right)\right) + V_{\tilde{r},I}^u\right)$, which becomes $V_e^u\left(t_{e,j+1}^{a-}\right) - V_e^u\left(t_{e,j}^a\right) \leq \left(1 - \frac{V_{\hat{e}}^u\left(\hat{e}_e\left(t_{e,j}^a\right)\right)}{V_{\hat{e}}^u(e_{e,M} - \tilde{e}_{e,M})}\right)\left(V_{\tilde{e},M}^u - V_{\tilde{r},I}^u\right)$. Therefore, over a single cycle, $V_e^u(e_e(t))$ decreases if $V_{\hat{e}}^u\left(\hat{e}_e\left(t_{e,j}^a\right)\right) > V_{\hat{e}}^u(e_{e,M} - \tilde{e}_{e,M})$, increases if $V_{\hat{e}}^u\left(\hat{e}_e\left(t_{e,j}^a\right)\right) < V_{\hat{e}}^u(e_{e,M} - \tilde{e}_{e,M})$, and remains constant if $V_{\hat{e}}^u\left(\hat{e}_e\left(t_{e,j}^a\right)\right) = V_{\hat{e}}^u(e_{e,M} - \tilde{e}_{e,M})$. Since $V_{\hat{e}}^u\left(\hat{e}_e\left(t_{e,j}^a\right)\right)$ approaches $V_{\hat{e}}^u(e_{e,M} - \tilde{e}_{e,M})$ as $t \to \infty$, $\|\hat{e}_e\left(t_{e,j}^a\right)\|$ approaches $e_{e,M} - \tilde{e}_{e,M}$, and hence, $\|e_e\left(t_{e,j}^a\right)\|$ approaches $e_{e,M}$ as $t \to \infty$. $\quad\square$

5.4 Design Example

In this section, an example of applying Theorems 5.1-5.4 is presented. Consider an unmanned ground vehicle (UGV) as the exploring agent and an unmanned airborne vehicle (UAV) as the relay agent, both equipped with velocity and bearing measurement units. Specifically, a two-wheeled mobile robot serves as the UGV while a quadcopter serves as the UAV.

5.4.1 Relay Agent

To control the UAV, a single-layer neural network will be used to learn the drift dynamics. Let $x_r(t) = [x_{rx}(t), x_{ry}(t), x_{r\theta}(t)] \in \mathbb{R}^3$ denote the UAV's Euclidean coordinate and yaw. The UAV is assumed to operate at a fixed height, and hence the control on altitude is not considered. Under Assumption 5.2 and Assumption 5.3, the Universal Function Approximation Theorem (cf. [80, 81]) may be invoked to approximate the drift dynamics as

$$f_r(x_r(t)) \triangleq W^T \sigma(x_r(t)) + \varepsilon(x_r(t)) \tag{5–23}$$

and

$$\hat{f}_r(\hat{x}_r(t)) \triangleq \hat{W}^T(t)\, \sigma(\hat{x}_r(t)), \tag{5–24}$$

where $W, \hat{W}(t) \in \mathbb{R}^{L \times 3}$ are the ideal and estimated weights, $\sigma : \mathbb{R}^3 \to \mathbb{R}^L$ is the activation function, $\varepsilon : \mathbb{R}^3 \to \mathbb{R}^3$ is the function approximation error bounded by $\bar{\varepsilon} \in \mathbb{R}^3$, and $L \in \mathbb{N}$ is the number of activation functions in the neural network. Hence, the error between the ideal and estimated weights is defined as

$$\tilde{W}(t) \triangleq W - \hat{W}(t). \tag{5–25}$$

Based on (5–23), the dynamics in (5–2) can be expressed as

$$\dot{x}_r(t) = W^T \sigma(x_r(t)) + v_r(x_r(t), t) + \varepsilon(x_r(t)) + d_r(t), \qquad (5\text{–}26)$$

Consider the neural network controller designed as

$$v_r(x_p(t), t) \triangleq \dot{x}_{aux}(t) - \hat{W}^T(t)\sigma(x_p(t))$$
$$- \left(k_r + \frac{(\bar{\varepsilon} + \bar{d}_r)^2}{\epsilon}\right)(x_p(t) - x_{aux}(t)), \qquad (5\text{–}27)$$

where $x_p(t) = x_r(t)$ when $p_r = a_r$ and $x_p(t) = \hat{x}_r(t)$ when $p_r = u_r$, $k_r \in \mathbb{R}^{3\times3}$ is a constant, positive-definite gain matrix, x_{aux} and $\dot{x}_{aux}$ are subsequently designed, and $\epsilon \in (0, 1]$ is a design parameter. In (5–27), the design structure remains the same for all $p_r \in \mathscr{S}_r$, where only the input signal switches between using $x_r(t)$ and $\hat{x}_r(t)$. The state estimate update law is designed as

$$\dot{\hat{x}}_r(t) \triangleq \hat{W}^T(t)\sigma(\hat{x}_r(t)) + v_r(x_o(t), t). \qquad (5\text{–}28)$$

Based on an integral concurrent learning approach described in [82], the parameter estimation update law is given as

$$\dot{\hat{W}}(t) \triangleq \begin{cases} proj(\Gamma\sigma(x_r(t)) e_r^T(t)), & p_r = a_r \wedge t < T, \\ 0_{L\times3}, & p_r = u_r \wedge t < T, \\ proj(\Gamma\sigma(x_r(t)) e_r^T(t) + k_{CL}\Gamma G), & p_r = a_r \wedge t \geq T, \\ proj(k_{CL}\Gamma G), & p_r = u_r \wedge t \geq T, \end{cases} \qquad (5\text{–}29)$$

where $proj(\cdot)$ is a smooth projection operator (e.g., [67] and [68]), $G \triangleq \sum_{l=1}^{N} \mathcal{Y}_l \left(\int_{t_l-\Delta t}^{t_l}\left(\dot{x}_r^T(\tau) - v_r^T(x_r(\tau), \tau)\right)d\tau - \mathcal{Y}_l^T\hat{W}(t)\right) \in \mathbb{R}^{L\times3}$, $t_l \in [t_0 + \Delta t, t]$, $\Gamma \in \mathbb{R}^{L\times L}$ is a constant, positive definite diagonal gain matrix, $k_{CL} \in \mathbb{R}_{>0}$ is a constant, positive gain, $\Delta t \in \mathbb{R}_{>0}$ is the integration window, and $\mathcal{Y}_l$ is the regressor for $\int_{t_l-\Delta t}^{t_l}\sigma(x_r(\tau))d\tau$.

Specifically, the history stacks are collected and updated using the method provided in [75, 83] whenever the relay agent is inside the feedback-available region, and remains the same throughout $\Delta t_{r,i}^u$, $\forall i \in \mathbb{N}$.

Assumption 5.6. The system of the relay agent is sufficiently excited over a finite duration of time. Specifically, there exists a $\underline{\lambda} \in \mathbb{R}_{>0}$ and $T \in \mathbb{R}_{>\Delta t}$ such that the minimum eigenvalue of $\sum_{l=1}^N \mathcal{Y}_l \mathcal{Y}_l^T \geq \underline{\lambda}$, $\forall t \geq T$.

Assumption 5.7. The bound on the ideal weights is known, such that $\left\| W - \hat{W}(t) \right\| \leq \bar{W}$.

After taking the time derivative of (5–6)-(5–8) and substituting in (5–2) and (5–23)-(5–29), the following closed-loop error dynamics are obtained

$$\dot{e}_r(t) = -\bar{k}_r e_r(t) + \tilde{W}^T \sigma(x_r(t)) + \varepsilon(x_r(t)) + d_r(t), \; p_r = a_r, \tag{5–30}$$

$$\dot{\hat{e}}_r(t) = -\bar{k}_r \hat{e}_r(t), \; p_r = u_r, \tag{5–31}$$

$$\dot{\tilde{e}}_r(t) = W^T \sigma(x_r(t)) - \hat{W}^T(t)\sigma(\hat{x}_r(t)) + \varepsilon(x_r(t)) + d_r(t), \; p_r = u_r, \tag{5–32}$$

where $\bar{k}_r \triangleq \left(k_r + \frac{(\bar{\varepsilon}+\bar{d}_r)^2}{\epsilon} \right) \in \mathbb{R}_{>0}$.

When $p_r = a_r$, a candidate Lyapunov-like functional is selected

$$V_\zeta^a(\zeta_r(t)) \triangleq \frac{1}{2} e_r^T(t) e_r(t) + \frac{1}{2} tr\left(\tilde{W}^T(t) \Gamma^{-1} \tilde{W}(t) \right). \tag{5–33}$$

where $\zeta_r(t) \triangleq \left[e_r^T(t), vec(\tilde{W}^T(t)) \right]^T$ and $vec(\cdot)$ is the vectorization operator. Based on Assumption 5.6 and the update law design in (5–29), taking the time-derivative of (5–33), and substituting in (5–30), (5–32) and (5–29) yield

$$\dot{V}_\zeta^a(\zeta_r(t)) \leq -k_r \|e_r(t)\|^2 + \epsilon, \tag{5–34}$$

$\forall t \in [t_{r,i}^a, t_{r,i}^u) < T,\ \forall i \in \mathbb{N}$, and

$$\dot{V}_\zeta^a(\zeta_r(t)) \leq - k_r \|e_r(t)\|^2 - k_{CL}\lambda_{min} tr\left(\tilde{W}^T(t)\tilde{W}(t)\right) + \delta_r^a$$

$$\leq - \lambda_r^a V_\zeta^a(\zeta_r(t)) + \delta_r^a, \tag{5–35}$$

$\forall t \in [t_{r,i}^a, t_{r,i}^u) \geq T,\ \forall i \in \mathbb{N}$, where $\lambda_r^a \triangleq 2\min(k_r, k_{CL}\lambda_{min})$, $0 < \lambda_{min} \in \mathbb{R}$ is the minimum eigenvalue of $\sum_{l=1}^N \mathcal{Y}_l \mathcal{Y}_l^T$, and $\delta_r^a \triangleq \|k_{CL}\sum_{l=1}^N \int_{t_l-\Delta t}^{t_l}\left(\varepsilon^T(x_r(\tau)) + d_r^T(\tau)\right)d\tau \tilde{W}^T(t)\mathcal{Y}_l\| + \epsilon$. Therefore, (5–10) from Assumption 5.5 is satisfied.

When $p_r = u_r$, three candidate Lyapunov-like functionals are selected as

$$V_{\hat{r}}^u(\hat{e}_r(t)) \triangleq \frac{1}{2}\hat{e}_r^T(t)\hat{e}_r(t), \tag{5–36}$$

$$V_{\tilde{r}}^u(\tilde{e}_r(t)) \triangleq \|\tilde{e}_r(t)\|, \tag{5–37}$$

$$V_{\tilde{W}}^u(\tilde{W}(t)) \triangleq \frac{1}{2}tr\left(\tilde{W}^T(t)\Gamma^{-1}\tilde{W}(t)\right). \tag{5–38}$$

After taking the time-derivatives of (5–36)-(5–38) and substituting in (5–31)-(5–29) yields

$$\dot{V}_{\hat{r}}^u(\hat{e}_r(t)) \leq -\bar{k}_r\|\hat{e}_r(t)\|^2, \tag{5–39}$$

$$\dot{V}_{\tilde{r}}^u(\tilde{e}_r(t)) \leq c_1\|\tilde{e}_r(t)\| + \bar{\varepsilon} + \bar{d}_r + \left\|\tilde{W}(t)\right\|(c_2\|\hat{e}_r(t)\| + c_3), \tag{5–40}$$

$$\dot{V}_{\tilde{W}}^u(\tilde{W}(t)) \leq \begin{cases} 0, & \forall t < T, \\ -k_{CL}\lambda_{min}tr\left(\tilde{W}^T(t)\tilde{W}(t)\right) + c_4 & \forall t \geq T, \end{cases} \tag{5–41}$$

where c_1, $c_2 \in \mathbb{R}$ are known, positive constants, $c_3 \in \mathbb{R}$ is the maximum bound on $\sigma(x_\sigma(t))$, and $c_4 \triangleq \left\|k_{CL}\sum_{i=1}^N \int_{t_l-\Delta t}^{t_l}\left(\varepsilon^T(x_r(\tau)) + d_r^T(\tau)\right)d\tau \tilde{W}^T\mathcal{Y}_i\right\|$. The generalized solutions to (5–39) and (5–41) can be derived as

$$V_{\hat{r}}^u(\hat{e}_r(t)) \leq V_{\hat{r}}^u(\hat{e}_r(t_{r,i}^u))e^{-2\bar{k}_r\left(t-t_i^u\right)}, \tag{5–42}$$

$$V_{\tilde{W}}^u(\tilde{W}(t)) \leq \begin{cases} V_{\tilde{W}}^u(\bar{W}), & \forall t < T, \\ \delta_W + \left(V_{\tilde{W}}^u(\bar{W}) - \delta_W\right) e^{-k_{CL}\lambda_{min}(t-T)}, & \forall t \geq T, \end{cases} \tag{5–43}$$

where $\delta_W \triangleq \frac{c_4}{k_{CL}\lambda_{min}}$. Based on (5–42), (5–43) and the projection algorithm, $\|\hat{e}_r(t)\|$ and $\|\tilde{W}(t)\|$ can be upper bounded by

$$\|\hat{e}_r(t)\| \leq \left\|\hat{e}_r(t_{r,i}^u)\right\| e^{-\bar{k}_r\left(t-t_{r,i}^u\right)}, \tag{5–44}$$

$$\left\|\tilde{W}(t)\right\| \leq \begin{cases} \bar{W}, & \forall t < T, \\ \sqrt{V_{\tilde{W}}^u(\tilde{W}(t))}, & \forall t \geq T, \end{cases} \tag{5–45}$$

By substituting (5–44) and (5–45) into (5–40) yields

$$\dot{V}_{\tilde{r}}^u(\tilde{e}_r(t)) \leq c_1 \|\tilde{e}_r(t)\| + \bar{\varepsilon} + \bar{d}_r + \left\|\tilde{W}(t_{r,i}^u)\right\| \left(c_2 \left\|\hat{e}_r(t_{r,i}^u)\right\| + c_3\right),$$

$$\leq \lambda_r^u V_{\tilde{r}}^u(\tilde{e}_r(t)) + \delta_{r,}^u \tag{5–46}$$

where $\delta_r^u = \|\tilde{W}(t_{r,i}^u)\| \left(c_2 \left\|\hat{e}_r(t_{r,i}^u)\right\| + c_3\right) + \bar{\varepsilon} + \bar{d}_r$ and $\lambda_r^u = c_1$. From here, Equation 5–13 from Assumption 5.5 is satisfied, and hence, Theorem 5.1 may be applied to obtain the dwell-time conditions for the UGV. Based on Assumption 5.6, Assumption 5.7, and the update law design in (5–29), $\left\|\tilde{W}(t_{r,i}^u)\right\| \leq \bar{W}, \forall t < T$ and $\left\|\tilde{W}(t_{r,i}^u)\right\| \leq \sqrt{\left(V_{\tilde{W}}^u(\bar{W}) - \delta_W\right) e^{-k_{CL}\lambda_{min}(t-T)} + \delta_W}, \forall t \geq T$. This implies that after a finite time of excitation, the maximum dwell-time condition in (5–15) is relaxed as the $\tilde{W}(t) \to \sqrt{\delta_W}$.

5.4.2 Exploring Agent

Consider a two-wheeled mobile robot serving as the exploring agent. A unicycle model with an exogenous disturbance is assumed for the UGV as

$$\dot{q}_e\left(t\right) \;\triangleq\; \begin{bmatrix} \cos q_{e\theta} & 0 \\[4pt] \sin q_{e\theta} & 0 \\[4pt] 0 & 1 \end{bmatrix} v_e\left(\hat{q}_e\left(t\right)\right) + d_e\left(t\right), \qquad (5\text{--}47)$$

where $q_e\left(t\right) = \left[q_{ex}\left(t\right),\ q_{ey}\left(t\right),\ q_{e\theta}\left(t\right)\right] \in \mathbb{R}^3$ is the two dimensional Euclidean position and orientation of the UGV with respect to the inertial frame and $v_e\left(\hat{q}_e\left(t\right)\right) \in \mathbb{R}^2$ is the control input. A reference trajectory is generated by a reference kinematic model given as

$$\dot{q}_{ref}\left(t\right) \;\triangleq\; \begin{bmatrix} \cos q_{r\theta} & 0 \\[4pt] \sin q_{r\theta} & 0 \\[4pt] 0 & 1 \end{bmatrix} v_{ref}\left(q_{ref}\left(t\right)\right), \qquad (5\text{--}48)$$

where $q_{ref}\left(t\right) = \left[q_{rx}\left(t\right),\ q_{ry}\left(t\right),\ q_{r\theta}\left(t\right)\right] \in \mathbb{R}^3$ and $v_{ref}\left(q_{ref}\left(t\right)\right) \in \mathbb{R}^2$ are the desired Euclidean pose and control input, respectively. The estimate of $q_e\left(t\right)$ is denoted by $\hat{q}_e\left(t\right)$ and its update law is defined as

$$\dot{\hat{q}}_e\left(t\right) \triangleq \begin{bmatrix} \cos q_{e\theta} & 0 \\[4pt] \sin q_{e\theta} & 0 \\[4pt] 0 & 1 \end{bmatrix} v_e\left(\hat{q}_e\left(t\right)\right), \qquad (5\text{--}49)$$

where $q_{e\theta}\left(t\right)$ is assumed to be measurable.

Assumption 5.8. The orientation with respect to the inertial frame, $\theta_e\left(t\right)$, is measurable through on-board measurement units such as a gyroscope or a compass.

Given (5–48) and (5–49), exponentially stable controllers may be implemented from existing literature, such as [84, 85]. Since the stability analysis for the error system $\|\hat{e}_e\left(t\right)\| = \|\hat{q}_e\left(t\right) - q_d\left(t\right)\|$ is identical with a change of variable from $x_e\left(t\right)$ to $\hat{q}_e\left(t\right)$ and $x_d\left(t\right)$ to $q_d\left(t\right)$, it has been omitted to avoid redundancy. To satisfy Assumption 5.5, select a candidate Lyapunov-like function $V_{\tilde{e}}^u\left(\tilde{e}_e\left(t\right)\right) \triangleq \|\tilde{e}_e\left(t\right)\|$. By taking time derivative of

$V_{\tilde{e}}^{u}\left(\tilde{e}_e\left(t\right)\right)$ and substituting in (5–47) and (5–49) yield,

$$
\begin{aligned}
\dot{V}_{\tilde{e}}^{u}\left(\tilde{e}_e\left(t\right)\right) &\leq \|\dot{\tilde{e}}_e\left(t\right)\|, \\
&\leq \bar{d}_e\left(t\right).
\end{aligned}
$$

Therefore, (5–14) in Assumption 5.5 is satisfied. Along with the selection on $\tilde{e}_{e,M}$, Theorem 5.2 may be invoked to yield the dwell-time condition. Then, the control gain for the exploring agent can be determined by selecting a desired bound, $e_{e,M}$, and applying Theorem 5.4. Specifically, the selections on $\tilde{e}_{r,I}$ and $\tilde{e}_{e,M}$ must obey the relationship of $\tilde{e}_{r,I} + \tilde{e}_{e,M} + \|\hat{x}_e - \hat{x}_r\| \leq R_{com}$ because $\|x_r\left(t\right) - x_e\left(t\right)\| = \|x_r\left(t\right) - \hat{x}_r\left(t\right) - x_e\left(t\right) + \hat{x}_e\left(t\right) + \hat{x}_r\left(t\right) - \hat{x}_e\left(t\right)\| \leq \|x_r\left(t\right) - \hat{x}_r\left(t\right)\| + \|x_e\left(t\right) - \hat{x}_e\left(t\right)\| + \|\hat{x}_e\left(t\right) - \hat{x}_r\left(t\right)\|$, which must be less than R_{com} at $t = t_{e,j}^a$. However $\|\hat{x}_e\left(t\right) - \hat{x}_r\left(t\right)\|$ may be made arbitrarily small (including zero) by utilizing an auxiliary trajectory design as illustrated in the following subsection.

5.4.3 Auxiliary Trajectory

An auxiliary trajectory $x_{aux}\left(t\right)$ is designed for the relay agent to track so that $x_r\left(t\right)$ may reach $x_e(t)$ within the given dwell-time conditions in (5–15) such that $\|x_r\left(t\right) - x_e\left(t\right)\| \leq R_{com}$. While $x_r\left(t\right) \in \mathcal{F}^c$, $\|e_r\left(t\right)\|$ can be upper bounded by $\tilde{e}_{r,T}$ when the maximum dwell-time condition in (5–15) is reached, implying that there exists a bounded set $\mathcal{B} = \{z \in \mathbb{R}^2 | \|z - x_{aux}\left(t\right)\| \leq \tilde{e}_{r,T}\}$ such that $x_r\left(t\right) \in \mathcal{B}$, $\forall t$. In this case, let $\mathcal{A}$ be defined as the compact set of the inscribed ball of $\mathcal{F}$, $\tilde{e}_{r,T}$ be equal to its radius, and x_ϵ be defined as the center of $\mathcal{A}$. Therefore, the requirement of $x_r\left(t\right) \in \mathcal{B} \subseteq \mathcal{F}$ can be satisfied if $x_{aux}\left(t\right)$ coincides with x_ϵ when the maximum dwell-time is reached.

To illustrate the design of the auxiliary trajectory, an example of $x_{aux}\left(t\right)$ is given as

$$
x_{aux}\left(t\right) \triangleq \begin{cases} \rho_1 \hat{x}_r\left(t_{e,j}^a - t_{r,i}^a\right)\left(t\right) + \left(1 - \rho_1\right)\hat{x}_e\left(t\right), & \forall t \in \left[t_{e,j}^a - t_{r,i}^a,\ t_{e,j}^a\right), \\ \rho_2 \hat{x}_r\left(t_{r,i+1}^a - t_{e,j}^a\right) + \left(1 - \rho_2\right)x_\epsilon\left(t\right), & \forall t \in \left[t_{r,i+1}^a - t_{e,j}^a,\ t_{r,i+1}^a\right). \end{cases} \tag{5–50}
$$

where ρ_1, $\rho_2 \in \mathbb{R}$ are time-based ratios designed as $\rho_1 \triangleq \frac{t-t_{r,i}^a}{t_{e,j}^a-t_{r,i}^a}$ and $\rho_2 \triangleq \frac{t-t_{e,j}^a}{t_{r,i+1}^a-t_{e,j}^a}$.

Using this design, $\|\hat{x}_e(t) - \hat{x}_r(t)\| = 0$ at $t = t_{e,j}^a$, the condition for parameter selection, $\tilde{e}_{r,I} + \tilde{e}_{e,M} + \|\hat{x}_e - \hat{x}_r\| \leq R_{com}$, is relaxed. Other transition functions may also be utilized to achieve similar effects, such as the smoother-step function as described in Chapter 4.

5.5 Experimental Results

An experiment is performed to verify the theoretical results and demonstrate the performance of the developed approach. As depicted by Figure 5-1, a region with state feedback, $\mathcal{F} \in \mathbb{R}^2$, is defined by a circle with a radius of 0.6 meters centered at the origin, a desired path, $x_d \subset \mathcal{F}^c \subset \mathbb{R}^2$, is defined by a circular trajectory with a radius of 1.8 meters from the origin, and the communication radius of the relay agent is selected to be 0.6 meters. The overall goal of this experiment is to represent a scenario where a two-wheeled mobile robot is utilized as an exploring agent, tasked with following x_d, while a quadcopter is utilized as the relay agent that services the exploring agent intermittently. Specifically, the objective is to demonstrate the boundedness of the tracking error $e_e(t)$ and verify the results in Theorems 5.1-5.4.

For this experiment, a Parrot Bebop 2.0 quadcopter and a Clearpath Robotics Turtlebot 2 with a Kobuki base are used for the UAV and UGV, respectively. The experimental setup are described in Chapters 3. Although a single ground station is used, the respective control algorithms for the relay and exploring agent are implemented to simulate the behavior and interaction both agents would experience had the algorithms been implemented separately and on-board the agents. State measurements from the motion capture system are made available to the quadcopter whenever the quadcopter is inside the prescribed feedback-available region, and the pose difference between the two agents are utilized whenever the agents are within the communication range of one another (i.e., only the vector $\|x_e(t) - x_r(t)\|$ is made available by Assumption 5.4, rather than the independent measurements of $x_e(t)$ and $x_r(t)$). The measured pose difference
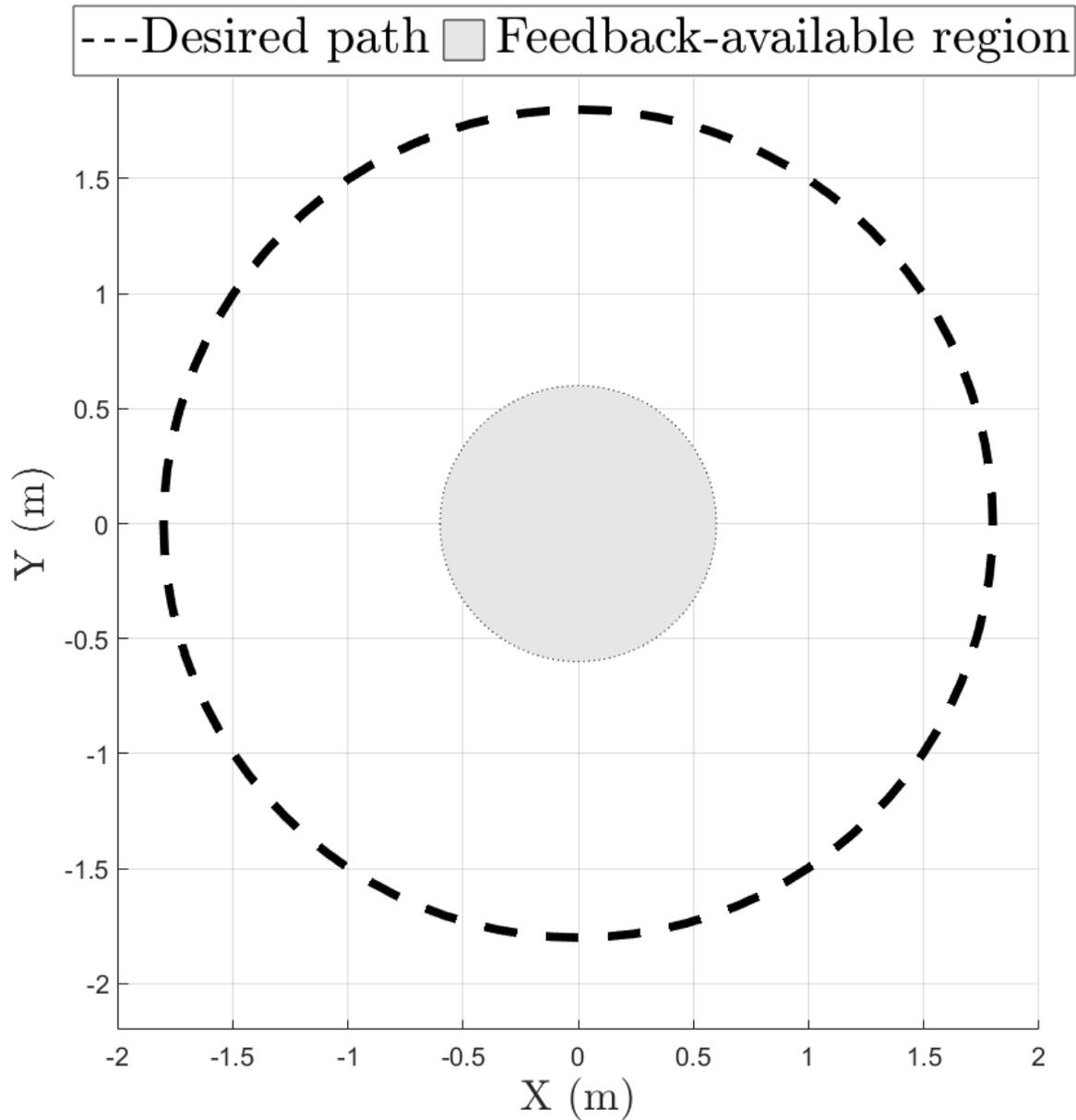
Figure 5-1. A representation of the experimental setup. The gray region denotes the feedback-available region, which is 0.6 meters in radius, and the black dotted line denotes x_d, which is a circular path with a radius of 1.8 meters. As a comparison, the ratio between the radius of the desired path and the feedback-available region is 300%, versus 150% in Chapter 4 (1 meter radius for the feedback-available region and 1.5 meters for the desired circular path).

is then added to the relay agent's estimate of its own pose to generate a reset signal that is communicated to the exploring agent through the WiFi channel.

Dynamics described by (5–26) and (5–47) are used for the relay and exploring agent, respectively, where the control design described by (5–27)-(5–29) are utilized for the relay agent, and the control design in [85] and the estimate update law in (5–49) are implemented for the exploring agent. Specifically, the bound on the disturbances are assume to be $\bar{d}_r = 0.01$ and $\bar{d}_e = 0.0067$, the gain conditions and parameters for the relay agent are selected as $k_r = 0.8I_3$, $\epsilon = 0.01$, $\bar{W} = 2.0$, $k_{CL} = 0.7$, and hyperbolic tangent for the activation function in the neural network. The gain conditions for the exploring agent are selected to match the selections in [85], such that $\lambda_e^a = 0.18$. Based on the experimental scenario, desired error bounds are selected as $\tilde{e}_{e,M} = 0.4$, $\tilde{e}_{r,I} = 0.2$ and $\tilde{e}_{r,M} = 0.6$. The dwell-time conditions resulting from the selected gain conditions and parameters are $\Delta t_{r,i}^u \leq 6.97$ seconds before the relay agent reaches the exploring agent, $\Delta t_{r,i}^u \leq 17.56$ seconds before the relay agent must return to $\mathcal{F}$, and $\Delta t_{e,j}^u \leq 30.0$ seconds between each state estimate update for the exploring agent. Obeying the dwell-time conditions, an auxiliary trajectory is designed to bring the the estimates of the relay agent to and from the exploring agent. The results are shown in Figures 5-3-5-6.

Figure 5-2 demonstrates the overall tracking result from a top-down view of the trajectories generated by the agents. As shown in the figure, the exploring agent is able to follow the prescribed path by a bounded error, and the relay agent is able to service the exploring agent and return to the feedback-available region intermittently. To quantify the performance, Figure 5-3 illustrates the instantaneous values of $\|e_e(t)\|$ with respect to time. Over each state estimate update, $\|e_e(t)\|$ becomes discontinuous due to the use of reset maps. The average path-following error of $\|e_e(t)\|$ is calculated to be 0.1257 meters, which translate to approximately 10.5% in ratio compared to the distance from $\mathcal{F}$. In Figure 5-4, the root-mean-square (RMS) error for $\|\tilde{e}_e(t)\|$ is 0.1429 meters and the peak is bounded below the desired threshold $\tilde{e}_{e,M} = 0.45$ meters.
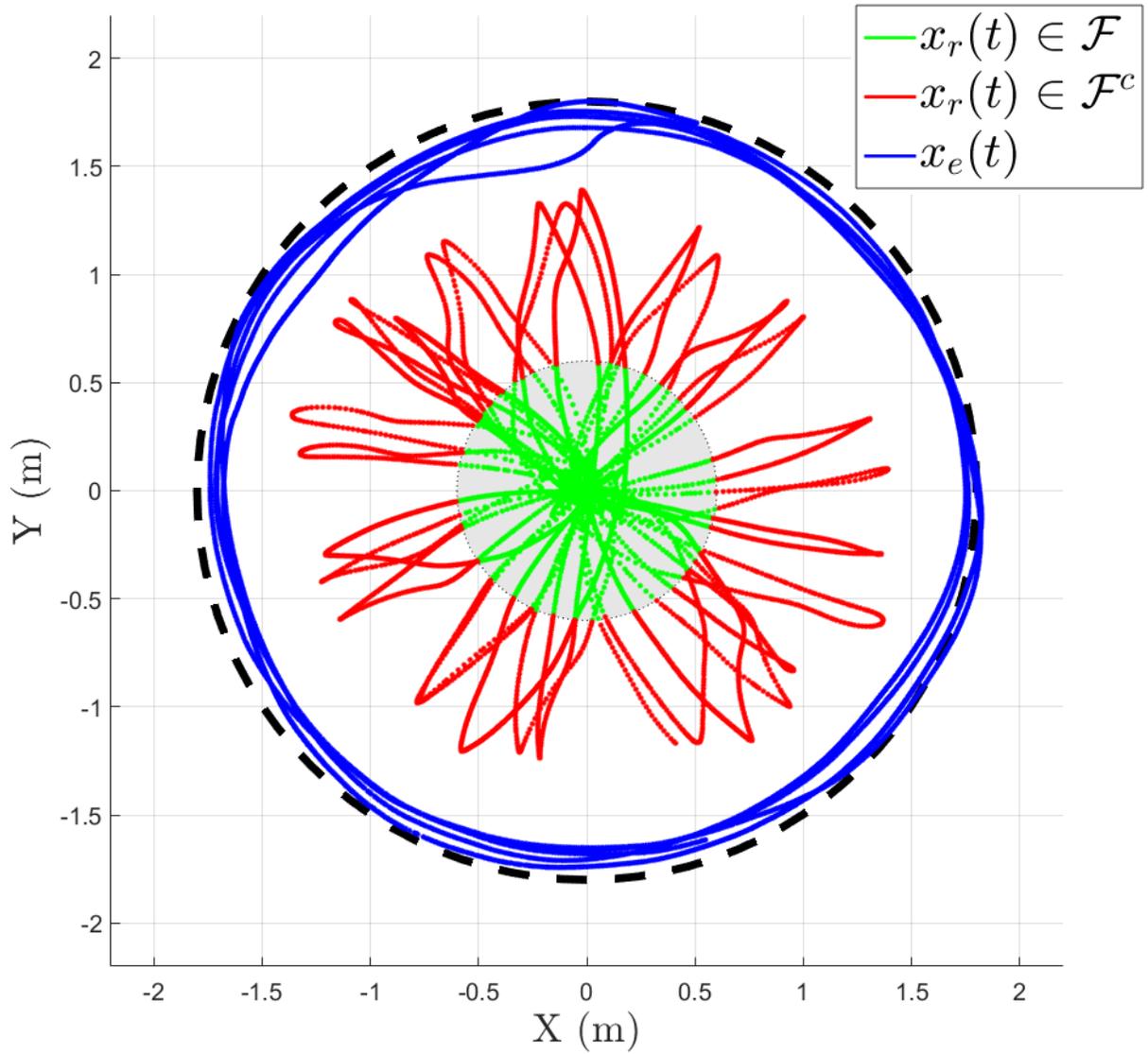
Figure 5-2. The overall tracking result for the relay and exploring agent. The green and red lines denote the trajectories of the relay agent when inside and outside the feedback-available region, respectively. The blue line represents the trajectory of the exploring agent, which is initialized at $(0.5, 1.7)$.
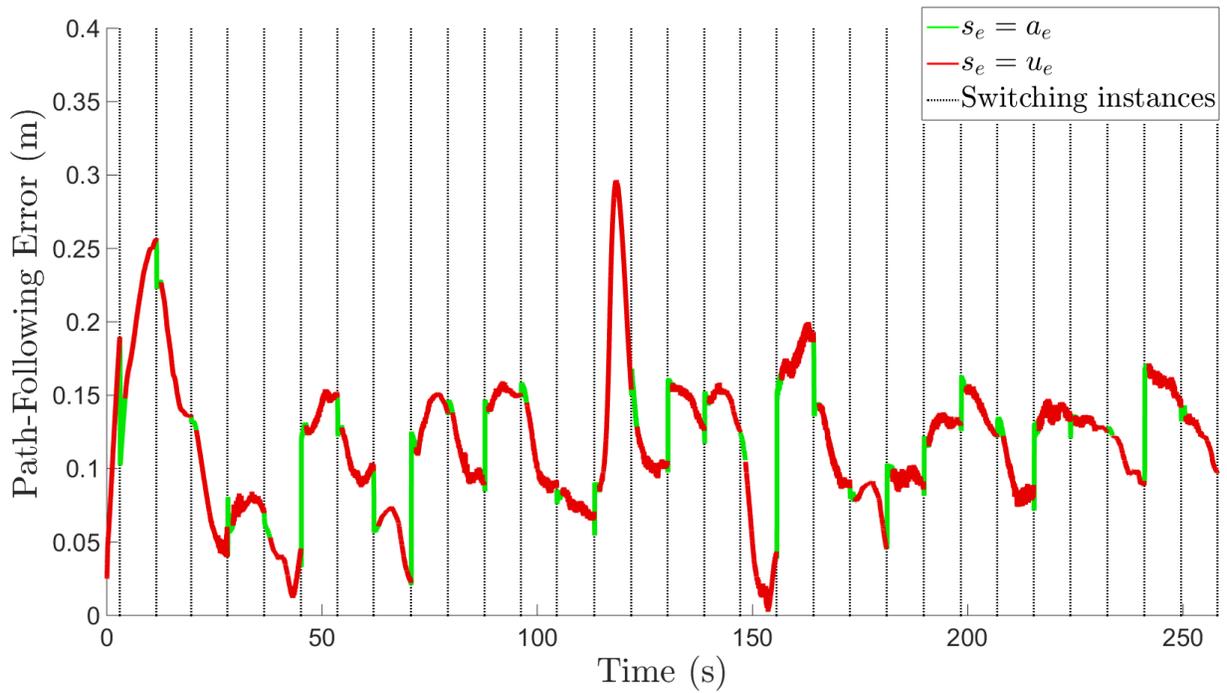
Figure 5-3. The tracking performance plot for $\|e_e(t)\|$. The green and red trajectories denote the change in $\|e_e(t)\|$ when the agents are within and outside the communication range, respectively. The vertical dotted lines denote the time instances when the relay agent transmitted an estimated pose information to the exploring agent (i.e., $t^a_{e,j}$).
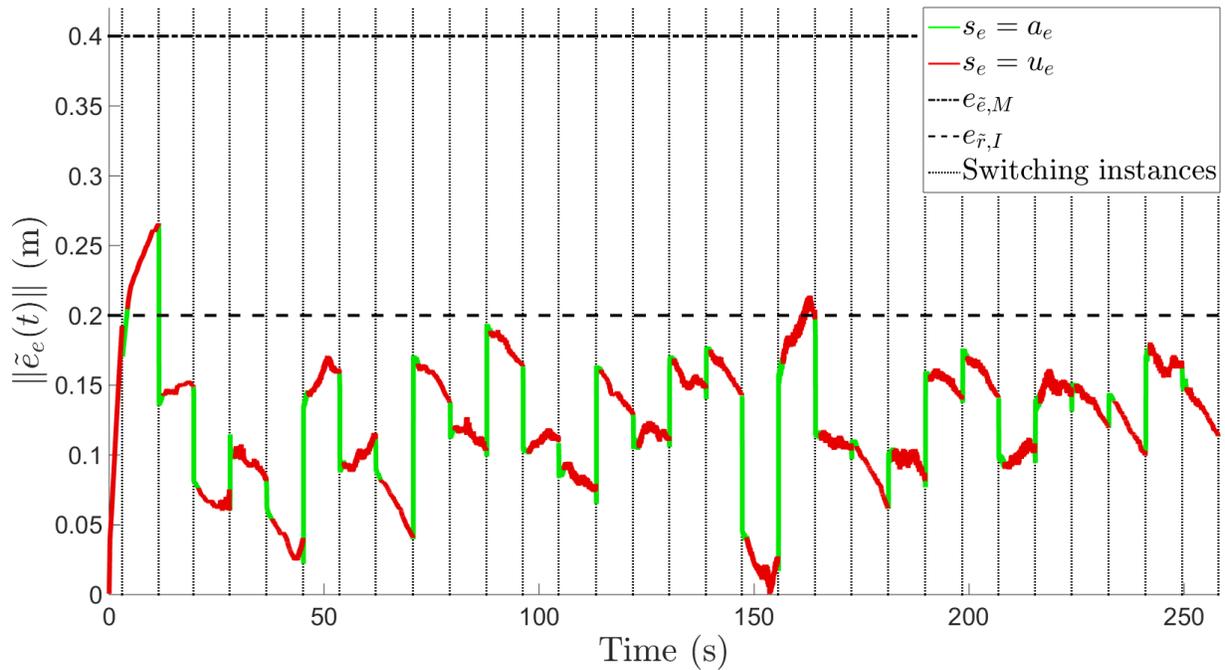
Figure 5-4. The tracking performance plot for $\|\tilde{e}_e(t)\|$. The green and red trajectories denote the change in $\|\tilde{e}_e(t)\|$ when the agents are within and outside the communication range, respectively. The vertical dotted lines denote the time instances when the relay agent transmitted an estimated pose information to the exploring agent (i.e., $t_{e,j}^a$).
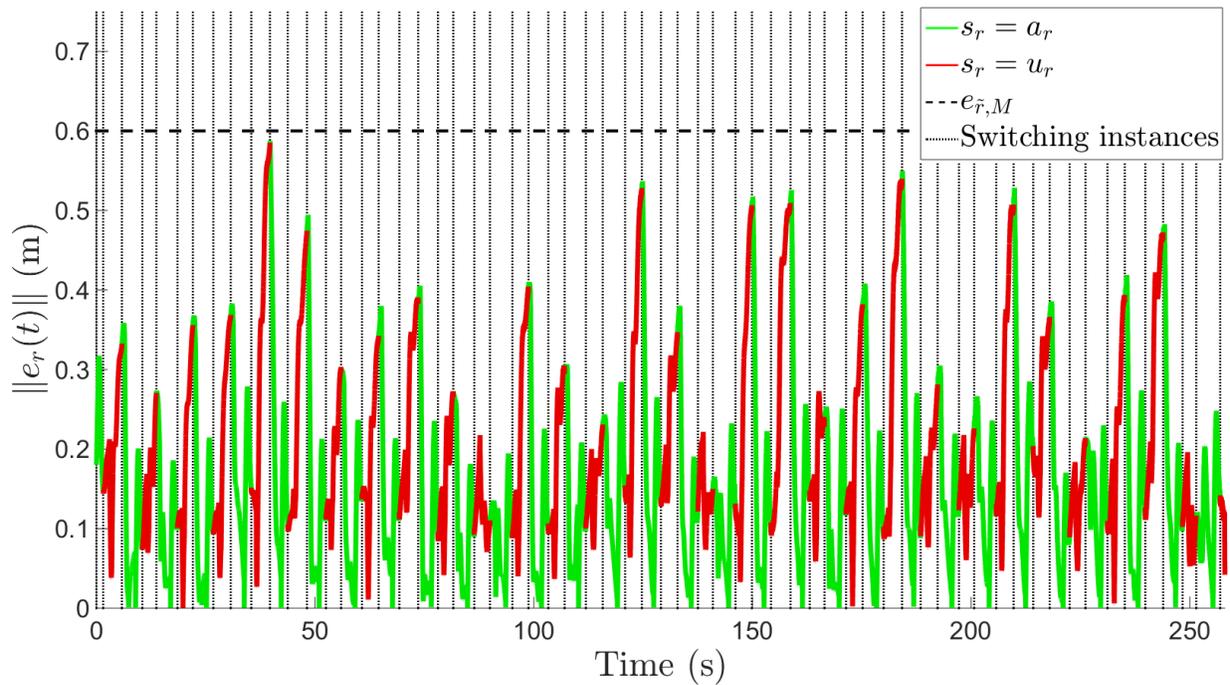
Figure 5-5. The tracking performance plot for $\|e_r(t)\|$. The green and red trajectories denote the change in $\|e_r(t)\|$ when the relay agent is inside and outside the feedback-available region, respectively. The vertical dotted lines denote the time instances when the relay agent crosses the boundaries of the feedback-available region (i.e., $t_{r,i}^a$ and $t_{r,i}^u$).
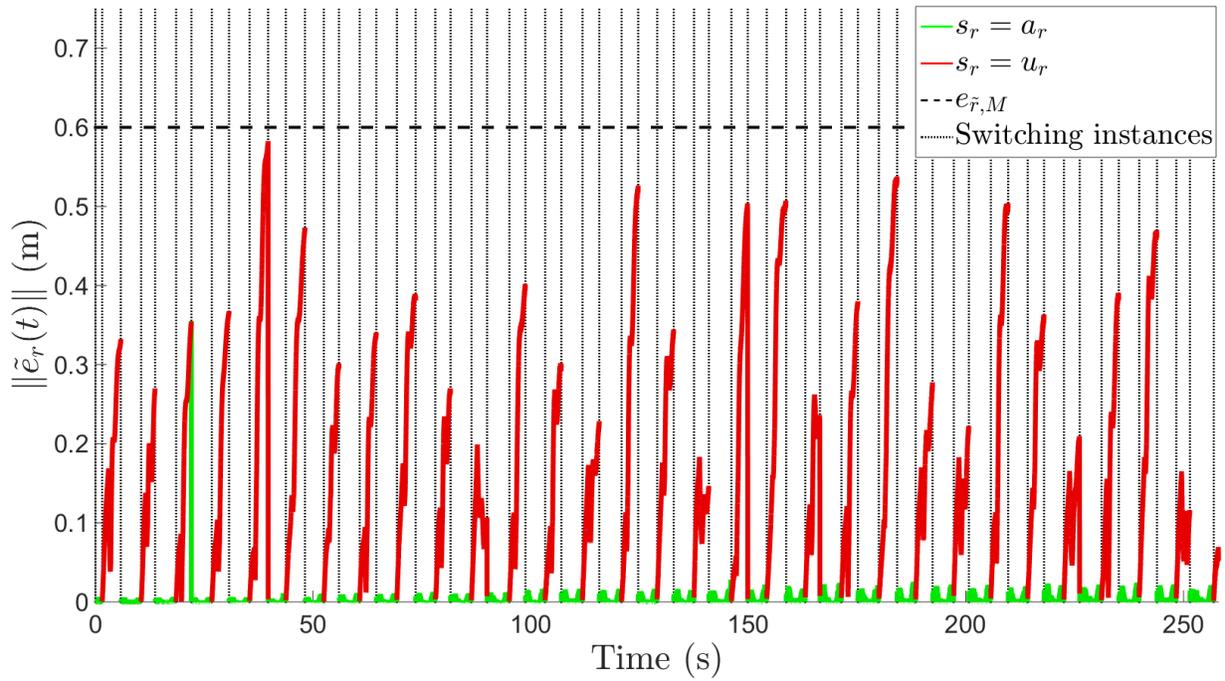
Figure 5-6. The tracking performance plot for $\|\tilde{e}_r(t)\|$. The green and red trajectories denote the change in $\|\tilde{e}_r(t)\|$ when the relay agent is inside and outside the feedback-available region, respectively. The vertical dotted lines denote the time instances when the relay agent crosses the boundaries of the feedback-available region (i.e., $t_{r,i}^a$ and $t_{r,i}^u$).
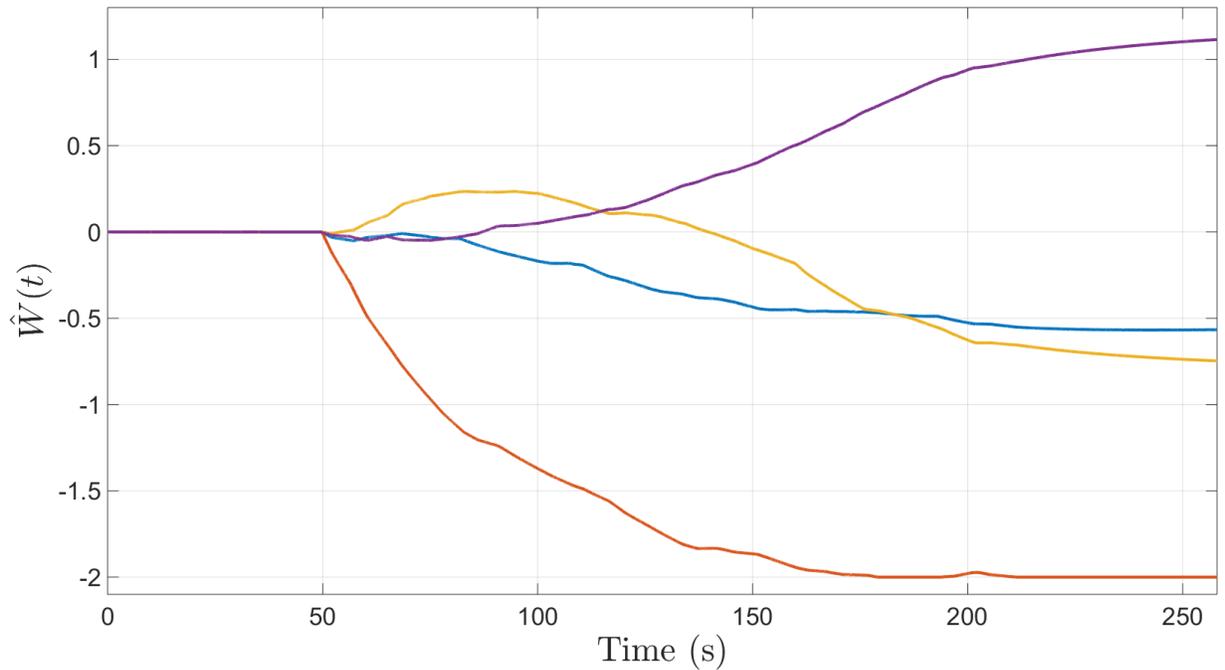

Figure 5-7. The estimated weights of the single-layered neural network.

Figure 5-5 and 5-6 illustrate the tracking error and the state estimation error for the relay agent. As the results indicate, both $\|e_r(t)\|$ and $\|\tilde{e}_r(t)\|$ are bounded above by the desired threshold $\tilde{e}_{r,M} = 0.6$ meters, which is a sufficient condition to ensure stability. The effects of the reset maps can be clearly seen in Figure 5-6 where $\|\tilde{e}_r(t)\|$ is immediately reset to zero upon every entry to the feedback-available region. Figure 5-7 provides an depiction of the change of $\hat{W}(t)$ with respect to time. However, since the ideal weights W are unknown in neural network, an error plot for $\|\tilde{W}(t)\|$ cannot be provided.

Based on the results, the experiment illustrated the performance of the developed method. Compared with the most similar result in [66], the results demonstrated the ability to operate further away from the feedback-available region. Specifically, the ratio between the radius of the desired path and the feedback-available region is 300% in this experiment (1.8 meters versus 0.6 meters), whereas 150% in [66] (1.5 meters versus 1.0 meter). In addition, the path-following error also performs better, where the average over the distance from $\mathcal{F}$ is approximately 10.5% in the developed method versus 34.3% in [66].

Since the calculated maximum dwell-time condition for the exploring agent is 30 seconds, the relay agent will remain in $\mathcal{F}$ for up to 20 seconds because every service cycle is approximately 10 seconds based on the experimental design. To further demonstrate the capability of the developed method, an extended experiment is performed in which three exploring agents are utilized. The gains and parameter selections remains the same from the previous experiment, and the relay agent cycles through the three exploring agents, servicing one agent at a time. The overall tracking result in shown in Figure 5-8. As indicated by 5-8, the exploring agents, whose states are represented by $x_{e1}(t)$, $x_{e2}(t)$ and $x_{e3}(t)$, respectively, are able to converge towards the desired path,

despite being initialized away from the path. The extended experiment further demonstrates the potential applications in formation control and herding problems where a single leader agent and multiple follower agents are involved.

5.6   Summary

A novel method for using a relay agent to assist an exploring agent to path-follow in a state feedback-denied region is presented. Specifically, the exploring agent may remain and operate in the feedback-denied region without having to return to the feedback-available region, while the relay agent intermittently leaves the feedback-available region to update state information for the exploring agent. The relay agent also contains unknown drift dynamics, and a neural-network-based learning method is utilized to approximate the drift dynamics. Both the exploring and relay agent rely on a state predictor to generate state estimates while outside the feedback-available region. Through a Lyapunov-based switched systems analysis, dwell-time conditions for the relay and exploring agent are developed. Provided that the dwell-time conditions are satisfied, the dynamical systems for both relay and exploring agents are proven to be stable, such that the tracking and estimation errors are bounded above by a user defined parameter.

To demonstrate the application of this method, examples of controller and predictor update laws for both agents are provided, a single-layer neural network is implemented using an integral concurrent learning approach, and an auxiliary trajectory for the relay agent is given to ensure the fulfillment of the dwell-time conditions. Based on the design examples, an experiment is performed using a two-wheeled mobile robot as the exploring agent and a quadcopter as the relay agent. The experimental results and respective error plots are provided, accompanied by discussions to illustrate the performance of the presented method.
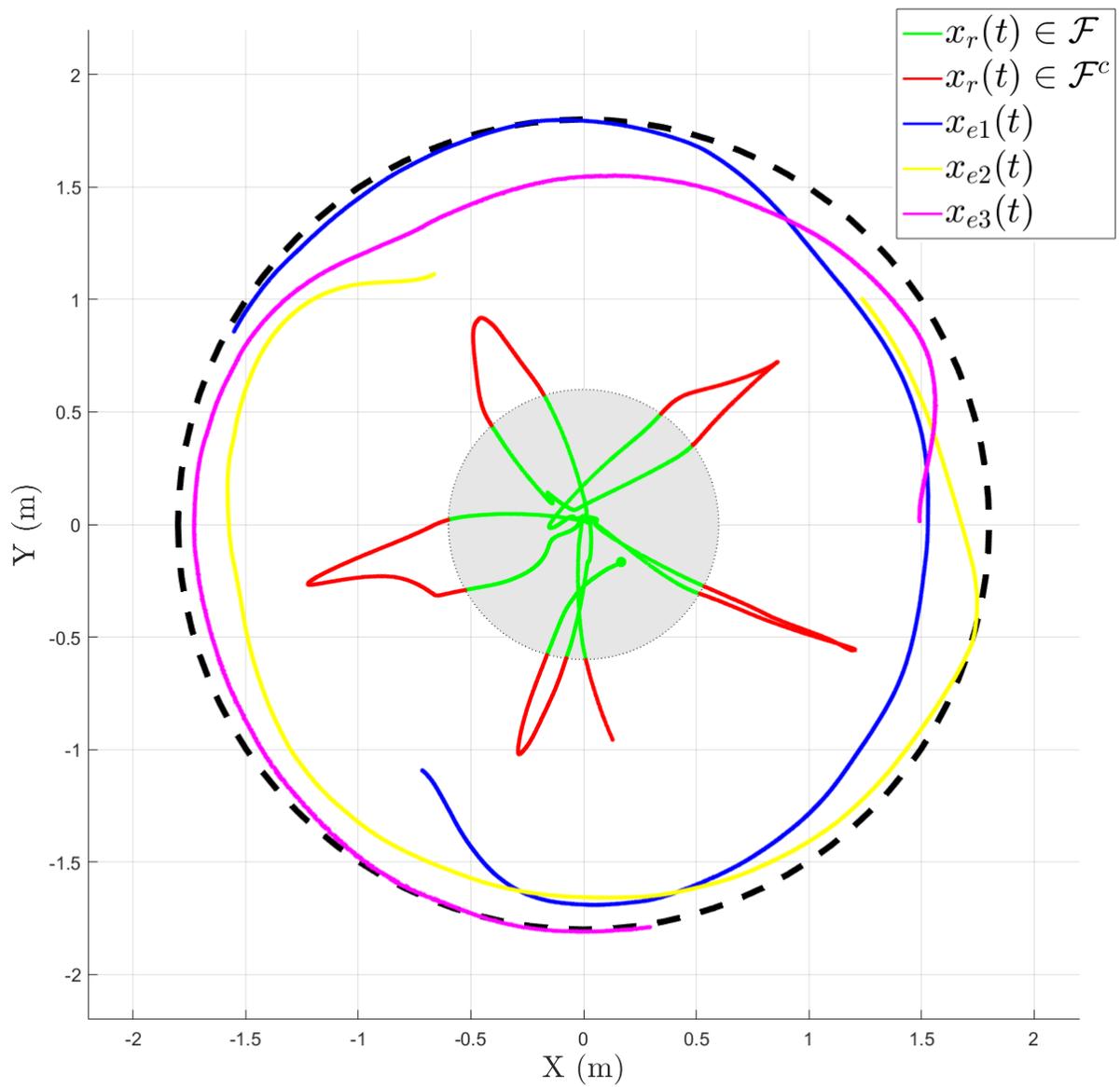
Figure 5-8. The overall tracking result with one relay agent servicing three exploring agent.

CHAPTER 6
CONCLUSION

In many scenarios, factors such as task definition, operating environment, or sensor modality can result in temporary loss of feedback for autonomous agents (e.g., communication may be limited or feedback may be provided by sensors such as cameras which are limited by sensing distance and field-of-view (FOV) constraints, and are vulnerable to occlusions). Such factors have motivated the development of various path planning and control methods that seek uninterrupted feedback, where the desired trajectory or behavior of such systems is inherently constrained. Systems with nonholonomic constraints may experience limited, sharp-angled or non-smooth trajectories to keep a navigational landmark in the FOV using a visual servoing approach. In lieu of constraining the system to ensure uninterrupted feedback, the work in this dissertation allows intermittent loss of state feedback for systems operating in feedback-denied regions. Some applications where this framework is useful include underwater operations that require vehicles to resurface to acquire GPS, navigation within urban canyons where GPS is occluded, and exploration of areas where absolute positioning systems have not been established.

Chapter 2, a novel method to WMR vision based trajectory tracking utilizing a switched systems approach is presented. In contrast to past literature, the approach presented in this chapter does not require constant image feedback of landmark features. State estimates are used for the control input instead of the true states, and are updated via an observer or a predictor when the landmark is visible or not, respectively. Chapter 2 represents novel approach to dealing with controlling a dynamical system under intermittent state feedback, where the system may navigate without state feedback for up to a developed dwell-time. It is shown that using the developed dwell time conditions for the nonlinear observer, trajectories can be designed to allow the landmark

to leave the FOV for periods of time. The stability analysis indicates the controller en-sures the tracking error is globally uniformly ultimately bounded. The bounded result implies that image feedback of landmark features is not required for a duration less than or equal to the maximum dwell time, allowing for intermittent state feedback. Given that the landmark may leave the FOV for periods of time, the WMR is able to operate over larger environments. A simulation and an experiment for the developed control scheme are provided.

Further extending the result, Chapter 3 aims to achieve a path-following objec-tive despite intermittent loss of feedback. The novelty of the result in this chapter is guaranteeing the stability of following a path which lies outside a region with feedback while maximizing the amount of time the agent spends in the feedback-denied envi-ronment. Unlike Chapter 2, where the objective is to regulate a nonholonomic vehicle to a set-point in the presence of intermittent feedback, the difficulty of path following in this chapter arises when the system is outside the feedback region. Switched systems methods are used to develop a state estimator and predictor when state feedback is available or not, respectively. Since switching occurs between a stable subsystem when feedback is available and an unstable subsystem when feedback is not available, dwell time conditions are developed that determine the minimum time that the agent must be in the feedback region versus the maximum time the agent can be in the feedback de-nied region. Using these dwell time conditions, a switching trajectory is designed based on the dwell time conditions that leads the agent in and out of the feedback denied region so that the overall system remains stable. An experiment using a quadcopter is performed to illustrate this approach.

To generalize the approach developed in the previous chapters, development in Chapter 4 is focused on the relaxation of the necessity to alter existing controllers and associated stability analysis, while maximizing the amount of time the agent is allowed in the feedback-denied environment. Furthermore, the current result allows

a reset map to be used with no minimum dwell-time condition. These contributions allow a wide class of controllers, observers, or predictors to be used, and allows the agent to spend more time following the path in the feedback denied region. Using Lyapunov-based stability methods, a framework is developed to allow state estimators and predictors to be used when state feedback is or is not available, respectively, and switched systems analysis determines the stabilizing dwell-time conditions based on a prescribed tolerance on the tracking error. According to the developed dwell-time conditions, an auxiliary trajectory is designed to guide the nonlinear dynamic system in and out of the feedback denied region so that the overall system remains stable. Two experiments using a quadcopter are provided to demonstrate the performance of the approach.

Building on the developed framework and taking into account uncertainty in the dynamics, Chapter 5 investigates an assisted path-following objective involving a relay agent and an exploring agent. Specifically, the presented method allows an exploring agent to remain and operate in the feedback-denied environment indefinitely, while a relay agent is utilized to intermittently visit the exploring agent to update its state estimate. The unique challenge in this method is that the relay agent also loses state feedback once it enters the feedback-denied region, and hence must rely on its state estimate to reach the exploring agent and then return to the feedback-available region in time. In addition, the drift dynamics of the relay agent are assumed to be unknown, and hence, a neural-network-based learning method is utilized to approximate the drift dynamics. To address the stability of the overall system, a Lyapunov-based, switched systems approach is used to develop dwell-time conditions to determine the maximum time the relay agent may remain in the feedback-denied region and the maximum time an exploring agent is allowed to operate without a state update given a prescribed tolerance on the estimation error. An experiment is performed, and results are presented with discussions. As an extension, the experiment is reproduced with

three exploring agents to demonstrate that under admissible physical conditions (i.e., minor environmental disturbances, measurement noise, etc.), the results in Chapter 5 may be extended to include multiple exploring agents.

The developments in this dissertation provides a foundation for various intermittent feedback research problems. One direction to extend is the development of a generalized path-planning strategy to replace the auxiliary trajectories described in this dissertation. The auxiliary trajectories described in this dissertation are arbitrarily designed to satisfy the dwell-time conditions and are ad-hoc in nature. However, a significant contribution can be made from utilizing (sub)optimal path-planning methods, such as model predictive control and online approximate optimal control methods, to yield a more general solution.

Furthermore, the relaxation of the dwell-time conditions may be investigated through other types of state estimation. As motivated in the literature review, the development in this dissertation is based on using a predictor to propagate state estimates when feedback is unavailable to demonstrate stability in the worst case scenario. However, integration with other sensors may improve state estimation, and hence, prolong the maximum dwell-time a system can operate without true state update. For example, although not included in this dissertation, preliminary results during the development of this work suggest that odometry from encoders on WMR's may provide a more accurate estimation than predictors under minimal slip conditions. In addition, vision-based odometry may also be utilized to update state estimate, which is typically the case for many commercial quadcopters. However, online quantification of estimation error accumulation for these methods and integration with the results in this dissertation are currently open challenges.

While the results of this dissertation involve a known, stationary feedback region, future research may also focus on time-varying, unknown or multiple regions. Based on the result in Chapter 5, if the relationship between agents is measurable when the

agents are sufficiently close, the exploring agent may be treated as a local landmark, and the relay agent may utilize the measured relationship as a local state feedback (with respect to the exploring agent). Thus, the local feedback information is similar to achieving localization with respect to a topology graph in SLAM approaches. Therefore, future research may potentially investigate global loop-closure techniques to estimate the topology between non-overlapping feedback-available regions. As a result, formation control and network problems are also potential research directions stemming from the development of this dissertation.

REFERENCES

[1] N. Gans, S. Hutchinson, and P. Corke, "Performance tests for visual servo control systems, with application to partitioned approaches to visual servo control," *Int. J. Rob. Res.*, vol. 22, no. 10, pp. 955–981, 2003.

[2] S. Hutchinson, G. Hager, and P. Corke, "A tutorial on visual servo control," *IEEE Trans. Robot. Autom.*, vol. 12, no. 5, pp. 651–670, Oct. 1996.

[3] N. Gans, G. Hu, K. Nagarajan, and W. E. Dixon, "Keeping multiple moving targets in the field of view of a mobile camera," *IEEE Trans. Robot. Autom.*, vol. 27, no. 4, pp. 822–828, 2011.

[4] N. Gans, G. Hu, J. Shen, Y. Zhang, and W. E. Dixon, "Adaptive visual servo control to simultaneously stabilize image and pose error," *Mechatron.*, vol. 22, no. 4, pp. 410–422, 2012.

[5] G. Hu, N. Gans, and W. E. Dixon, "Quaternion-based visual servo control in the presence of camera calibration error," *Int. J. Robust Nonlinear Control*, vol. 20, no. 5, pp. 489–503, 2010.

[6] G. Hu, N. Gans, N. Fitz-Coy, and W. E. Dixon, "Adaptive homography-based visual servo tracking control via a quaternion formulation," *IEEE Trans. Control Syst. Technol.*, vol. 18, no. 1, pp. 128–135, 2010.

[7] G. Hu, W. Mackunis, N. Gans, W. E. Dixon, J. Chen, A. Behal, and D. Dawson, "Homography-based visual servo control with imperfect camera calibration," *IEEE Trans. Autom. Control*, vol. 54, no. 6, pp. 1318–1324, 2009.

[8] J. Chen, D. M. Dawson, W. E. Dixon, and V. Chitrakaran, "Navigation function based visual servo control," *Automatica*, vol. 43, pp. 1165–1177, 2007.

[9] J. Chen, D. M. Dawson, W. E. Dixon, and A. Behal, "Adaptive homography-based visual servo tracking for fixed and camera-in-hand configurations," *IEEE Trans. Control Syst. Technol.*, vol. 13, pp. 814–825, 2005.

[10] G. Palmieri, M. Palpacelli, M. Battistelli, and M. Callegari, "A comparison between position-based and image-based dynamic visual servoings in the control of a translating parallel manipulator," *J. Robot.*, vol. 2012, 2012.

[11] N. Gans and S. Hutchinson, "Stable visual servoing through hybrid switched-system control," *IEEE Trans. Robot.*, vol. 23, no. 3, pp. 530–540, 2007.

[12] G. Chesi and A. Vicino, "Visual servoing for large camera displacements," *IEEE Trans. Robot. Autom.*, vol. 20, no. 4, pp. 724–735, 2004.

[13] P. Deptula, R. Licitra, J. A. Rosenfeld, and W. E. Dixon, "Online approximate optimal path-planner in the presence of mobile avoidance regions," in *Proc. Am. Control Conf.*, 2018, pp. 2515–2520.

[14] N. R. Gans and S. A. Hutchinson, "A stable vision-based control scheme for nonholonomic vehicles to keep a landmark in the field of view," in *Proc. IEEE Int. Conf. Robot. Autom.*, Roma, Italy, Apr. 2007, pp. 2196–2201.

[15] G. L. Mariottini, G. Oriolo, and D. Prattichizzo, "Image-based visual servoing for nonholonomic mobile robots using epipolar geometry," *IEEE Trans. Robot.*, vol. 23, no. 1, pp. 87–100, Feb. 2007.

[16] G. Lopez-Nicolas, N. R. Gans, S. Bhattacharya, C. Sagues, J. J. Guerrero, and S. Hutchinson, "Homography-based control scheme for mobile robots with nonholonomic and field-of-view constraints," *IEEE Trans. Syst. Man Cybern.*, vol. 40, no. 4, pp. 1115–1127, Aug. 2010.

[17] E. Garcia and P. J. Antsaklis, "Adaptive stabilization of model-based networked control systems," in *Proc. Am. Control Conf.*, San Francisco, CA, USA, Jul. 2011, pp. 1094–1099.

[18] S. S. Mehta, W. MacKunis, S. Subramanian, E. L. Pasiliao, and J. W. Curtis, "Stabilizing a nonlinear model-based networked control system with communication constraints," in *Proc. Am. Control Conf.*, Washington, DC, Jun. 2013, pp. 1570–1577.

[19] E. Garcia and P. J. Antsaklis, "Model-based event-triggered control for systems with quantization and time-varying network delays," *IEEE Trans. Autom. Control*, vol. 58, no. 2, pp. 422–434, Feb. 2013.

[20] M. J. McCourt, E. Garcia, and P. J. Antsaklis, "Model-based event-triggered control of nonlinear dissipative systems," in *Proc. Am. Control Conf.*, Portland, Oregon, USA, Jun. 2014, pp. 5355–5360.

[21] N. E. Leonard and A. Olshevsky, "Cooperative learning in multi-agent systems from intermittent measurements," in *Proc. IEEE Conf. Decis. Control*, Florence, Italy, Dec. 2013, pp. 7492–7497.

[22] J. Liang, Z. Wang, and X. Liu, "Distributed state estimation for discrete-time sensor networks with randomly varying nonlinearities and missing measurements," *IEEE Trans. Neural Netw.*, vol. 22, no. 3, pp. 486–496, Mar. 2011.

[23] Y. Shi, H. Fang, and M. Yan, "Kalman filter-based adaptive control for networked systems with unknown parameters and randomly missing outputs," *Int. J. Robust Nonlinear Control*, vol. 19, no. 18, pp. 1976–1992, Dec. 2009.

[24] Z. Wang, B. Shen, and X. Liu, "H_∞ filtering with randomly occurring sensor saturations and missing measurements," *Automatica*, vol. 48, no. 3, pp. 556–562, Mar. 2012.

[25] X. Yao, L. Wu, and W. X. Zheng, "Fault detection filter design for Markovian jump singular systems with intermittent measurements," *IEEE Trans. Signal Process.*, vol. 59, no. 7, pp. 3099–3109, 2011.

[26] Y. Zhao, J. Lam, and H. Gao, "Fault detection for fuzzy systems with intermittent measurements," *IEEE Trans. Fuzzy Syst.*, vol. 17, no. 2, pp. 398–410, 2009.

[27] J. You and S. Yin, "H_∞ filtering for time-delay t-s fuzzy systems with intermittent measurements and quantization," *J. Franklin Inst.*, Feb. 2013.

[28] H. Gao, Y. Zhao, J. Lam, and K. Chen, "H_∞ fuzzy filtering of nonlinear systems with intermittent measurements," *IEEE Trans. Fuzzy Syst.*, vol. 17, no. 2, pp. 291–300, Apr. 2009.

[29] K. You, M. Fu, and L. Xie, "Mean square stability for Kalman filtering with Markovian packet losses," *Automatica*, vol. 47, no. 12, pp. 2647–2657, Dec. 2011.

[30] H. Zhang and Y. Shi, "Observer-based H_∞ feedback control for arbitrarily time-varying discrete-time systems with intermittent measurements and input constraints," *J. Dyn. Syst., Meas., and Control*, vol. 134, no. 6, Sep. 2012.

[31] B. Shen, Z. Wang, H. Shu, and G. Wei, "On nonlinear H_∞ filtering for discrete-time stochastic systems with missing measurements," *IEEE Trans. Autom. Control*, vol. 53, no. 9, pp. 2170–2180, 2008.

[32] S. C. Smith and P. Seiler, "Optimal pseudo-steady-state estimators for systems with markovian intermittent measurements," in *Proc. Am. Control Conf.*, vol. 4, 2002, pp. 3021–3027.

[33] J. You, S. Yin, and H. R. Karimi, "Robust estimation for discrete markov system with time-varying delay and missing measurements," *Math. Probl. Eng.*, 2013.

[34] H. M. Faridani, "Performance of kalman filter with missing measurements," *Automatica*, vol. 22, no. 1, pp. 117–120, 1986.

[35] Z. Wang, F. Yang, D. W. C. Ho, and X. Liu, "Robust finite-horizon filtering for stochastic systems with missing measurements," *IEEE Signal Process. Lett.*, vol. 12, no. 6, pp. 437–440, Jun. 2005.

[36] Z. Wang, D. W. Ho, Y. Liu, and X. Liu, "Robust H_∞ control for a class of nonlinear discrete time-delay stochastic systems with missing measurements," *Automatica*, vol. 45, no. 3, pp. 684–691, 2009.

[37] Z. Wang, F. Yang, D. W. Ho, and X. Liu, "Robust H_∞ filtering for stochastic time-delay systems with missing measurements," *IEEE Trans. Signal Process.*, vol. 54, no. 7, pp. 2579–2587, 2006.

[38] F. O. Hounkpevi and E. E. Yaz, "Robust minimum variance linear state estimators for multiple sensors with different failure rates," *Automatica*, vol. 43, no. 7, pp. 1274–1280, 2007.

[39] H. Liang and T. Zhou, "Robust state estimation for uncertain discrete-time stochastic systems with missing measurements," *Automatica*, vol. 47, no. 7, pp. 1520–1524, 2011.

[40] L. Ma, Z. Wang, J. Hu, Y. Bo, and Z. Guo, "Robust variance-constrained filtering for a class of nonlinear stochastic systems with missing measurements," *Signal Process.*, vol. 90, no. 6, pp. 2060–2071, Jun. 2010.

[41] J. Liang, Z. Wang, and X. Liu, "State estimation for coupled uncertain stochastic networks with missing measurements and time-varying delays: the discrete-time case," *IEEE Trans. Neural Netw.*, vol. 20, no. 5, pp. 781–793, 2009.

[42] S. Kluge, K. Reif, and M. Brokate, "Stochastic stability of the extended Kalman filter with intermittent observations," *IEEE Trans. Autom. Control*, vol. 55, no. 2, pp. 514–518, 2010.

[43] L. Li and Y. Xia, "Stochastic stability of the unscented kalman filter with intermittent observations," *Automatica*, vol. 48, no. 5, pp. 978–981, 2012.

[44] S. Deshmukh, B. Natarajan, and A. Pahwa, "Stochastic state estimation for smart grids in the presence of intermittent measurements," in *IEEE Lat.-Am. Conf. Commun.*, 2012, pp. 1–6.

[45] Z. Wang, D. W. Ho, and X. Liu, "Variance-constrained filtering for uncertain stochastic systems with missing measurements," *IEEE Trans. Autom. Control*, vol. 48, no. 7, pp. 1254–1258, 2003.

[46] S. S. Mehta, G. Hu, A. P. Dani, and W. E. Dixon, "Multi-reference visual servo control of an unmanned ground vehicle," in *Proc. AIAA Guid. Navig. Control Conf.*, Honolulu, Hawaii, Aug. 2008.

[47] B. Jia and S. Liu, "Switched visual servo control of nonholonomic mobile robots with field-of-view constraints based on homography," *Control Theory Technol.*, vol. 13, no. 4, pp. 311–320, 2015.

[48] G. Klein and D. Murray, "Parallel tracking and mapping for small ar workspaces," in *IEEE ACM Int. Symp. Mixed Augment. Real.*, 2007, pp. 225–234.

[49] A. J. Davison, I. D. Reid, N. D. Molton, and O. Stasse, "Monoslam: Real-time single camera slam," *IEEE Trans. Pattern Anal. Mach. Intell.*, vol. 29, no. 6, pp. 1052–1067, Jun. 2007.

[50] D. Cremers, "Direct methods for 3d reconstruction and visual slam," in *IEEE IAPR Int. Conf. Mach. Vis. Appl.*, 2017, pp. 34–38.

[51] B. Williams, M. Cummins, J. Neira, P. Newman, I. Reid, and J. Tardós, "A comparison of loop closing techniques in monocular slam," *Robot. Auton. Syst.*, vol. 57, no. 12, pp. 1188–1197, 2009.

[52] C. Cadena, L. Carlone, H. Carrillo, Y. Latif, D. Scaramuzza, J. Neira, I. Reid, and J. Leonard, "Past, present, and future of simultaneous localization and mapping: Towards the robust-perception age," *IEEE Trans. Robot.*, vol. 32, no. 6, pp. 1309–1332, 2016.

[53] M. Labbé and F. Michaud, "Online global loop closure detection for large-scale multi-session graph-based slam," in *IEEE/RSJ Int. Conf. Intell. Robot. Syst.*, Sept 2014, pp. 2661–2666.

[54] R. Kümmerle, G. Grisetti, H. Strasdat, K. Konolige, and W. Burgard, "G2o: A general framework for graph optimization," in *IEEE Int. Conf. on Robot. Autom.*, May 2011, pp. 3607–3613.

[55] D. Liberzon, *Switching in Systems and Control*. Birkhauser, 2003.

[56] G. Zhai, B. Hu, K. Yasuda, and A. N. Michel, "Stability analysis of switched systems with stable and unstable subsystems: An average dwell time approach," *Int. J. Syst. Sci.*, vol. 32, no. 8, pp. 1055–1061, Nov. 2001.

[57] M. A. Müller and D. Liberzon, "Input/output-to-state stability and state-norm estimators for switched nonlinear systems," *Automatica*, vol. 48, no. 9, pp. 2029–2039, 2012.

[58] A. Parikh, T.-H. Cheng, H.-Y. Chen, and W. E. Dixon, "A switched systems framework for guaranteed convergence of image-based observers with intermittent measurements," *IEEE Trans. Robot.*, vol. 33, no. 2, pp. 266–280, April 2017.

[59] H.-Y. Chen, Z. I. Bell, R. Licitra, and W. E. Dixon, "Switched systems approach to vision-based tracking control of wheeled mobile robots," in *Proc. IEEE Conf. Decis. Control*, 2017, pp. 4902–4907.

[60] W. E. Dixon, D. M. Dawson, E. Zergeroglu, and F. Zhang, "Robust tracking and regulation control for mobile robots," *Int. J. Robust Nonlinear Control*, vol. 10, pp. 199–216, 2000.

[61] J.-H. Hwang, R. C. Arkin, and D.-S. Kwon, "Mobile robots at your fingertip: Bezier curve on-line trajectory generation for supervisory control," in *Intelligent Robots and Systems, 2003.(IROS 2003). Proceedings. 2003 IEEE/RSJ International Conference on*, vol. 2. IEEE, 2003, pp. 1444–1449.

[62] G. J. Yang and B. W. Choi, "Smooth trajectory planning along bezier curve for mobile robots with velocity constraints," *International Journal of Control and Automation*, vol. 6, no. 2, pp. 225–234, 2013.

[63] F. Zhou, B. Song, and G. Tian, "Bezier curve based smooth path planning for mobile robot," *Journal of Information & Computational Science*, vol. 8, no. 12, pp. 2441–2450, 2011.

[64] B. Lau, C. Sprunk, and W. Burgard, "Kinodynamic motion planning for mobile robots using splines," in *2009 IEEE/RSJ International Conference on Intelligent Robots and Systems*, Oct. 2009, pp. 2427–2433.

[65] H.-Y. Chen, Z. I. Bell, P. Deptula, and W. E. Dixon, "A switched systems approach to path following with intermittent state feedback," *IEEE Trans. Robot.*, submitted (see also arXiv:1803.05584).

[66] ——, "A switched systems framework for path following with intermittent state feedback," *IEEE Control Syst. Lett.*, vol. 2, no. 4, pp. 749–754, Oct. 2018.

[67] M. Krstic, I. Kanellakopoulos, and P. V. Kokotovic, *Nonlinear and Adaptive Control Design*. New York, NY, USA: John Wiley & Sons, 1995.

[68] W. E. Dixon, A. Behal, D. M. Dawson, and S. Nagarkatti, *Nonlinear Control of Engineering Systems: A Lyapunov-Based Approach*. Birkhauser: Boston, 2003.

[69] K. Dupree, N. Gans, W. Mackunis, and W. E. Dixon, "Euclidean calculation of feature points of a rotating satellite: A daisy chaining approach," in *Proc. Am. Control Conf.*, York, NY, Jul. 2007, pp. 3874–3879.

[70] N. R. Gans, A. Dani, and W. E. Dixon, "Visual servoing to an arbitrary pose with respect to an object given a single known length," in *Proc. Am. Control Conf.*, Seattle, WA, USA, Jun. 2008, pp. 1261–1267.

[71] W. MacKunis, N. Gans, K. Kaiser, and W. E. Dixon, "Unified tracking and regulation visual servo control for wheeled mobile robots," in *IEEE Multi-Conf. Syst. and Contr.*, Suntec City, Singapore, Oct. 2007, pp. 88–93.

[72] M. Fiala, "Artag, a fiducial marker system using digital techniques," in *2005 IEEE Computer Society Conference on Computer Vision and Pattern Recognition (CVPR'05)*, vol. 2, Jun. 2005, pp. 590–596 vol. 2.

[73] E. Olson, "Apriltag: A robust and flexible visual fiducial system," in *Robotics and Automation (ICRA), 2011 IEEE International Conference on*. IEEE, 2011, pp. 3400–3407.

[74] A. Dani, N. Fischer, Z. Kan, and W. E. Dixon, "Globally exponentially stable observer for vision-based range estimation," *Mechatron.*, vol. 22, no. 4, pp. 381–389, Special Issue on Visual Servoing 2012.

[75] Z. I. Bell, H.-Y. Chen, A. Parikh, and W. E. Dixon, "Single scene and path reconstruction with a monocular camera using integral concurrent learning," in *Proc. IEEE Conf. Decis. Control*, 2017, pp. 3670–3675.

[76] D. S. Ebert, *Texturing & modeling: a procedural approach*. Morgan Kaufmann, 2003.

[77] "bebop_autonomy library," http://bebop-autonomy.readthedocs.io.

[78] M. Branicky, "Multiple Lyapunov functions and other analysis tools for switched and hybrid systems," *IEEE Trans. Autom. Control*, vol. 43, pp. 475–482, 1998.

[79] P. Peleties and R. DeCarlo, "Asymptotic stability of m-switched systems using lyapunov-like functions," in *Proc. Am. Control Conf.*, 1991, pp. 1679–1684.

[80] F. L. Lewis, R. Selmic, and J. Campos, *Neuro-Fuzzy Control of Industrial Systems with Actuator Nonlinearities*. Philadelphia, PA, USA: Society for Industrial and Applied Mathematics, 2002.

[81] J. A. Farrell and M. M. Polycarpou, *Adaptive approximation based control: Unifying neural, fuzzy and traditional adaptive approximation approaches*, ser. Adaptive and Learning Systems for Signal Processing, Communications and Control Series. John Wiley & Sons, 2006, vol. 48.

[82] A. Parikh, R. Kamalapurkar, and W. E. Dixon. (2015) Integral concurrent learning: Adaptive control with parameter convergence without PE or state derivatives. arXiv:1512.03464.

[83] ——, "Target tracking in the presence of intermittent measurements via motion model learning," *IEEE Trans. Robot.*, vol. 34, no. 3, pp. 805–819, 2018.

[84] C. Samson, "Control of chained systems application to path following and time-varying point-stabilization of mobile robots," *IEEE Trans. Autom. Control*, vol. 40, no. 1, pp. 64–77, 1995.

[85] L. E. A. M., P. Soueres, M. Courdesses, and S. Fleury, "Robust path-following control with exponential stability for mobile robots," in *Proc. IEEE Int. Conf. Robot. Autom.*, vol. 4, May 1998, pp. 3279–3284 vol.4.

BIOGRAPHICAL SKETCH

      Hsi-Yuan Chen received his bachelor's degree from the Department of Mechanical Engineering at the National Taiwan University of Science and Technology in 2014. As an undergraduate, he joined the Center for Intelligent Robots, where he spent two years researching robotic vision and navigation theories. Hsi-Yuan joined the Nonlinear Controls and Robotics laboratory at the University of Florida for his graduate studies. He received his Master of Science in mechanical engineering (2016) with a Computer Engineering Minor as well as his Doctor of Philosophy degree (2018) under the supervision of Dr. Dixon. His primary research interests include switched systems theory, intermittent sensing, simultaneous localization and mapping, and other vision-based control systems.